Electronic Thesis and Dissertation Repository

8-23-2017 12:00 AM

Force Sensing Surgical Grasper with Folding Capacitive Sensor

Dave BP Tripp, *The University of Western Ontario*

Supervisor: Dr. Michael Naish, *The University of Western Ontario*
A thesis submitted in partial fulfillment of the requirements for the Master of Engineering Science degree in Electrical and Computer Engineering
© Dave BP Tripp 2017

Follow this and additional works at: https://ir.lib.uwo.ca/etd

Part of the Biomedical Commons, and the Biomedical Devices and Instrumentation Commons

Recommended Citation
Tripp, Dave BP, "Force Sensing Surgical Grasper with Folding Capacitive Sensor" (2017). *Electronic Thesis and Dissertation Repository*. 4854.
https://ir.lib.uwo.ca/etd/4854

Force Sensing Surgical Grasper with Folding Capacitive Sensor

Dave Tripp

M.E.Sc. Thesis, 2017
Department of Electrical and Computer Engineering
The University of Western Ontario

Abstract

Minimally-invasive surgery (MIS) has brought many benefits to the operating room, however, MIS procedures result in an absence of force feedback, and surgeons cannot as accurately feel the tissue they are working on, or the forces that they are applying. One of the barriers to introducing MIS instruments with force feedback systems is the high cost of manufacturing and assembly. The instruments must also be sterilized before every use, a process that can easily destroy any embedded sensing system. An instrument that can be disposed of after a single use and produced in bulk at a low cost is desirable.

Printed circuit micro-electro-mechanical systems (PCMEMS) is an emerging manufacturing technology that may represent an economically viable method of bulk manufacturing small, single-use medical devices, including surgical graspers. This thesis presents the design and realization of a PCMEMS surgical grasper that can fit within a 5 mm trocar, and can accurately measure forces in 3 axes, over a range of ± 4 N.

The designed instrument is the first PCMEMS grasper to feature multi-axis sensing, and has a sensing range twice as large as current PCMEMS devices. Experimental results suggest that the performance of the sensing system is similar to conventionally-manufactured MIS instruments that use capacitive force transducers. The techniques applied in this thesis may be useful for developing a range of PCMEMS devices with capacitive sensors. Improvements to the design of the grasper and the sensing system are suggested, and several points are presented to inform the direction of future work related to PCMEMS MIS instruments.

Acknowledgements

I feel very fortunate to have had Dr. Michael Naish as my MESc supervisor. Before I began my MESc, I emailed him to discuss the possibility of pursuing other opportunities, and he provided me with fair and honest advice. When I decided to return to Western he allowed me the freedom to choose a thesis topic that interested me. I would like to thank him for his continued guidance and support. Dr. Naish was always available to meet and discuss ideas, and at times was the only person keeping me on track. Further, he always made sure I had the resources necessary to do my work, including securing me good TA positions. His help was invaluable to the success of this project.

The staff at CSTAR were always very welcoming, and allowed me to use CSTAR equipment whenever I needed—including the computer that I typed this thesis on. I would especially like to thank Abelardo (Abe) Escoto. Abe taught me how to use the Atometric micro milling machine, and helped me through the difficulties of machining with 25 μm and 50 μm end mills. He was a great source of information for all things related to MIS devices and helped fix many of my poor designs for parts and fixtures. When I needed to use the wire EDM, or needed training or assistance with any number of problems, Abe always made time to meet with me.

I like to think of the WearME group as our "sibling" lab. I would like to thank Dr. Trejos and the WearME research group for letting me freely borrow tools or equipment.

The knowledge from the Electronics Shop in SEB is what brought my circuit designs to life: Eugen Porter, Rob Barbeito, Trent Steensma, Ken Strong, and Ron Struke put in a lot of work that helps the university and its students. Thank you for working with me when I needed to try things that were new and difficult. Rob and Eugen helped me figure out the best way to make my

laser printed flexible circuits, something that saved me a tremendous amount of time. Eugen was a great source of ideas and problem solving solutions when I would stop in to discuss my (ongoing) issues. He also always made time to 3D print pieces that I needed or run the laser cutter for me.

I would also like to thank Chris Vandelaar for all his guidance in machining and fabrication. Chris was instrumental in my research and taught me the basics of CNC machining. He answered many questions about the best way to fixture, machine, cut, and make everything from simple to impossible parts. Chris saved me many hours by letting me know when I needed to abandon certain ideas, and provided me with much better alternatives.

I'd like to thank my summer student Claire, who helped in the design and testing of the first generation prototype, and was a source of good ideas and conversation. Thanks to my friend and roommate Brandon Edmonds, for ensuring my time outside of the lab was well spent.

Contents

List of Figures

List of Tables

Nomenclature and Acronyms

Acronyms

2D	Two-Dimensional
3D	Three-Dimensional
AC	Alternating Current
AWG	American Wire Gauge
CAD	Computer-Aided Design
CDC	Capacitance to Digital Converter
CFRP	Carbon Fiber Reinforced Plastic
CNC	Computer Numerically Controlled
CSTAR	Canadian Surgical Technologies & Advanced Robotics
DOF	Degree Of Freedom
DPSS	Diode-Pumped Solid State
EDM	Electrical Discharge Machining
FBG	Fiber Bragg Grating
FEA	Finite Element Analysis
FPCB	Flexible Printed Circuit Board
GUI	Graphical User Interface
IC	Integrated Circuit

LED   Light Emitting Diode

MEMS   Micro-Electro-Mechanical Systems

MFI   Micromechanical Flying Insect

MIS   Minimally Invasive Surgery

MMM   Micro Milling Machine

PC   Personal Computer

PCB   Printed Circuit Board

PCMEMS   Printed-Circuit MEMS

PDMS   Polydimethylsiloxane

PVDF   Polyvinylidene Fluoride

RMS   Root Mean Square

rpm   revolutions per minute

SL1   Sublaminate 1

SL2   Sublaminate 2

SL3   Sublaminate 3

USP   United States Pharmacopeia

UV   Ultraviolet

Variables

A Overlapping area between electrodes

δA Change in overlapping area between electrodes

C Capacitance

C'_A Adjusted axial capacitance response

C_A Axial sensor capacitance response

$C_\mathrm{A,N}$ Normal coupled response on axial load

$C_{\mathrm{A,T}}$	Transverse coupled response on axial load
C_{N}'	Adjusted normal capacitance response
C_{N}	Normal sensor capacitance response
$C_{\mathrm{N,A}}$	Axial coupled response on normal load
$C_{\mathrm{N,T}}$	Transverse coupled response on normal load
C_{T}'	Adjusted transverse capacitance response
C_{T}	Transverse sensor capacitance response
$C_{\mathrm{T,A}}$	Axial coupled response on transverse load
$C_{\mathrm{T,N}}$	Normal coupled response on transverse load
E	Young's modulus
E_{A}	Equation of force response for axial sensor
E_{N}	Equation of force response for normal sensor
E_{T}	Equation of force response for transverse sensor
F_{A}	Force response of axial sensor
F_{N}	Force response of normal sensor
F_{T}	Force response of transverse sensor
ε_0	Relative permittivity of air
ε_{r}	Relative permittivity of dielectric
F	Force
G	Shear modulus
γ	Shear strain
L	Width of capacitive electrode
t	Distance between electrodes in capacitor
Δt	Change in distance t
τ	Shear force
ν	Poisson's ratio

x_s Linear displacement of electrode

Units

°C   degrees Celsius

cm   centimeters

dB   decibels

g   grams

Hz   hertz

N   newtons

Nm   newton-meters

Nmm   newton-millimeters

min   minutes

mil   0.001 inches

mg   milligrams

mm   millimeters

mN   millinewtons

mV   millivolts

μm   micrometers

Ω ohms

pF   picofarad

psi   pounds per square inch

s   seconds

V   volts

W   watts

Chapter 1

Introduction

1.1 Motivation

Minimally invasive surgery (MIS) is a surgical technique performed through small incisions in the body. Compared to traditional open surgery, MIS offers many benefits including reduced blood loss, less pain, lower infection rates, shorter hospital stays, as well as high patient satisfaction and improved cosmesis [2–4]. The drawbacks of MIS are also well noted: a steeper learning curve, increased equipment costs, and a lack of force feedback.

Without force feedback, surgeons must rely on visual cues to determine tissue characteristics and estimate the amount of force that they are applying. Surgeons perform many procedures with limited or no force feedback—with a high rate of success—but there is plenty of evidence to support the benefits of force feedback: when tying knots for suturing, three studies have shown force feedback allows surgeons to be more consistent and tie tighter knots without breaking the thread [5–7]; force feedback also improves the accuracy of palpation tasks [8]; and without force feedback errors in a blunt dissection task increased by a factor of three [9].

One of the barriers to introducing force feedback in MIS instruments is the high cost of manufacturing and assembly. The instruments must also be sterilized before every use, a process that can easily destroy any embedded sensing system. Therefore, an instrument that can be disposed of after a single use and produced in bulk at a low cost is desirable.

A relatively new technology known as printed circuit micro-electro-mechanical systems (PCMEMS)

has shown promise for creating devices that are small, complex, and inexpensive. Several PCMEMS medical devices have been developed, including MIS graspers [10–16]. PCMEMS is well suited for developing medical devices, however the current designs of MIS graspers only measure forces in one axis, and are designed for a small force range (± 1.5 N) [11].

The availability of a more robust PCMEMS grasper that offers a larger measurement range and can measure forces in 3 axes would help to progress towards commercially viable PCMEMS medical devices, as well as single use medical devices. The development of a commercially viable force sensing surgical grasper must be considered from many different perspectives—this thesis aims to explore one of these.

1.2   General Problem Statement

MIS instruments that accurately measure forces can provide a benefit to many surgical procedures; however, the cost of these instruments must be low enough to justify widespread adoption. Reasonable cost is achieved through devices that can be reprocessed and sterilized, or disposed of after a single use. Sterilization and multiple uses often degrade performance when using force sensors, and conventional manufacturing techniques usually fail to produce MIS instruments that perform well enough, and are inexpensive enough for a single use.

PCMEMS is an emerging manufacturing technology that may be an economically viable method of bulk manufacturing small, single-use medical devices, including surgical graspers. However, improvement to the function of PCMEMS surgical graspers is required before they can be of clinical use. This thesis aims to contribute to the development of single-use disposable graspers by creating a PCMEMS grasper with greater functionality than exists in current literature, and by reducing barriers to fabricating PCMEMS devices.

1.3   Research Objectives

The primary goal of this thesis is to improve the development of MIS PCMEMS devices by expanding on PCMEMS fabrication techniques and developing a PCMEMS grasper with greater functionality than existing PCMEMS graspers. The following objectives were outlined to help

reach this goal.

- Explore layer fabrication methods other than laser-cutting machines normally used in PCMEMS, to reduce barriers for researchers who may not have access to this equipment.

- Include three-axis force sensing in the grasper—researching various sensing modalities to determine which are best suited for PCMEMS devices.

- Design, build, and evaluate a PCMEMS MIS grasper that has three-axis force sensing over a range of ± 4 N and can fit through a 5 mm trocar.

1.4 Scope

Many force sensing MIS graspers have been presented in literature, with many more in development. The focus of this thesis is not to create the most robust or functional MIS grasper, but to create the most robust and functional PCMEMS MIS grasper. Only PCMEMS manufacturing techniques will be considered, and the thesis will focus only on creating a grasper small enough to fit through a 5 mm trocar—a size suitable for arthroscopic surgery. To justify the development of the grasper, the completed device should be comparable in function and form to existing force sensing graspers, as determined through the state of the art. A small section of the thesis will be devoted to showcasing the benefits of force feedback in MIS, and the advantages of locating sensors at the tool tip (a benefit of using PCMEMS). Further justification of the benefits of PCMEMS will be explored strictly from a literature review perspective—no independent experiments to explore the advantages of PCMEMS manufacturing will be performed. This thesis requires the development of a mechanical structure and layer designs for the PCMEMS device, such that the device can pop-up and be assembled easily, and the development of a complete sensing system. Previous PCMEMS graspers have been developed that measure forces in 1 axis only; the sensing system for this grasper will feature 3 axes of force sensing. The grasper will be evaluated on the useful range, dynamic response, accuracy, and repeatability of the measurements.

1.5   Overview of the Thesis

The structure of the remainder of the thesis is as follows:

Chapter 2   Literature Review: Summarizes the state of the art for PCMEMS technology and current force sensing MIS graspers. Provides background information on the benefits of force feedback in minimally invasive surgery.

Chapter 3   First Prototype: Details the work done for the development and manufacturing of the first-generation grasper. Includes the evaluation and discussion of this version of the instrument.

Chapter 4   Second Generation Grasper: Describes the changes and improvements made for the design and fabrication of the second-generation grasper. The design is evaluated and the results are discussed.

Chapter 5   Conclusions and Future Work: Showcases the outcomes and contributions of this thesis. Suggests improvements for the design and future areas of work.

Chapter 2

Literature Review

2.1 Introduction

The primary goal of the research was to further explore the use of printed-circuit MEMS (PCMEMS) manufacturing to create a force sensing surgical instrument suitable for minimally invasive surgery. Expanding on existing research to create an instrument using new techniques and materials, with a larger force sensing range than current PCMEMS devices. To first ensure that the designed grasper is a useful development, Section 2.2 provides a brief overview on when and how force sensing in minimally invasive surgery is advantageous. Section 2.3 then discusses the process and capabilities of PCMEMS, and why this may be useful for a MIS device. Examples of existing PCMEMS devices are discussed, as well as general manufacturing guidelines. In Section 2.4, technologies used for sensing forces are summarized. These technologies were reviewed for their relative usefulness, but also for how well they can be incorporated into a PCMEMS device. A perceived advantage of PCMEMS is inexpensive bulk manufacturing and efficient assembly when compared to traditional manufacturing techniques—sensing methods that eliminate or reduce these advantages are considered in less detail. The chosen sensing modality for the instrument—capacitance based sensing—is then explored in greater depth in Section 2.5.

2.2　Force Sensing in MIS

It is intuitive to think that limiting the sense of touch, which is so heavily relied on by surgeons, could be very detrimental to surgical outcomes. However many MIS procedures are currently performed with limited or removed haptic feedback, with a high rate of success. Every process has room for improvement though, and gains in intuitiveness or safety would justify the use of haptic feedback. Therefore, the question to ask isn't whether we need haptic feedback to successfully perform a surgery, but what improvements may result from including haptic feedback. This section examines the challenges of measuring forces during MIS procedures, and how force sensing may add value in surgery.

2.2.1　Is Force Sensing Needed?

To understand if force sensing is needed, it is important to look at some factors that can cause errors between perceived and actual forces in surgery. In traditional MIS, a trocar is placed through a small incision in the body, and an instrument is inserted through the trocar. The trocar serves to protect the tissue surrounding the incision. When working without force feedback, contact between the instrument and the trocar, as well as contact with surrounding tissue, can interfere with the surgeon's ability to determine how much force is being applied. These forces are combined with a leverage effect from the tool pivoting at the insertion point, and possible friction and backlash within the instrument itself. Trejos *et al.* discuss the magnitudes of these errors, shown in Figure 2.1 [17].
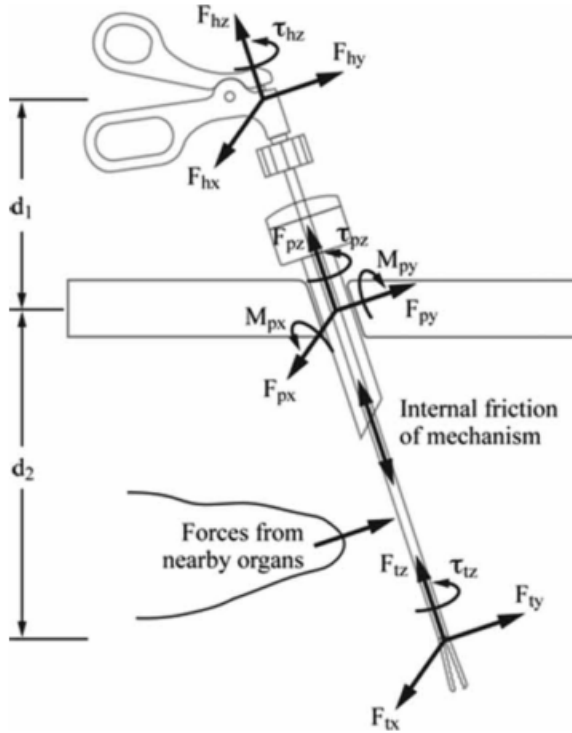
Figure 2.1: Forces acting on minimally invasive instruments [17].

- Forces at the handle are 2 to 6 times greater than tip forces [18].

- Friction at the trocar: 0.25–3 N [19, 20].

- Torques created by the abdominal wall: up to 0.7 Nm [20].

- Internal instrument friction losses: 58% to 92% [21].

- Forces and torques at the tip: 0.5–10 N, 0–0.1 Nm. [20].

Of course, surgeons feel these forces only when using handheld MIS instruments; in robotic or telesurgical procedures, no force feedback at all is provided to clinicians. Many studies have been performed to determine how a lack of force feedback (in manual and robotic MIS procedures) may negatively affect surgical performance. It can be seen from these studies that the task being performed influences the degree to which force sensing is needed. In three studies done on knot tying for suturing, force feedback allowed surgeons to be more consistent, and create tighter knots without fear of breaking the thread [5–7].

Palpation tasks also show better results when force feedback is involved. In a study by Mac-Farlane *et al.*, a force feedback device was significantly better than a standard grasper at rating tissue compliance, however it was still not as successful as using manual palpation with fingers [8]. The method of transmitting the force feedback information to clinicians can effect the results as well, as shown by Gwilliam *et al.* [22]. Force information can be displayed graphically, to visualize forces being applied, or with haptic feedback, so that surgeons can feel the forces that they are ap-

plying. It was found by Gwilliam that displaying graphical force information combined with haptic feedback was best for inexperienced users, however experienced surgeons also showed significant error reduction using only haptic feedback. While the presentation of force feedback information is outside the scope of this thesis, it is useful to note that force feedback can be used to reduce palpation error for both experienced and inexperienced users.

It was also found that without direct force feedback, excessive force in tissue manipulation, dissection, or retraction procedures can increase the risk of tissue trauma [23, 24]. A study simulating a blunt dissection task found that by removing force feedback, the number of errors that resulted in damaged tissue increased by a factor of 3 [9]. In the same study force feedback reduced peak forces applied during surgery by a factor of 2–6.

These examples illustrate that there is value in adding force sensing to minimally invasive surgical systems. Furthermore, with the steep learning curve of MIS, systems with force feedback can be valuable for training and simulation, allowing real world performance to be predicted more accurately. To establish direct force feedback, sensors must be somehow integrated into a surgical instrument.

2.2.2   Sensor Location

The placement of the sensors on the tools is another important consideration. Sensors can be placed in four possible locations: at the tool tip, on the instrument shaft inside of the patient's body, on the instrument shaft outside of the patient's body, or at the actuation mechanism. Placing the sensors at the tool tip has been shown to provide the most accurate force information because the forces shown in Figure 2.1 (friction, reaction forces at the incision, inertia, and backlash) will not interfere with the measurement of tool–tissue interaction forces. Unfortunately, placing the sensors at the tool tip also has the strictest limitations on available space. A summary of sensor locations based on a review article by Puangmali *et al.* [2], is shown in Table 2.1.

PCMEMS is excellent for building small systems on the scale of 1–10 mm, therefore it can be used to overcome the size constraints for locating sensors at the tip of an instrument. As noted earlier, this location also provides the greatest accuracy.

Location	Advantages	Disadvantages
Tool tip	Force measurements are obtained directly, no disturbance from other forces.	Information must be transmitted the furthest distance, strictest limitations on size. Must be sterile.
On shaft inside the body	Not affected by friction and reaction forces at incision.	Drive and assembly mechanics can still disturb measurements. Must be sterilizeable, limitations on size.
On shaft outside of the body	Does not need to sterilized, relaxed size constraints.	Subject to friction and reaction forces at the entry port of the instrument, Measurements are not as accurate.
At actuation mechanism	Does not need to be sterilized, most relaxed size constraints. Some information can be measured directly, such as motor currents.	Measurements are subject to internal friction, backlash, inertia, and interference with tool shaft. Indirect force measurement, least accurate.

Table 2.1: Locations of force sensors for minimally invasive surgical instruments [2].

2.3   PCMEMS

PCMEMS is a relatively new manufacturing method, first described in 2011 [1]. The process is sometimes termed PopUp MEMS, and it appears that no clear distinction between the two exists. Using actuation mechanisms to "pop-up" components (unfolding like a pop-up book) is a key principle of PopUp MEMS. However, devices using the same pop-up mechanisms have been termed PCMEMS by their authors [25]. Although the terms appear to be used interchangeably, herein all such devices will be referred to as PCMEMS for clarity.

The term "printed-circuit" MEMS was coined due to the similarity of the layer-by-layer manufacturing process to that used in the manufacture of printed circuit boards for electronics—an efficient and effective method of both precise and large-scale manufacturing. Similarly, PCMEMS allows for advances in the large scale manufacture of complex electromechanical devices by using a single set of streamlined operations.

PCMEMS are best suited for devices in the 1–10 mm size range, where traditional MEMS manufacturing (surface and bulk micromachining) is very time consuming, difficult to create truly three-dimensional structures, and can only use a limited variety of materials [1]. Conventional techniques for larger devices also fail on this scale: traditional hinges, linkages, and joints become increasingly expensive and time consuming (if not impossible) to fabricate as size decreases. Fur-

ther, the efficiency of traditional hinges decreases as the required precision cannot be met with conventional techniques. PCMEMS is especially suited for MIS instruments. This is explored more thoroughly in [11], where the following points are discussed:

1. Planar (two-dimensional) manufacturing allows many devices to be created in parallel, reducing fabrication time, and cost.

2. Integrating sensors, circuits, and actuators directly during the manufacturing can eliminate time consuming alignment and assembly procedures.

3. Friction and wear are reduced with the flexure based joints. Kapton hinges (used in PCMEMS) have been shown to withstand 10^6 cycles before failure.

4. A large range of materials can be used with PCMEMS, including medical grade alloys and many materials that are biocompatible.

PCMEMS was chosen as the method to fabricate the grasper presented herein, and this technology was studied extensively. Previous PCMEMS papers were studied for joint design, material selection, folding methods, geometric design, and to establish manufacturing parameters .

2.3.1 Manufacturing PCMEMS

In PCMEMS, devices are a combination of many thin layers of materials. The layers within a device can be structural, flexible, adhesive, electrically/thermally conductive, provide actuation, or add sensing [11]. Layers are stacked on top of each other to create a two dimensional layup. The layup is then laminated, using sheet adhesive placed between layers to bond everything together and form a continuous device. After lamination, pre-machined hinges and linkages can fold to "pop-up" the device into a three-dimensional structure. The diverse layer materials can be combined to create a wide range of integrated kinematics, sensing, and actuation.

To manufacture a PCMEMS device, a unique pattern is cut into each layer. This first cut defines the individual layer geometry. A diode-pumped solid state (DPSS) laser is commonly used for cutting operations, but is not required (a CNC or traditional milling machine may be used). Holes for alignment pins are usually included in the first cut—dowel pins can then be used to align

layers that need to be laminated together. By using alignment pins in the material layers, it was shown that alignment accuracies of 1–5 μm are typical after bonding layers [1].

To prepare for lamination, the layers are cleaned and processed to promote adhesion. Cleaning can involve soaking the layers in alcohol, ultrasonic cleaning, or an argon plasma etch [1]. After cleaning, adhesive sheets are "back tacked". Back tacking is a process of depositing the adhesive sheets onto structural layers. This is done to improve the transfer of the adhesive sheets from their protective paper backing. In back tacking, the adhesive layer is pressed to a structural layer under 50 psi of pressure at 130 °C for 1 minute [11].

After back tacking all the layers are stacked on top of each other for the full bonding procedure. The stack is placed under heat and pressure to bond and form a continuous laminate. The standard manufacturing procedure for all of the PCMEMS devices listed in section 2.3.2 held the lamination for two hours at 200 °C under 50–60 psi of pressure. The most common adhesive used was DuPont FR1500 acrylic sheet adhesive. [1, 11–16, 25–28]. Devices in these papers were manufactured using a diode-pumped solid-state laser, with a focused beam diameter of 8 μm.

Discrete components such as sensors, actuators, and integrated circuits can be added to the laminate at any point during construction and add functionality to a device. The basic lamination procedure is shown in Figure 2.2.

After lamination, the device undergoes a second round of laser cutting. This usually frees up any joints and movement needed to assemble the device. Assembly can be guided, forcing important features to move into place by having a moving support frame, or devices can be assembled by hand. To keep the assembled structure permanent, some devices use slots and tabs to lock into place [16], some are soldered [25], and some use an internal spring force [12]. If a support frame is used to help assemble the device, once the final shape is secure, the frame is removed.

2.3.2 PCMEMS Devices

In the first paper on PCMEMS, a linked chain, 1:900 scale airplane, and flexible hexagonal prism were all manufactured using the technique [1]. This paper demonstrated fundamentally that devices with many layers and large three-dimensional features were easily achieved using the
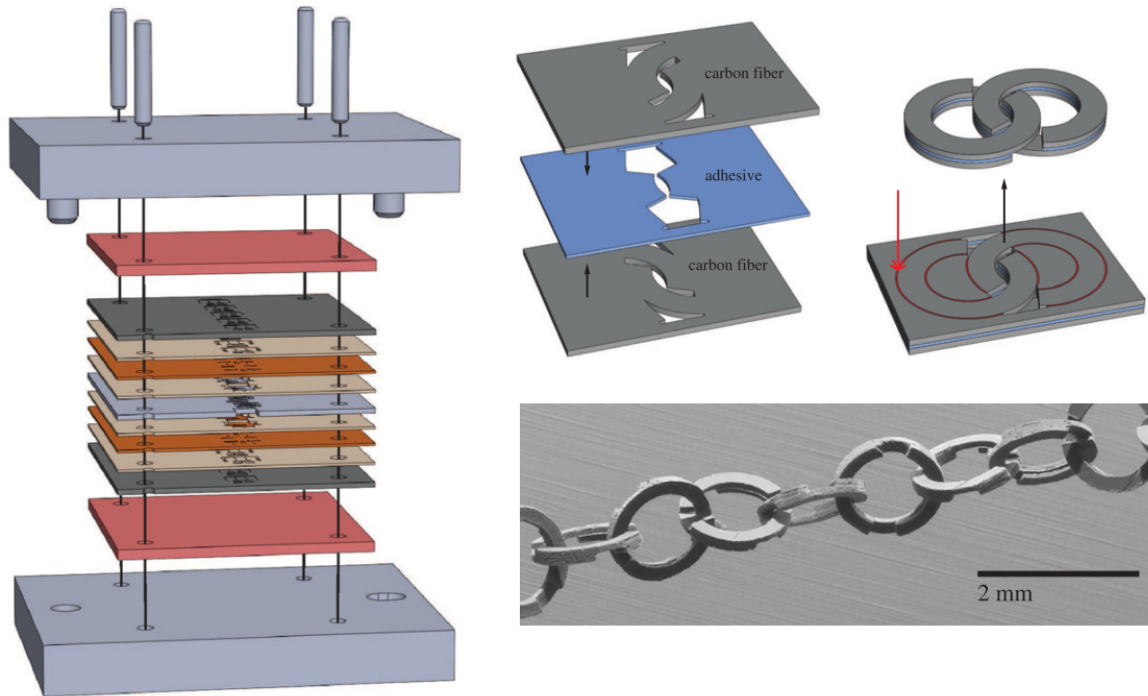
Figure 2.2: Alignment process for small chain [1].

PCMEMS method. Materials used in the devices included steel, polyimide, and carbon fiber—steel and carbon fiber provide structural strength, while polyimide acts as a flexible layer that can be used to form joints and hinges. The hexagonal prism used an internal spring, made of spring steel, to self-assemble. The spring was machined into the layer then laminated in a stretched position. After being released from support material, the spring pulled inwards, popping-up the device. This process is shown in Figure 2.3.

In 2012, a flying micro robotic insect (Mobee) was constructed using PCMEMS [25]. Mobee featured many high DOF joints and piezoelectric actuators. To achieve the necessary lift-to-weight ratio, Mobee used a variety of materials including carbon fiber reinforced plastic (CFRP), titanium, polyimide, and brass. The brass was used on the top layer of the device as a way to fix joints in place—after folding the device into its final shape, adjacent brass pads were soldered together to prevent any unwanted motion. Precision manufacturing and alignment allowed for component features as small as 10 μm, and a total weight of only 90 mg.

Mobee used a complex scaffolding system to support the device during construction, and to
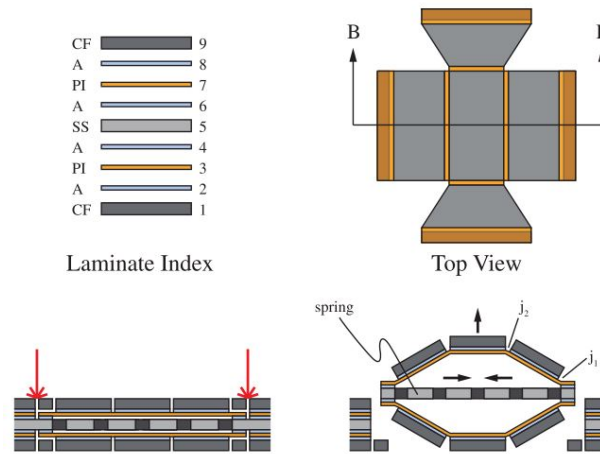
Figure 2.3: Self assembling PCMEMS hexagonal prism [1].

make folding the device easier and more precise—the folding is similar to "pop up" books, where a single actuation can create many out of plane features. The scaffold connected to any mechanisms that needed to fold out of plane, and was based on a Sarrus linkage to pull pieces vertically into position. Using the standard PCMEMS techniques, start-to-finish manufacturing time was less than 24 hours [25]. Additional work on the wing hinge designs revealed that a small increase in hinge length can drastically improve the lifespan of the wing hinges [27]. Rounding the corners of the structural materials surrounding the joints did not seem to improve lifespan though.

Mobee can also be used to compare PCMEMS to other layered manufacturing procedures. A comparable design for a small flying insect that used a simple layered manufacturing technique—not PCMEMS—is the Micromechanical Flying Insect (MFI) [29]. The MFI had a total of 26 joints, including some assemblies allowing 2, 4, and 5 DOF to articulate the wings. Two piezoceramic actuators in each wing generated lift. Composite materials were used for most of the structural elements, and non-solid designs (honeycombs) on some beams provided a higher stiffness to weight ratio than traditional beams. The first difference between the MFI and Mobee is that the MFI was hand assembled, it did not "pop up" into shape. Secondly, layer alignment with dowel pins was not used for the MFI—pieces were aligned and assembled manually under a microscope, adding significantly to the manufacturing time.
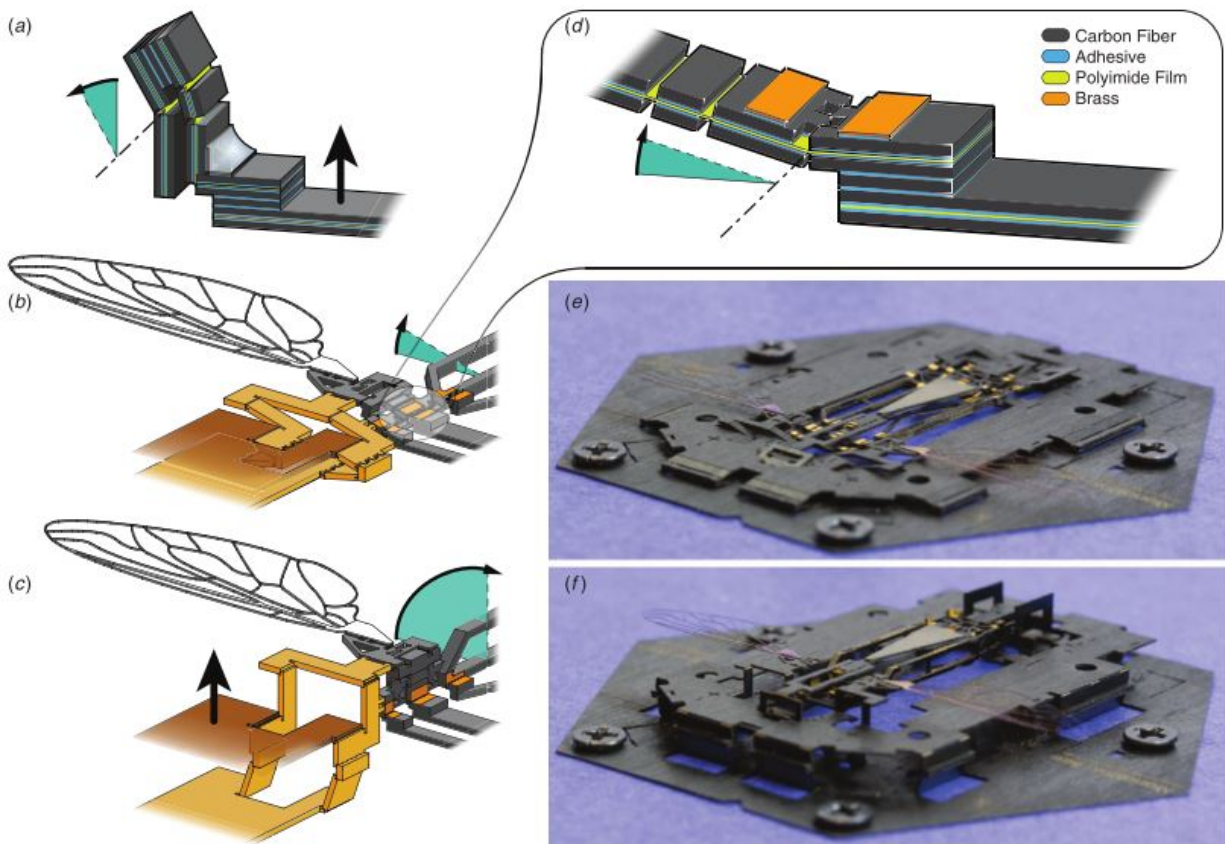
Figure 2.4: Folding assembly of Mobee PCMEMS device. (*a*) A four bar linkage turns linear actuation into rotation, also showing solder locking a joint in place. (*b*) The wing during and after (*c*) assembly. (*d*) A castellated joint, showing multiple layers of the device. (*e*) Mobee before and after (*f*) assembly with the scaffold frame [25].

The MFI weighed 28 g, which is very heavy when compared to the 90 mg of Mobee. These differences illustrate that comparatively, PCMEMS allows for smaller and more precise components with faster manufacturing than more basic layered manufacturing procedures.

Several PCMEMS medical devices have been developed, including other MIS graspers. The first, by Gafford *et al.* (Figure 2.5) was constructed from 11 separate layers of material with an 18 mm by 7.5 mm overall footprint [15]. The materials used were 50 μm thick 304 stainless steel for structural layers, 25 μm thick polyimide as a flexible layer, and DuPont FR1500 acrylic adhesive to join the layers together. The grasper used three castellated hinges for articulation: one hinge on each side of the body to support and guide the movement of the jaws, and one hinge in the middle of the jaws that was attached to a cable for actuation. Strength tests were performed on the hinges

and it was determined that this hinge design could tolerate shear stresses of 26.8 ± 0.53 N/mm^2, and torques of 22.8 ± 2.15 Nmm per mm of hinge width before failure. Failure was predictable, and it was found that the torsional strength of the hinges could be greatly improved by rounding the corners of the steel in the castellated hinges to prevent tearing the polyimide.
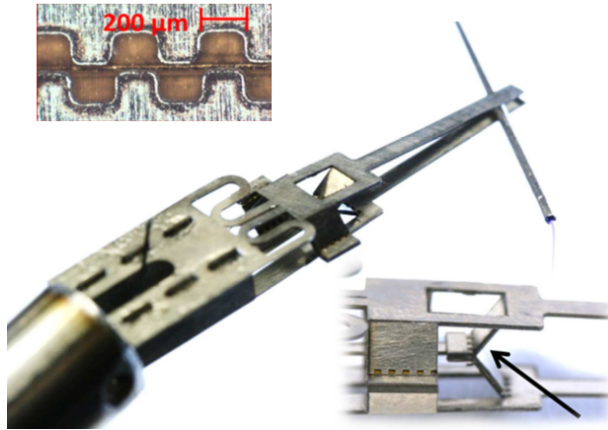
Figure 2.5: PCMEMS minimally ivasive surgical grasper. Inset showing castellated hinges [15].

The grasper uses a serpentine spring as a passive restoring force, such that the jaws rest open when no actuation load is applied. The jaws were were 1 mm wide and 10 mm in length, able to lift objects up to 200 mg. Heavier weights could not be lifted due to a combination of a lack of friction on the surface of the jaws, and compliance in the jaws themselves. It was noted by the authors that adding out of plane features to the jaws could greatly improve stiffness.

Gafford created a second version of the grasper, adding the aforementioned stiffness improvement, and adding an integrated strain gauge force sensor. The sensor was designed to measure grasping forces up to 1.5 N in a single axis [16]. Unfortunately, a 1:1 scale prototype of this design was not created, only a 2:1 model. The grasper was constructed from 15 individual layers of material including stainless steel, polyimide, FR1500 acrylic adhesives, and constantan alloy (used for the strain gauge material). The constantan alloy was added as the top layer of the laminate, with the strain gauge pattern not appearing until after the device was laminated. A diode-pumped solid state (DPSS) laser was used to ablate material from the constantan layer, forming the winding shape of the strain gauges. A sensitivity of 408 mV/N was observed with the force sensor, and a maximum load of about 1.5 N was applied. The device is shown Figure 2.6.
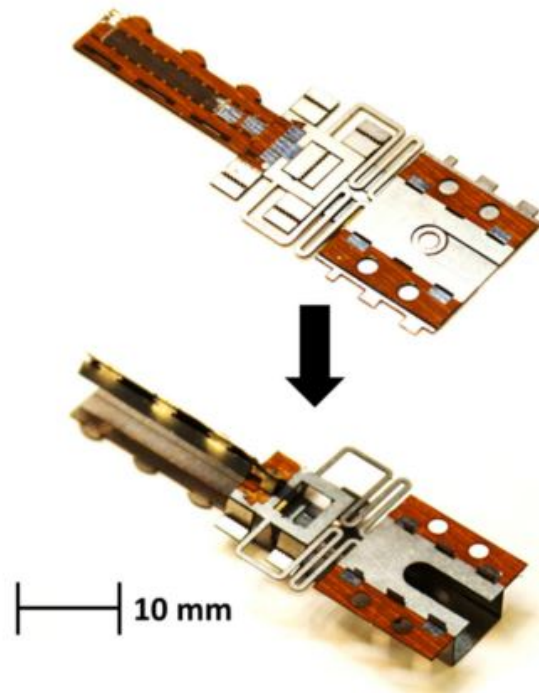
Figure 2.6: Force sensing PCMEMS minimally invasive surgical grasper [16] © 2013 IEEE.

The jaw design was altered to include two out of plane folds, creating a triangular shape with improved stiffness. The authors' analysis show that jaw stiffness is increased by 200 times over the original planar design. One more castellated hinge was added to each side of the jaws, to allow the jaws to remain parallel to each other when opening and closing. The additional hinges also increased the jaw strength. Although the grasper was designed to handle tip loads of only 1 N, the additional hinges allowed for maximum tip loads of approximately 4 N. Importantly, it is noted by the authors that the low cost of materials and labour make the device suitable for single-use, eliminating the need for sterilization.

The most recent iteration of a PCMEMS grasper was manufactured to be suitable for micro-surgery [11]. Although exact dimensions are not given, it appears that the grasper is approximately 5 mm wide. The triangular jaw structure of [16] was not used for this model—the grasper was designed for relatively small forces, and therefore the increased stiffness may not have been neces-sary. Similar to [16], a strain gauge with an on-board half-bridge was used to sense grasping forces. The strain gauge was formed by laser ablation of constantan alloy, and the half-bridge circuit was

added as layer during the construction of the device. Two simulated tasks—needle driving and tissue retraction—were used as initial tests of the grasper, measuring forces up to 300 mN, with a resolution of 5 mN. The grasper was then attached to a robotic micro-manipulation platform and 1 mm diameter steel balls were stacked into a pyramid using the grasper.

A microsurgical PCMEMS articulated arm was proposed, which used expanding bladders to control movement [10]. The device was unique in that it was constructed primarily from soft material, using various combinations of polydimethylsiloxane (PDMS) and Dragonskin 0020 to create structural layers of varying stiffnesses that were soft and flexible. Microfluidic lines controlled fluid flow into bladders. Depending on the desired function, bladders were attached to the other layer of the device, and sandwiched between layers. A capacitive sensor was formed by adding a layer of Pyralux (copper clad polyimide) patterned with capacitive electrodes to the each side of the bladder. The sensor could then determine inflation position of the bladder. Three proposed joint types using the expanding bladders are shown in Figure 2.7.
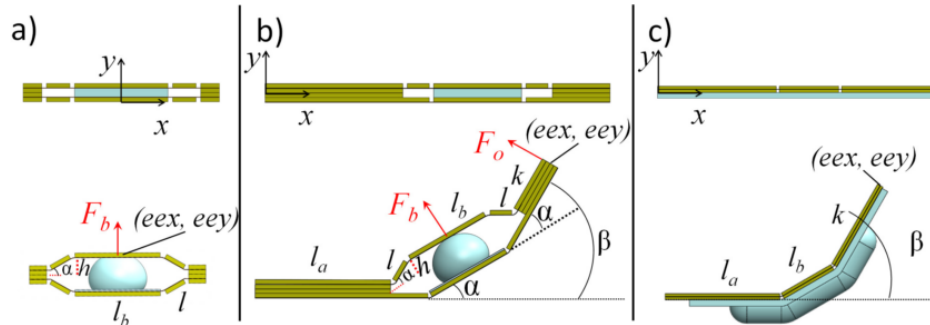
Figure 2.7: PCMEMS joints using expandable bladders. a) A linear actuator based on a Sarrus linkage. b) Bending mechanism with one side of the Sarrus linkage fixed. c) Bending mechanism with bladder mounted externally [10] © 2016 IEEE.

A flexible wrist designed to enhance endoscopic mobility was created with PCMEMS [13]. The wrist is designed for single-use, and is made to fit on to the distal end of existing endoscopic instrument shafts. 15 layers of material were used in the construction of the device including 75 μm 304 stainless steel for structural layers, 25 μm polyimide for joints, 18 μm copper clad 25 μm polyimide (Pyralux) for flexible printed circuits, and FR0100 acrylic sheet adhesive. The device uses a pin system for aligning layers, and is mounted on a separate jig to actuate the assembly

scaffold. The jig uses push pins to actuate the pop-up mechanisms in the design, with Sarrus linkages in the assembly frame to guide the structure, Figure 2.8.
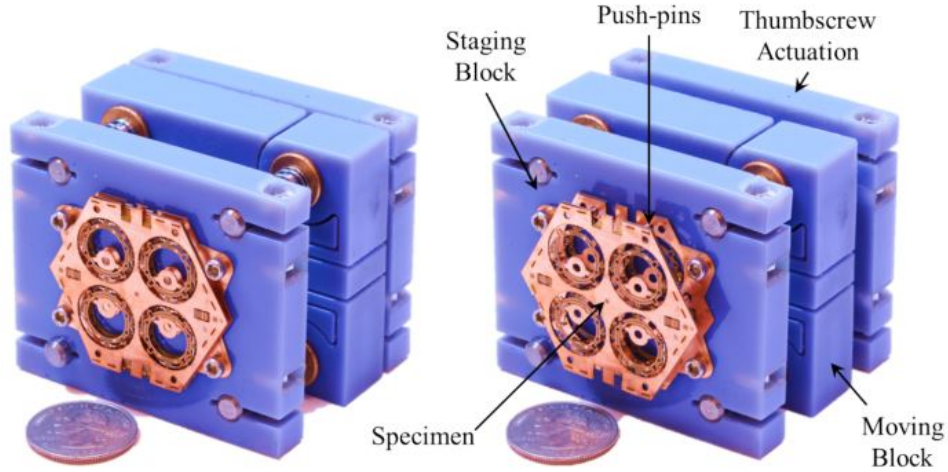
Figure 2.8: Thumbscrew actuated jig for assembly scaffold of PCMEMS endoscopic wrist [13] © 2016 IEEE.

Two standalone PCMEMS force sensors were created by Gafford *et al.*. One of the sensors measures forces in a single axis using light intensity modulation (LIM) [12], and one measures forces in three axes using strain gauges in a cross configuration [14]. Both sensors use 50 μm 304 stainless steel for structural layers, 25 μm polyimide for joints, copper clad 25 μm polyimide for flexible printed circuits, and FR1500 acrylic sheet adhesive, shown in Figure 2.9.

The sensor using LIM had a range of 200 mN and a resolution of 0.8 mN. With a footprint of only 2.7 mm, the sensor was designed to fit through the working port of an 8.6 mm endoscope for MIS. The structure of this sensor is very similar to that seen in the hexagonal prism created in [1]. An emitter is mounted to one side of a hexagonal prism structure, across from it is the detector. The sensor features an internal spring that is pre-tensioned before lamination. The internal spring allows the sensor to self-assemble—when release cuts are made, the stored tension in the spring pulls the sides of the sensor together, raising it into its working position. This spring also provides the elastic element that couples the emitter to the detector. After assembly, the sensor was encapsulated in a UV cured epoxy.

The three-axis force sensor is described by the authors as designed for use in minimally invasive

surgery, although a direct application is not stated. The sensor measures 1x1x2 cm, including the signal conditioning circuitry. A strain gauge is located on both sides of each arm, for a total of 8 gauges. Similar to [11, 16] the strain gauges were formed by ablating constantan alloy. The strain gauge beam width was 30 μm. The gauges were then connected to the remaining circuitry by adding a layer of etched copper clad polyimide.

The sensor was made more rigid by folding and locking the outer flaps to form a box. These folds used a combination of castellated and plastic hinges (a fold with serrations where the material deforms plastically). The plastic hinges add some stiffness to the fold, making it more robust—this is useful for joints that will be locked in place. To lock the box together, the same method as [25] was used, with brass tabs soldered together. When tested, the device showed a range of -500 to 500 mN in the x and y directions, and -2.5 to 2.5 N in the z direction, with an RMS noise of 1.6 mN.
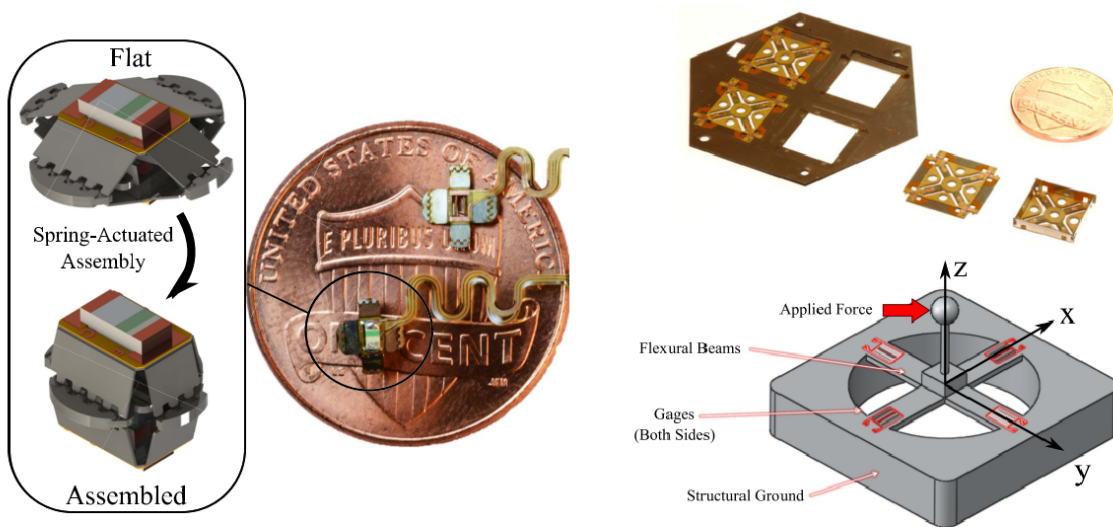
Figure 2.9: PCMEMS force sensors. (left) Self-assembling force sensor using light intensity modulation © 2016 IEEE. (right) Three-axis force sensor using strain gauges © 2014 IEEE.

Other devices using PCMEMS include a voice coil actuator that added pick-and-place components both before and after lamination [28]. The device incorporated rigid and flexible circuitry, with the circuitry added as a layer in the manufacturing process. A unique aspect of this design is that the device featured circuits in multiple layers that were connected after the lamination

process. The areas in the circuits that needed to be connected were tinned with solder, and reflow soldering was used to form connections that flowed over intermediate layers in the device.

2.4   Force Sensing Medical Instruments

Many minimally invasive surgical instruments have been designed to incorporate force sensing. Puangmali *et al.* performed a review of existing technologies for force and tactile sensing in MIS in 2008 [2], and Tiwana *et al.* provided a similar review in 2012 [30]. Sensor placement has been discussed in Section 2.2.2, and though it has been decided to place the sensors at the tip of instrument, it is useful to look a range of sensing technologies—including technologies that may not be used at the tip of the instrument. The designed PCMEMS grasper should ideally function at a level at least comparable to existing technologies. However, any technologies that cannot be incorporated into the tool tip of the instrument were explored in less detail.

Puangmali *et al.* included examples of sensorized instruments that measured force using displacement, resistance, capacitance, current, pressure, vibration, and optical sensors. These sensor technologies were compared to determine which would be best suited for a high accuracy PCMEMS device. Because the grasper is designed with the intention of being single-use, cost effective technologies were also given preference.

Some methods measure forces indirectly, such as a design by Tholey *et al.* that measured the current applied to drive motors to determine applied torques or forces [31]. This method was not very accurate though, because it failed to take into account secondary forces such as friction at joints or linkages, and the inertia of all involved mechanism. A position based design by Rosen *et al.* used a servo and encoder to measure position error, translated into a force feedback [32]. The system was teleoperative, removing common error sources such as internal friction and backlash. However, due to the relative complexity of systems such as these that use indirect sensing, these methods are not well suited to a single-use MIS grasper designed using PCMEMS, and are not considered further.

Optical sensors are a popular area of research for force sensing MIS instruments. Optical sensors usually have a good sensing range, high resolution, and are immune from electromagnetic

interference [30]. Fiber Bragg grating systems, a type of fiber optic sensor, are common but often feature very high cost signal conditioning and interrogation units to measure the signals. Attempts have been made to lower the cost, such as the fiber Bragg grating systems designed by Yurkewich *et al.* [33] and Tosi *et al.* [34]. Still, the optical fibers would need to be added as pick and place components in a PCMEMS device, and need to run the length of the instrument. This makes for a relatively more complex assembly process, and increases the cost of the needed components. Using simple LED and photo-transistor pairs to measure LIM is better suited for PCMEMS. This was seen in the endoscopic wrist module and self assembling force sensor developed by Gafford *et al.* [12, 13]. In order to measure forces in 3 DOF the system needs a minimum of three emitters, three collectors, an elastic element, and constraint hinges. Fitting all of this through a 5 mm trocar may be difficult.

The most common technology for force sensing in a MIS device is using strain gauges to measure force through changes in resistance. Strain gauges require flexure of the object under measurement, and there exists a trade-off between stiffness and sensor sensitivity—nonetheless, strain gauges are generally considered accurate and low-cost. Many MIS instruments have been designed using strain gauges. A relevant example is an instrument that placed strain gauges on the shaft close to the end effector [6]. The strain gauges were placed in opposing pairs designed to reduce noise. Accurate results were achieved, but only in two directions—forces along the shaft were not able to be measured using this method.

Fischer *et al.* developed a 3 DOF force sensing grasper with strain gauges mounted to the jaws [35]. The design used strain gauges in a full and half Wheatstone bridge, as well as a Poisson bridge for a total of eight strain gauges. Parts of the instrument could be sterilized with an autoclave, but others required ethylene oxide (EtO) sterilization. Trejos *et al.* worked on creating an easily sterilizable force sensing grasper, comparing coatings and adhesives to determine which would allow strain gauges to survive multiple autoclave cycles [36]. Their final prototype was able to survive multiple autoclave cycles, with a 0.10–0.21 N accuracy, 0.05–0.20 N repeatability, and hysteresis of 0.06–0.21 N, depending on the measurement direction. Strain gauges were mounted on the instrument shaft near the grasper jaws, shown in Figure 2.10.

The use of strain gauges in PCMEMS graspers has also been explored, as was described in
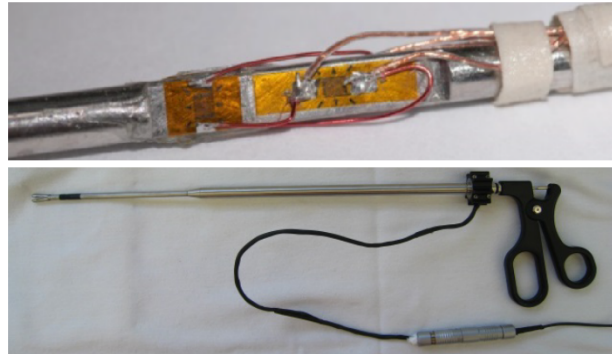
Figure 2.10: Sterilizable force sensing instrument. (top) Strain gauges installed on instrument inner shaft. (bottom) Sterilizable instrument with strain gauges mounted on shaft near end effector © 2014 IEEE.

Section 2.3.2. The PCMEMS surgical graspers that used strain gauges only measured forces in one axis, with a relatively small sensing range [16]. Better results were achieved in the stand-alone 3 DOF PCMEMS force sensor (also using strain gauges) [14]. One of the previous drawbacks of working with strain gauges was the time and precision required to install the often very fragile strain gauges on to the instruments. PCMEMS alleviated this problem by adding a solid layer of strain gauge material to the devices and using a laser to form the strain gauge pattern by ablating material. It should be noted though that this method requires access to a precise laser, which may not be possible with the available resources for this project.

Piezoelectric materials are often manufactured in very thin sheets or films, which may allow them to be integrated easily in a PCMEMS design. Polyvinylidene fluoride (PVDF) is a popular piezoelectric material that can output large voltages under relatively small deformations. Piezoelectrics *produce* voltage, requiring no external electrical power to be supplied to the sensing elements. Dargahi *et al.* used a PVDF film on the grasper jaws of a MIS instrument. The sensor had a measurement range of 2 N, and excellent sensitivity was reported [37]. A PVDF sensor element was designed by Sokhanvar *et al.* that could be usefully adapted to work with many MIS tools [38], shown in Figure 2.11. The sensor consisted of a beam structure with two PVDF films sandwiched under the end supports, and one under the flexible beam. The design allows the sensors to function directly as a grasping surface. By measuring both the direct force applied, and the deformation of the beam, the sensor can detect the softness or hardness of the material being

grasped. The sensor can be adapted for different force ranges by changing the Young's Modulus or dimensions of the flexible substrate.
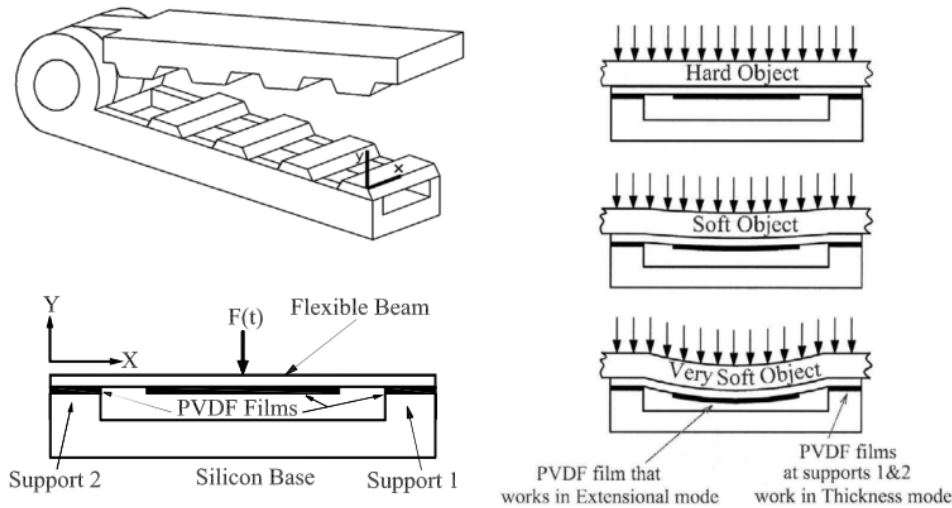
Figure 2.11: PVDF sensor design. Flexible beam design with three sensor films can measure object hardness.

Teo *et al.* used a commercially available 'flexiforce' sensor from Tekscan (a piezoresistive force sensor) [39] to measure grasping force. The smallest commercially available flexiforce sensor, the A101-1 (https://www.tekscan.com/products-solutions/force-sensors/a101) , is 7.6 mm wide. The sensor would need to be modified to fit within a 5 mm instrument.

In both Puangmali [2] and Tiwana's [30] review articles, the stated disadvantage of piezoelectric materials is that they are not as suitable for measuring static forces. This is because piezoelectric materials only measure changes in applied force, and are therefore subject to charge leakages under static forces. Many piezoelectric films are also sensitive to changes in temperature, or can become damaged at high temperatures. This is not ideal for a device that may need to be laminated at 200°C.

Capacitive sensing is the final technique to be included for consideration. Puangmali notes capacitive sensing offers an advantage over strain gauges of excellent sensitivity without temperature dependence [2], and Tiwana notes the additional advantages of a large dynamic range, and good spatial resolution [30]. In the literature it is seen that small capacitive sensors, and MIS graspers

using capacitive sensing for force measurement have been designed.

Chang and Allen used MEMS processes to fabricate capacitive pressure sensors with read out circuitry integrated directly into the sensor structure, by using lithography defined electrical traces [40]. Although the finished structure was too large for use in a MIS instrument (5.7 x 5.7 cm), it demonstrated the concept of integrated sensors and circuitry. Gray and Fearing fabricated a MEMS 8x8 array of capacitive sensor cells for tactile sensing that was less than 1 mm^2 [41]. The sensor array could measure millinewton forces and could be used in grasping applications.

A capacitive shear force sensor developed by Chen *et al.* was manufactured based on PCB techniques [42]. The prototype sensor consisted of a flexible dielectric layer (silicone rubber) sandwiched between two PCBs. Electrodes were directly patterned in the PCBs, forming a capacitive pair across the silicone. The back side of the PCB was clad in copper to serve as a ground plane and reduce electromagnetic interference. The silicone layer was added by injection molding, with dielectric ceramic powder added to increase sensitivity (0.14 volume fraction). The sensor operated on the principle of measuring differences in capacitance based on the shift and change in distance between two bottom electrodes and a common top electrode, this is shown in Figure 2.12. The sensor was tested to a maximum load of 10 N, with a resolution of 1 mN.
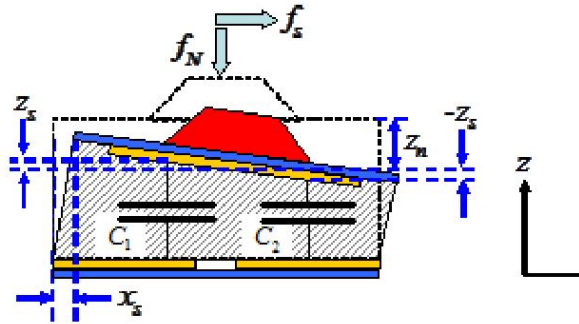
Figure 2.12: Capacitive shear sensor design principle. Shear force causes a translation and rotation of upper electrode. [42] © 2013 IEEE.

Capacitive sensors can integrate multiple axes of sensing in one unit. Multiple six-axis force-torque capacitive sensors have recently been presented in literature. Brookhuis *et al.* developed a MEMS fabricated six-axis sensor with a 9 x 9 mm footprint, capable of measuring 50 N of normal force, 10 N of shear force, and moments of 25 Nmm in each direction [43]. The sensor uses a

combination of triangular electrodes to measure the normal force and moments in the x and y directions, and a series of small overlapping "comb" electrodes to measure shear forces and moments in the z direction. Micromachined silicone pillars form the spring element of the sensor.

Kim *et al.* manufactured a sensor based on a flexible cross with grooves holding capacitive electrodes [44]. When a force deforms the cross, the distance between electrodes changes, providing force data. The sensor measured forces up to 10 N, but had a relatively low resolution of 0.5 N. Maximum measured torque was 0.16 Nm, with a resolution of 0.02 Nm.

Lee *et al.* created a sensor using a grounded top electrode disk, and three opposite electrodes located in a circle $120°$ apart [45]. The sensor has an elastic structure supporting the grounded disk, and an air gap between sensors, shown in Figure 2.13. The sensor electrodes are integrated into a PCB with the capacitance to digital converter (CDC), similar to the sensor described by Chen *et al.* [42]. Although the sensor is too large for a PCMEMS application, it demonstrated again the use of PCB techniques by combining sensing electrodes into a PCB with read out circuitry and a CDC.
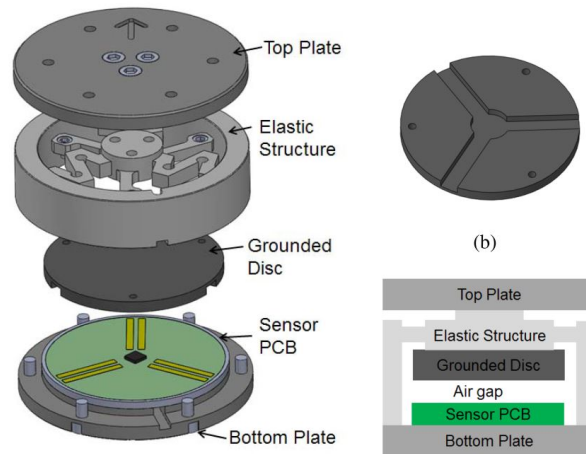
Figure 2.13: Six-axis capacitive sensor by Lee *et al.* [45] © 2016 IEEE.

Two papers by Kim *et al.* document the development of a small grasper with four-axis capacitive force sensing [46,47]. Both jaws on the grasper have a grounded electrode in a triangular prism shape separated from a pair of angled electrodes by a layer of polydimethylsiloxane (PDMS). The PDMS is a flexible dielectric and is deformed when forces are applied to the jaws. The method of

force sensing is shown in Figure 2.14. Electrodes in the top jaw are rotated $90°$ from those in the bottom jaw, allowing the two jaws to resolve shear forces in separate axes.
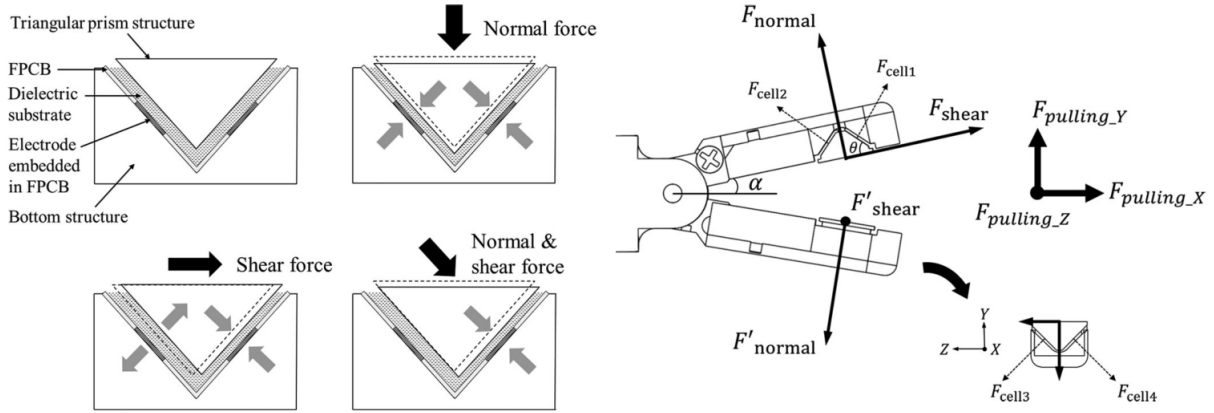
Figure 2.14: Principles of operation of capacitive force sensing grasper. (left) Triangular prism structures under normal and shear forces. (right) Force measurements using both jaws [47] © 2015 IEEE.

The electrodes are patterned on a FPCB that also holds the CDC. Minimizing the distance between the CDC and electrodes, and housing the CDC within the grasper jaws minimizes noise and stray capacitance. The case and base structure of the grasper jaws are also grounded to block out stray capacitance. A plastic insulator layer between the FPCB and base prevents shorting the circuit. Construction of the device is shown in Figure 2.15.

2.4.1 Force Sensing Summary

Although there are other force sensing technologies that may be used for MIS instruments, it is believed that optical sensors, piezoelectric films, strain gauges, and capacitive sensing are best suited for PCMEMS manufacturing. A summary of the force sensing technologies and their suitability for PCMEMS is shown in Table 2.2.

Comparing each sensing technology, it is likely that all will be able to meet the required sensing range. The remaining considerations are: accuracy, resolution, dynamic response, repeatability, size, circuit simplicity, PCMEMS manufacturability, and temperature sensitivity. However, the initial focus must be on ensuring the chosen sensor system is suitable for PCMEMS manufacturing, and will be able to fit within such a small device.

Fiber optics have not been previously used with PCMEMS, and aren't well suited for planar manufacturing. LIM sensors, if used similarly to those in existing PCMEMS devices [12] may require multiple emitters and detectors when measuring three axes of force, resulting in a bulky and complex system. Similarly, including three-axis force sensing with strain gauges and signal conditioning may prove too difficult to fit within such a small device—the previously demonstrated PCMEMS three-axis strain gauge force sensor was over two-times too long and wide for an MIS grasper application [14]. With piezoelectric films, no commercial solution exists that is small enough for this project, and the temperatures required by the lamination process may result in damage.

Capacitive sensors have been previously manufactured integrated into PCBs, including the read out circuitry and a CDC chip—a method that should translate well to PCMEMS designs. Capacitive sensors on FPCBs have successfully been integrated into a surgical grasper, showing that at the scale needed, reliable sensing was still achieved. An advantage over strain gauges was seen when incorporating multiple axes of force sensing—capacitive sensors were demonstrated to be compact, and one unit could be simplified by having a common ground electrode used for measuring multiple forces [42, 45–47]. Based on these advantages, capacitive sensors were chosen as the sensing method for this device.
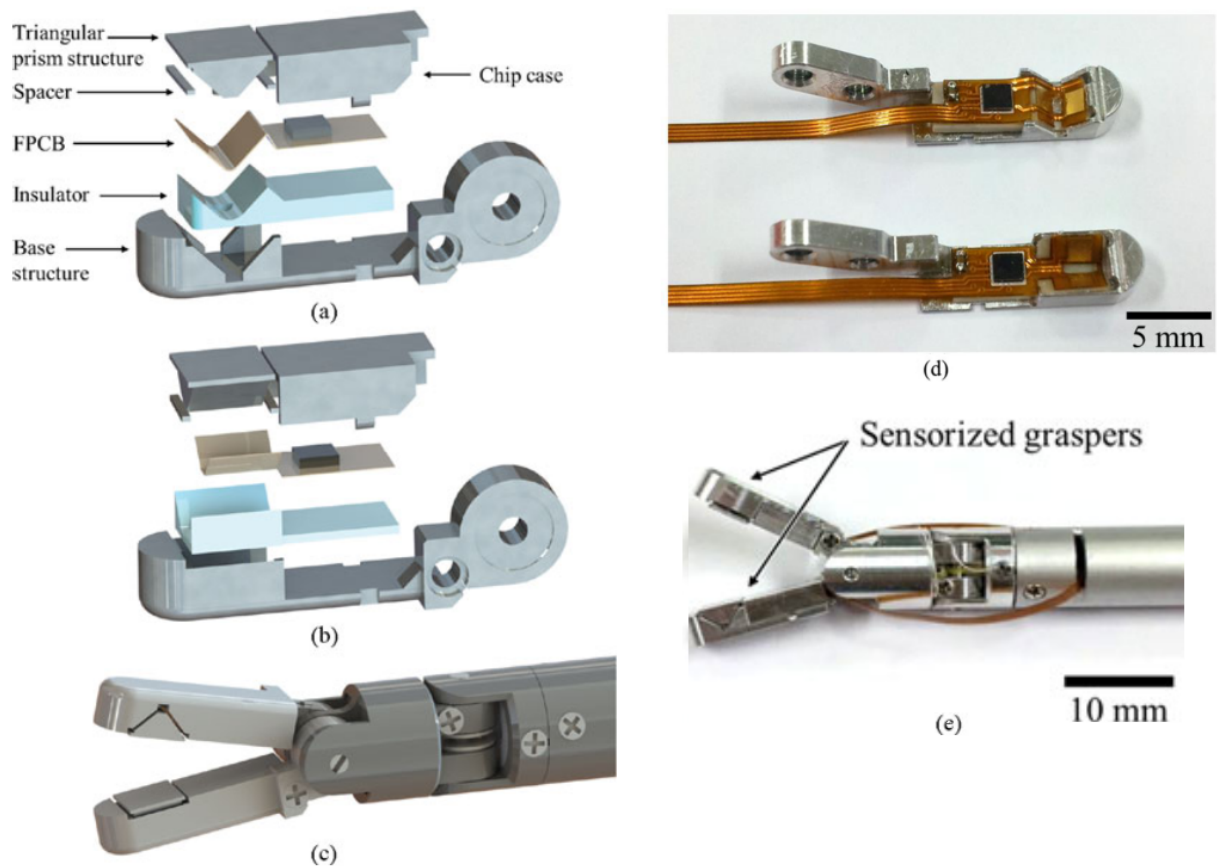
Figure 2.15: Construction of capacitive force sensing grasper. (a) Top grasper jaw. (b) Bottom grasper jaw. (c) CAD model of finished design. (d) View of FPCBs with CDC and electrodes. (e) Completed grasper prototype [47] © 2015 IEEE.

Technology	Advantages	Limitations	PCMEMS Considerations	Relevant Examples
Optical sensors (LED and Photo-diode)	LED and photo transistor pairings are simple and relatively small. Sensor information is digital and can be transmit relatively far.	Can be sensitive to other light sources. Multiple DOF can quickly increase complexity of system.	Has been used successfully in PCMEMS designs as pick and place components.	[33, 34]
Optical sensors (FBG)	High sensitivity with no hysteresis. One FBG fiber can sense multiple DOFs.	Can be sensitive to other light sources. Difficult to achieve small bending radii. Systems can be expensive.	Difficult to incorporate long fibers in a PCMEMS construction process for a disposable end effector.	[12, 13]
Piezoelectric	No additional power supply needed, generate their own voltage. Large force range, quick response time.	Very dependent on temperature. Subject to charge leakage under static forces.	Often available as thin films that could be added in PCMEMS process. Lamination procedure at 200°C may destroy some piezoelectric sensors.	[37–39]
Strain gauges	Small size, and relatively high sensitivity. Established technology used in many graspers.	Sensitive to temperature changes and electromagnetic noise. Trade-off between measurement sensitivity and structure stiffness.	Easily incorporated into PCMEMS designs. Can be manufactured quickly if laser is used to form strain gauges by ablation.	[6, 14, 16, 35, 36]
Capacitive sensing	High sensitivity, large dynamic range. Limited hysteresis and low temperature dependency.	Sensors are subject to stray capacitance. Require a CDC conversion chip near sensors.	Many capacitive sensors are manufactured in planar PCB processes.	[40, 42, 44–47]

Table 2.2: Force sensing technologies

2.5   Capacitive Force Sensing Principles

Many of the capacitive sensors that were looked at operate on the principle of two electrodes coupled by an elastic force element. As a force or torque is applied, the elastic element is deformed, changing the distance between the two electrodes and affecting a change in capacitance. In some cases this was an elastic element sandwiched between the electrodes [42, 47], or an elastic element that supported one of the electrodes [45]. The principle is the same though, and capacitance between two parallel plates is calculated as

$$C = \varepsilon_0 \varepsilon_{\mathrm{r}} \frac{A}{t}, \tag{2.1}$$

where ε_0 is the relative permittivity of air, ε_{r} is the relative permittivity of the dielectric material used between the plates (which may be the elastic element), A is the area that overlaps between electrodes, and t is the distance between the plates. Applying a normal force compresses the elastic element, changing t, and therefore changing the capacitance value. The change in t can be simply calculated using Hooke's Law as

$$\Delta t = \frac{Ft}{EA}, \tag{2.2}$$

where Δt is the change in thickness, E is the modulus of elasticity for the elastic element, and F is the applied force. (1) and (2) can be combined to determine the relationship between capacitance and applied force, with the change in capacitance expressed as

$$\Delta C = \varepsilon_0 \varepsilon_{\mathrm{r}} \frac{A}{t \left(1 - \frac{F}{AE}\right)}. \tag{2.3}$$

This equation works for a simple elastic element under a normal force. If the element is under shear however, a different set of equations must be considered. If the shear force moves the electrodes out of alignment, the effective overlapping area is reduced, reducing capacitance. This effect can be used to sense shear forces as done by Lee *et al.* [45], or can be mitigated by oversizing one of the electrodes, as by Kim *et al.* [47]. This effect is shown in shown in Figure 2.16. If the two electrodes are the same size and the shear causes a pure translation, Equation 2.1 is still true, and
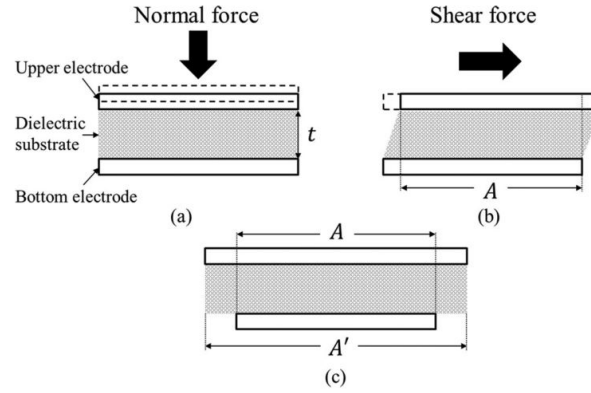
Figure 2.16: Capacitance changes under applied shear forces.(a) Capacitive sensor under normal force. (b) Capacitive sensor under shear, overlapping area A is decreased. (c) By increasing the size of the top electrode, overlapping area remains unchanged under shear forces [47].

the change in capacitance is simply related to the change in overlapping area, calculated as

$$
\begin{aligned}
\Delta C &= C_1 - C_2 \\
&= \varepsilon_0 \varepsilon_{\mathrm{r}} \frac{A}{t} - \varepsilon_0 \varepsilon_{\mathrm{r}} \frac{(A - \delta A)}{t} \\
&= \frac{\varepsilon_0 \varepsilon_{\mathrm{r}}}{t}(-\delta A) \\
&= \frac{\varepsilon_0 \varepsilon_{\mathrm{r}}}{t}(-L x_{\mathrm{s}}).
\end{aligned}
\tag{2.4}
$$

Where δA is the area that one electrode is displaced, which can be represented by the width of the electrode L multiplied by the linear displacement of the electrode x_{s}. Assuming the elastic element behaves linearly, Hooke's law for shear stress can be employed. First the shear modulus is calculated,

$$
G = \frac{E}{2(1+\nu)},
\tag{2.5}
$$

where G is the shear modulus, and ν is the Poisson's ratio of the material. Shear modulus is a material property that can be used to calculate shear strain,

$$
\begin{aligned}
G &= \frac{E}{2(1+\nu)} \\
\gamma &= \frac{\tau}{G} \\
\gamma &= \frac{2(1+\nu)}{E}\tau,
\end{aligned}
\tag{2.6}
$$

where γ is shear strain, expressed as the angle (in radians) caused by the shear stress, and τ is the applied shear force. γ is simply

$$
\gamma = \frac{x_\mathrm{s}}{t},
\tag{2.7}
$$

Combining shear and normal forces, it is important to note that a compression due to normal force will change the effective thickness of the elastic element under shear, thereby reducing the distance t used in Equation 2.7.

Of course, this deals only with linear deformations, and simple calculations. If more complex assessments of strain and deformation are required, using a finite element analysis would be the preferred method.

Chapter 3

Design and Realization of the First Prototype

3.1 Introduction

Based on the literature reviewed in Chapter 2, it was decided to focus on the use of PCMEMS manufacturing with capacitive force transducers to produce a sensorized minimally invasive surgical grasper. This chapter will examine the first prototype, including the development of the mechanical design from initial concept through its final shape, material selection, layer position, and layer patterning. The design of the sensing system is discussed in terms of function, theoretical measurements, and PCB design.

3.1.1 Manufacturing Notes

Before continuing with the discussion of the mechanical design, some specifics of the manufacturing process should be noted to clarify certain design specifications and design choices.

All the PCMEMS devices that were discussed in Chapter 2 were manufactured using a laser to cut and pattern the material layers. Unfortunately, a suitable laser was not available for use at Western University, therefore a micro milling machine (MMM) was used in its place. Although this was suitable for small-scale proof of concept and prototype creation, it should be noted that this method is not ideal for large scale production. A laser can cut patterns much faster, more

accurately, and rotating tools create edges that are less smooth than those produced by a laser. Therefore, aspects such as the bulk manufacturing and processing times are not representative of an optimal PCMEMS process.

The Atometric MMM used was capable of operating at sub-micron accuracy, with a maximum spindle speed of 90,000 rpm. The cutting tools purchased from Harvey Tool were 25, 50, 75, and 100 μm diameter flat endmills with a cutting length three times their diameter. In testing, the 25 μm endmills broke very frequently, and with a cutting depth of only 75 μm, would not be able to cut through a sublaminate (a laminated combination of multiple layers) of material. 50 and 75 μm endmills proved to be more durable, and were used for the majority of cuts. Therefore, the minimum interior corner radius for any feature was limited to 50 μm. Normally, the focused beam diameter in PCMEMS manufacturing is 5–10 μm, allowing for finer features to be machined [11]. The 50 μm tools were run at a spindle speed of 85,000 rpm, with a feed-rate of 90 mm/min for stainless steel, and 120 mm/min when cutting polyimide or adhesive.

Using the MMM, first each material layer was secured to a fixture block using cyanoacrylate adhesive. This was done to ensure that the layers remained as flat as possible, especially when small features were machined. If the layers were not properly secured, when small features were cut, internal tensions in the material would be released and it was possible for material to spring up into the cutting tool; this would damage the material and break the cutting tool. A face plate with a window for machining was then screwed on to further secure the material (Figure 3.1). Each layer was then individually patterned using the MMM to cut a 2D profile that created all of the necessary features in the layer.

The remainder of the manufacturing procedure was similar enough to that previously described in Section 2.3.1, that it does not warrant further discussion.

3.1.2 Design Specifications

The goal of this work was to create a versatile MIS grasping instrument that demonstrates the feasibility of a capacitive sensing system, that while similar to designs for existing MIS graspers, has yet to be used within a PCMEMS environment. Exploring the use of a micro-milling machine for PCMEMS manufacturing was also important. With these goals in mind, the specifications for
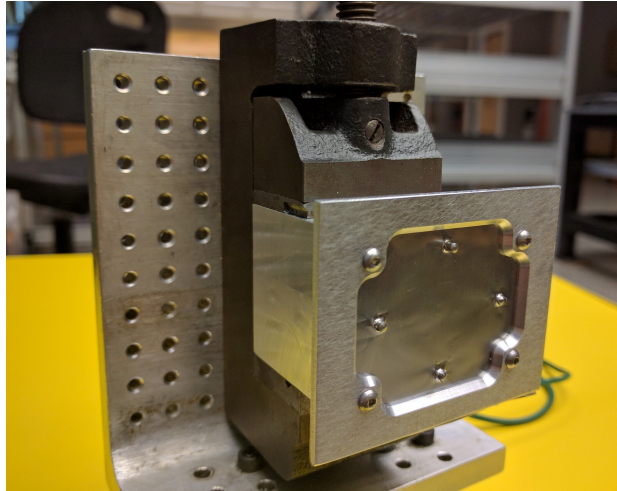
Figure 3.1: Fixture for micromilling machine. Faceplate is held on with four screws, and four alignment pins are used to position the layer for machining.

the instrument were as follows:

1. The grasper must fit through a standard 5 mm trocar. This represents a maximum outer shaft diameter of 5.6 mm.

2. The sensing system must measure forces in 3 axes: normal to the grasping surface, axial (in the direction of the instrument shaft), and transverse (perpendicular to the instrument shaft).

3. Force measurement sensitivity must be 0.1 N in all three axes to measure the changes in forces exerted on soft tissue.

4. Force measurement range must be at least from -4 to 4 N in all axes.

5. The grasper must be able to withstand forces of 4 N in all directions.

6. Due to its use in a surgical instrument, any materials and adhesives used must be fully biocompatible.

7. To ensure low cost of manufacture, the device must be designed in such a way that it can be bulk manufactured easily. This includes ensuring that the folding of the device is guided so that assembly can be automated.

8. The sensing system must be contained within the end effector of the grasper, in a way that it can be integrated directly into the manufacturing process.

9. The design must be compatible with both micro-milling and laser cutting manufacturing processes.

10. To manufacture the devices on the micro-milling machine, the smallest internal radius of any cut through a single layer of material is 50 μm, and through multiple material layers is 75 μm. This is due to the diameter and cutting length of available tools.

When deciding the usable force range to aim for with the grasper, it is important to remember that forces up to and greater than 20 N can be seen in some surgical procedures. However, given the design constraints for this problem, the limitations of planar manufacturing, and the force range of previous PCMEMS graspers, 20 N was not seen as a realistic goal. Some studies were examined that used a lower range of applied forces during various surgical tasks. Forces up to 2.5 N were seen in a suturing task [48], up to 1.8 N was measured to retract stomach tissue [49], and up to 3.5 N of force was applied in a tissue characterization test [50]. The chosen force range (± 4 N) is significantly more than existing PCMEMS graspers, allows for the grasper to be useful for the aforementioned tasks, and represents a step towards a universally useful disposable MIS device.

Although as much sensitivity as possible is desired, there must be design trade offs. Using tissues such as the liver as an example, damage has been shown to occur at 200 kPa [51]. With an approximate surface area of 24 mm^2 for the jaws, a 0.1 N increase only increases pressure by 4.17 kPa. This is 2% of the total damage threshold, and therefore should be suitable.

All materials used in the device must not cause adverse effects when exposed to human tissue or bodily fluid, and must not be affected by these as well.

The goal of fitting through a 5 mm trocar was chosen so that the grasper is suitable for a large variety of surgical procedures. This is a trocar size commonly used in arthroscopic surgical procedures.

3.2   Mechanical Design

There are a set number of shapes that are possible in a folding design, since any single fold can only move out of plane in one direction. Although it is possible to create very complex shapes using PCMEMS and origami folding techniques, increased complexity requires more complicated linkages for transforming between flat and folded states.

The design comprises three components: a body that will attach to the instrument shaft and two jaws, with one jaw containing the sensing system. To improve the strength of the device it was decided that the lower jaw and the body would be formed from one sublaminate. This requires the lower jaw to be fixed, therefore the upper jaw must actuate to open and close the grasper. Because the lower jaw is fixed, this is where the sensing system was placed. The mechanical design of the lower jaw is then based on fitting the sensing system and maximizing sensor sensitivity. However, there is more flexibility in the design of the upper jaw.

To create a strong design for the upper jaw it was decided to use a triangular shape, as this has been proven to be substantially stronger than a flat sheet of material with no out of plane features [16]. A set of possible triangular jaw designs for the grasper was developed, and finite element analysis was performed on these designs to determine which shape was the strongest. Modeling the combination of layers and layer interactions is complex, and does not guarantee accurate results, therefore the obtained FEA results were used strictly on a comparative basis between designs. Using SolidWorks simulation tools, three designs were compared with 5 N transverse shear and normal force loads, shown in Figure 3.2. The designs were modeled as 100 μm thick 304 stainless steel. Simulations were run using the SolidWorks Simulation package with a mesh size of 50 μm. The results of this comparison qualitatively suggest that Design b) is the strongest and most rigid jaw design.

Next, the goal was to design a complete structure that could be created from a combination of sublaminate structures. An iterative system was used—designs were modeled in SolidWorks, then 10:1 scale prototypes were produced rapidly using a 40 W laser cutter. The 10:1 prototypes were used to ensure that the folding kinematics behaved as modeled, and that the designed joints worked properly. The 10:1 scale prototypes were constructed using card stock paper for the rigid
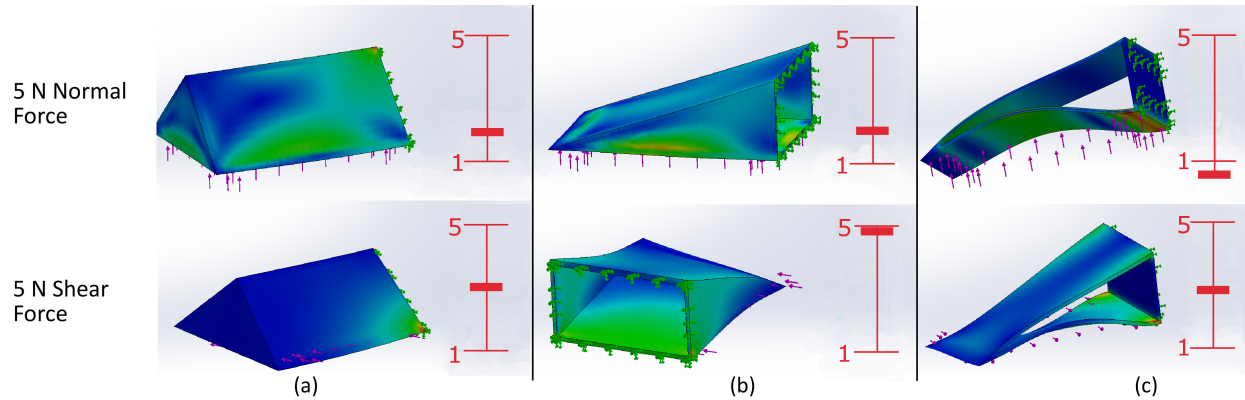
Figure 3.2: Comparison of upper jaw designs under 5 N loads. Bars inset in each image indicate the estimated factor of safety under 5 N loads.

layers and sheets of acetal for the flexible layers. These materials were used for the 10:1 scale prototypes because they were very easy to process and inexpensive. A 10:1 scale prototype is shown in Figure 3.3.
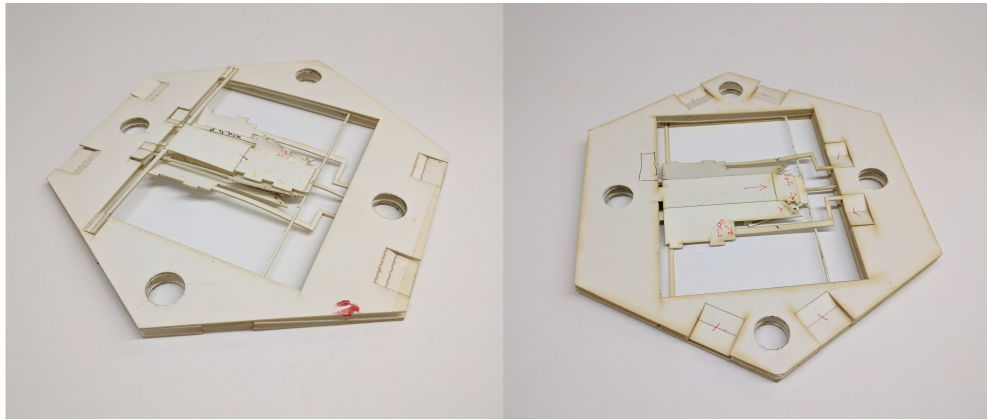
Figure 3.3: 10:1 prototype paper model in the unfolded position. Annotations can be seen written on the model to denote areas that require alteration.

The design of the layers included a support frame, shown in Figure 3.3. This is similar to other PCMEMS devices such as the endoscope wrist by Gafford (Figure 2.8). The frame serves to keep the layers and sublaminates aligned during construction. The support frames also include features designed to facilitate the folding of the device—Sarrus linakges on the edges of frames extend to push the sublaminates apart, while also pulling any sections that need to rotate into position.

The support frame design was successfully tested on the 10:1 scale prototype. However, when

the design was realized on the first 1:1 prototype, the time to machine each layer increased substantially; this also resulted in greater tool wear, and a larger number of broken tools. Therefore, it was decided that to decrease the production time, the 1:1 scale prototypes would not include the support frame and would be assembled manually. Due to the small number of prototype graspers being produced, this was not an issue. As a comparison, the total length of cuts in the layers (and therfore machining time) is increased 5 fold by including the support frame.

The finished first prototype design was created from a total of three sublaminates: sublaminate one (SL1) comprises the lower jaw, sensing system, and sides of the body; sublaminate two (SL2) contains the bottom and sides of the upper jaw, as well as a pull tab where the actuation cable is attached; sublaminate three (SL3) contains the top of the upper jaw, and the roof of the supporting body. When the device is folded, tabs in the top of the upper jaw (SL3) fit into slots in the sides of the upper jaw (SL2) to join SL2 and SL3 together. The roof of the body (SL3) has slots that fit tabs in the sides of the body (SL1) to lock the body of the grasper into place. The three sublaminates can be seen in Figure 3.4.

The front of the bottom jaw is angled, so that the two jaws will meet at a point. This was done to make grasping small objects easier, and to more closely mimic the form of existing MIS instruments. The top jaw is designed to be connected to a cable for actuation. The jaw rotates on a polyimide hinge about the roof of the supporting body. The hinge for the top jaw has a castellated design that has been shown to support torsional loads of 22.8 ± 2.15 Nmm per mm of hinge width [15]. The hinge width for this jaw is approximately 3 mm, and tip loads are at a maximum distance of 8 mm from the hinge. This allows for a conservative maximum allowable force of 7.74 N.

Figure 3.4: Completed sublaminate structures of first prototype. From left to right: sublaminates 1, 2 and 3.

The basic construction of the sublaminates is similar, with the exception of the added sensing system for the bottom jaw. Each sublaminate needs two structural layers for strength, a flexible layer to allow folding, and two adhesive layers to bond everything together. These five layers of materials are: 50 μm 304 stainless steel as the structural layers, 25 μm kapton (polyimide) as the flexible middle layer, and two layers of FR1500 sheet adhesive to bond the layers together. The folds on each sublaminate are realized by using castellated hinges to ensure both strength and folding accuracy. The layers of each sublaminate are shown in Figure 3.5.
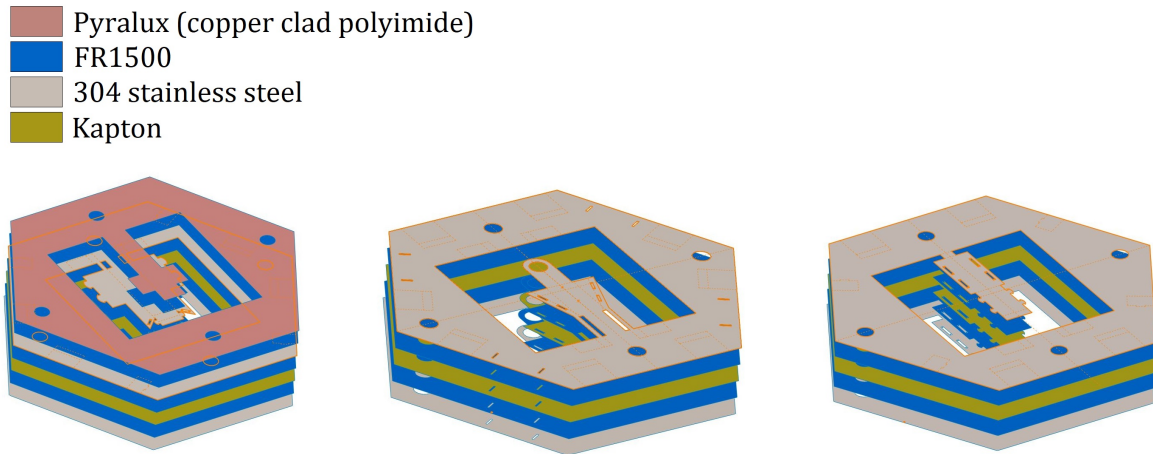
Figure 3.5: Layers of each sublaminate, from left to right: sublaminates 1, 2 and 3. Design is shown including support frame.

It was decided to use 304 stainless steel for the structural layers of the sublaminates. When compared to 316 stainless steel—a steel grade commonly used for medical applications—304 stainless steel is more readily available in thicknesses of 25–100 μm, and offers the same strength at a much less expensive price. Other materials such as titanium and carbon fiber reinforced polymers were also considered, however these were not chosen due to their higher cost and lower availability. Future work may focus on comparing designs made from different materials, but it is outside of the scope of this thesis. A summary of the chosen materials is shown in Table 3.1.

The overall size of the grasper depends largely on two factors: 1. the grasper must be small enough to fit into a shaft that can be inserted through a 5 mm trocar and 2. the grasper must be large enough to fit a capacitance to digital converter (CDC) chip. Further, the lower jaw must

Justification	Material	Layer
304 SS is biocompatible, high strength, available at thicknesses of 25 μm or 50 μm, and can be machined relatively easily.	304 stainless steel	Structural
Kapton has a high tensile strength and melting point, it is flexible, electrically insulating, and readily available in thicknesses of 25 μm.	Kapton (polyimide)	Flexible
The only material that has been used as a successful adhesive layer in PCMEMS devices. Very strong bonds and is available as thin as 12.5 μm.	FR1500	Adhesive

Table 3.1: Materials for body of grasper.

maximize the space available for sensors. Using a simple parallel plate capacitance model for the capacitive sensors, we see an increase in sensitivity by increasing electrode size. However, the height of the lower jaw can't be increased too far, or it will impact the structure of the upper jaw. Based on these constraints, the grasper is 4.3 mm wide and 4.0 mm tall. The finished grasper body can be seen next to the CAD model made in SolidWorks in Figure 3.6.
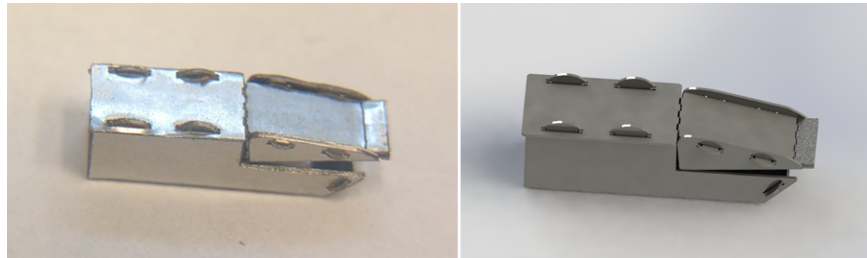
Figure 3.6: Completed grasper (left) with SolidWorks CAD model (right).

3.3   Sensing System Design

The grasper needs to be able to measure both normal (grasping) and shear forces applied at the tip of the instrument with enough sensitivity to detect changes in tissue characteristics and allow precise control during operations. A three-axis force sensing concept was created to work within the constraints of layered manufacturing and fit the needs of a minimally invasive surgical instrument.

The design uses four capacitive sensors; each sensor consists of a pair of electrodes separated

by a flexible dielectric layer. The sensors operate on the principles of parallel plate capacitors discussed in Section 2.5. When the grasper is unfolded (flat), there is one electrode positioned on each face of the lower jaw—the bottom, front, left and right. The electrodes become oriented in three separate planes once the device is folded into its final shape. The sensors on the left and right sides measure transverse shear forces, the sensor on the front measures axial shear forces, and the sensor on the bottom measures normal forces.

Due to the angle of the front of the bottom jaw, the axial shear sensor will also respond to changes in normal force. Therefore, the axial shear sensor will need to be decoupled from the normal force sensor. Similarly, it is possible that some amount of coupling will exist between all sensors. Decoupling the sensors will require the use of a calibration matrix. A model of the sensing system, unfolded, is shown in Figure 3.7. The sensor circuit can be manufactured as a flexible printed circuit board (FPCB) and added as a single layer to SL1 during construction.

To convert the sensor signals into a useable output, a CDC, the FDC1004 from Texas Instruments, sits within the body of the grasper. By minimizing the distance between the CDC and the sensors, noise and stray capacitance are minimized [46]. The only other components on the FPCB are two decoupling capacitors. This design also allows the instrument and sensing system to be manufactured together, and packaged as one unit.
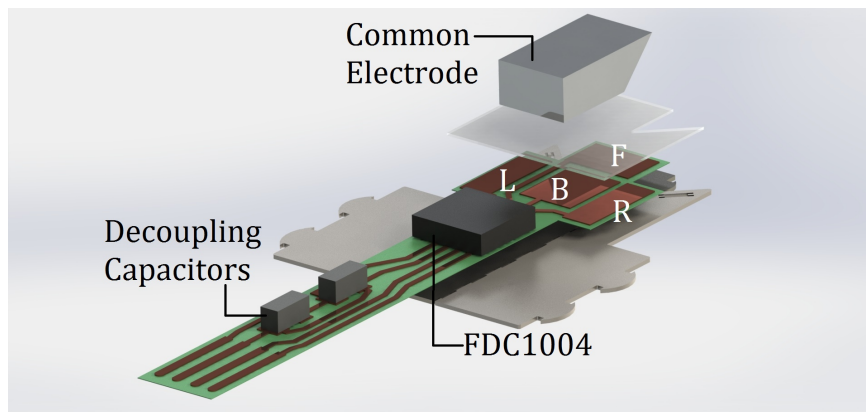
Figure 3.7: Expanded view of dielectric, FPCB, and structural layers. Sensing electrodes are labeled L and R (left and right: transverse shear), F (front: axial shear), and B (bottom: normal forces).

The FPCB was machined including pin alignment holes, and was laminated to the top layer of

stainless steel in SL1 using FR1500 sheet adhesive during the standard lamination process. After lamination, the FDC1004 and capacitors were soldered to the FPCB.

Once the FPCB was populated, a flexible dielectric sheet was adhered on top of the electrodes using cyanoacrylate adhesive. A sheet of silicone rubber with a thickness of 127 μm, and a shore hardness of 55A was used as the dielectric for the prototype. SL1 was then folded and locked into shape and a solid piece of aluminum was placed in the middle of the jaw on top of the dielectric, acting as the opposite electrode for all capacitive sensors, and as the grasping surface for the bottom jaw. The aluminum electrode was secured with cyanoacrylate adhesive by bonding it on all sides to the flexible dielectric. The sensing system in the bottom jaw (without the common electrode) can be seen in Figure 3.8
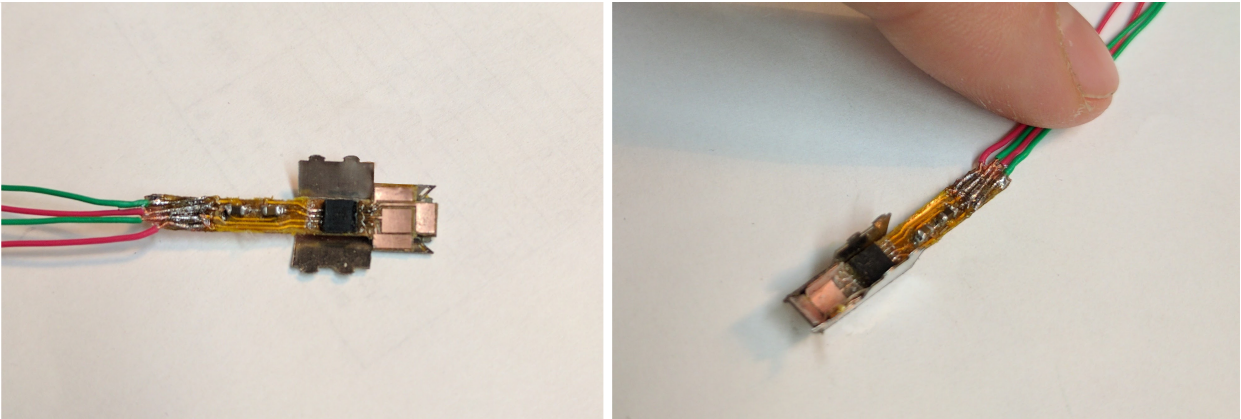
Figure 3.8: FPCB assembled with the grasper. (left) The FPCB added on top of the bottom jaw in the unfolded position. (right) The bottom jaw folded, with the FPCB installed. The flexible dielectric sheet covering the electrodes is in place in the right image. The aluminum plug that serves as the common electrode is then dropped into the jaw and attached with adhesive.

To improve the shielding of the sensors, a ground shield is needed. Although the FDC1004 comes equipped with two AC shielding channels, preliminary tests showed that using a ground plane was more effective than using the shielding channels. Therefore, the FPCB is copper clad on both sides. The underside of the FPCB—the layer of copper in contact with the grasper body—is connected to ground.

3.3.1 Manufacture of the Circuit Boards

The FPCBs for the prototype grasper were produced at Western University, using copper clad polyimide sheets obtained through DuPont. For the first prototype, the FPCB was manufactured using the Atometric MMM. By removing material from one face of a copper clad polyimide laminate (Pyralux, Dupont) circuit traces were formed. Using a similar procedure as when milling the other layers of the device, a Pyralux sheet was glued flat to a fixture and machined using a 75 μm endmill. To ensure that there was sufficient material behind the copper, it was necessary to use a sheet of Pyralux with a polyimide thickness of at least 50 μm. Ensuring that the fixture and laminate were completely uniform was difficult and time consuming, and removing only the copper required extremely precise depth control. Using a laminate with thinner polyimide resulted in cutting completely through the polyimide in some areas.
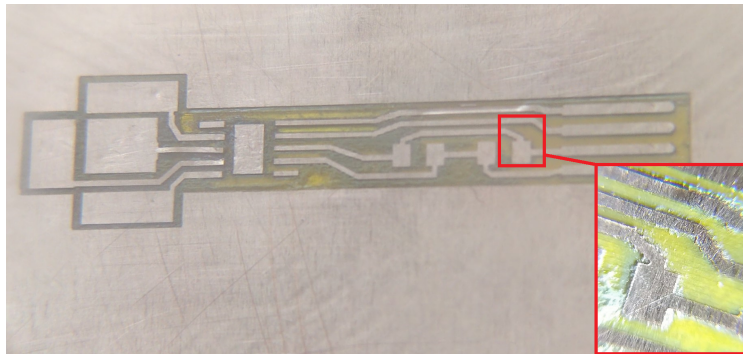
Figure 3.9: FPCB machined using the Atometric milling machine. Inset showing closer view of circuit traces.

3.4 Evaluation and Discussion—First Prototype

The testing that was performed was limited in scope, and was designed to demonstrate the feasibility of the sensing system, as well as to determine any areas that needed to be modified to improve the grasper's functionality. The conclusions from this evaluation drove the changes that were made for the next iteration of the grasper.

3.4.1 Experimental Setup

The first prototype grasper was assembled into an instrument shaft that could be inserted through a 5 mm trocar. A stainless steel tube was used as the instrument shaft for testing. The tube had an outer diameter of 5.56 mm, and an inner diameter of 4.14 mm. To hold the grasper, four slots were cut into the end of the tube using a wire EDM. This not only created a secure fit for the grasper, but added additional strength by supporting the walls of the grasper. The instrument shaft was then fixed to an optical table using 3D-printed mounts. With the grasper mounted in the shaft, four 32 AWG wires were connected to the FPCB and passed through the shaft to an evaluation board (FDC1004EVM, Texas Instruments) for data collection. The evaluation board was connected to a PC where the evaluation board software graphical user interface (GUI) allowed configuration and data collection. Data was exported from the evaluation GUI to MATLAB for analysis. To apply forces to the device, a small piece of 50 μm thick 304 stainless steel foil was fixed to the aluminum electrode in the bottom jaw using cyanoacrylate adhesive; the foil had small holes to allow for the secure attachment of a cable. The cable was run over a pulley and was used to hang calibrated weights in various positions, to apply a known force on each sensor in the grasper. The upper jaw of the grasper was then pulled tightly shut, to simulate a grasping task. The setup can be seen in Figure 3.10.
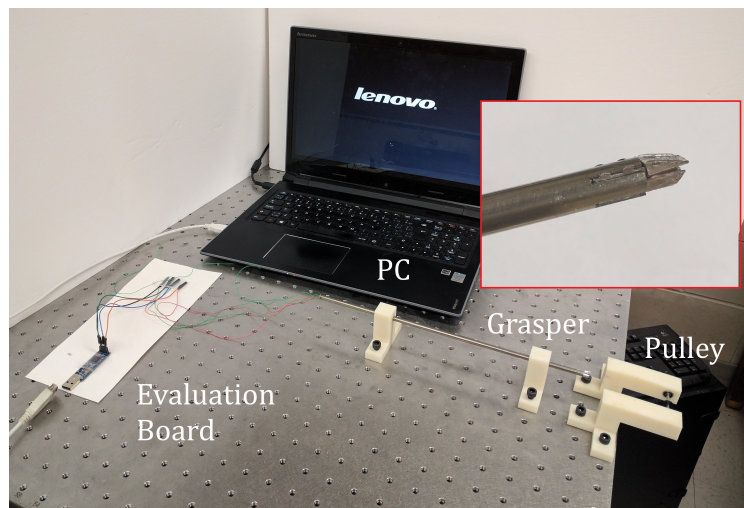
Figure 3.10: Testing setup for first prototype grasper. Inset shows grasper mounted into instrument shaft.

3.4.2   Experimental Results

Weights were hung from the testing setup in increments of 50 g to measure the response of the sensor: 50, 100, 150, 200, and 250 g, corresponding to forces of 0.49, 0.98, 1.47, 1.96, and 2.45 N. Although weights greater than 250 g were tested and supported by the jaw, the higher shear force dislodged the aluminum electrode on multiple occasions. Therefore, it was decided to reduce the testing to a maximum of 2.45 N. This falls short of the 4 N objective, however it still serves as a proof of concept for the sensor, and is more than twice as high as the forces measured in previous PCMEMS graspers. This problem can be addressed by using a stronger, more flexible adhesive.

When applying a load to one of the transverse shear sensors, it was seen that these sensors worked as a differential pair—as the electrode moved, an increase in capacitance in one sensor was accompanied by a decrease in the opposite sensor. The differential sensing is shown in Figure 3.11, and allows the two sensors to be used in combination, improving reliability when measuring transverse shear forces. It should also be noted that despite best efforts at shielding the system, there was still a small amount of noise present. The noise can be seen in Figure 3.11, unfiltered. Using MATLAB, the signal-to-noise ratio for the transverse shear sensors was calculated to be approximately 40 dB, with peak-to-peak noise of 0.04 pF. The normal force sensor performed similarly to the transverse sensors, with a signal-to-noise ratio of approximately 40 dB.
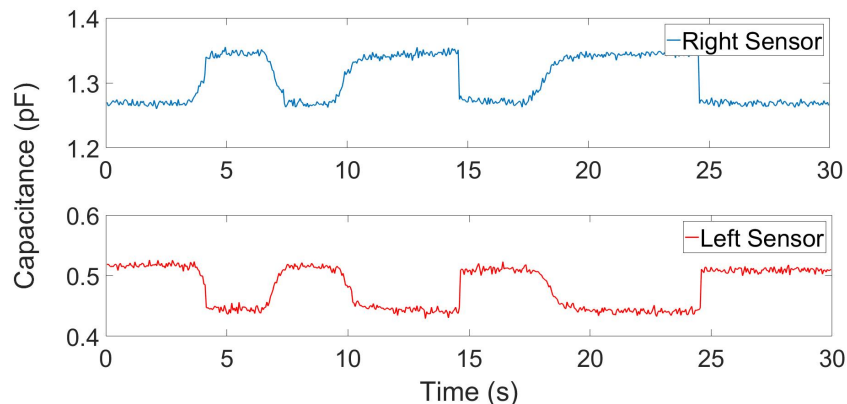
Figure 3.11: Differential sensing of transverse shear sensors. Left and right transverse shear sensors under repeated applications of a 0.49 N load. The measured capacitance values are taken from the raw sensor data.

Unfortunately, the front sensor did not respond to axial shear forces as planned. The front

sensor responded well to normal forces, however, the response to axial forces was not as strong as expected. The response was small enough that 0.5 N of applied force was indistinguishable from noise, even after passing the data through a low-pass filter. Figure 3.12 shows the response of the front sensor to 1.47 and 2.45 N of force. It can be seen that even under an applied force of 1.47 N, it is difficult to distinguish between the signal and noise; it must also be noted that the applied forces were manually hung weights, and therefore small vibrations and hand movements at the loading points will have contributed to the noise in the system.
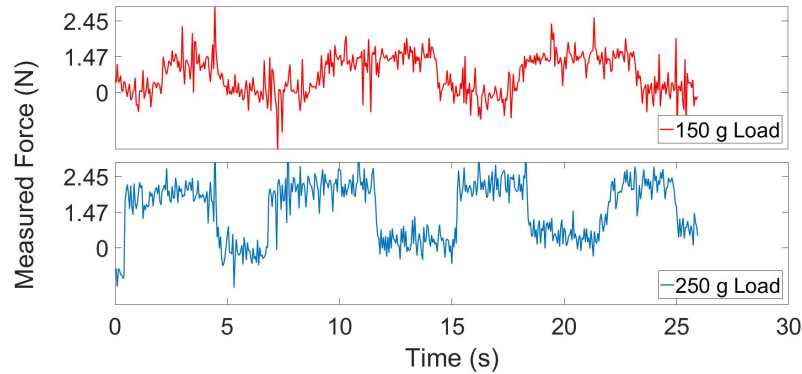
Figure 3.12: Response of axial shear sensor to 150 g and 250 g loads. Loads under 150 g could not be accurately measured.

For the transverse shear and normal force sensors, multiple applications of the same force were used to measure repeatability and accuracy. Data from the left transverse sensor is shown in Figure 3.13 as an example. By measuring the average output under each load, a graph of the force–capacitance response was first generated to characterize the sensor. Although the system somewhat follows the linear Hooke's Law approximation discussed earlier (R^2 value for a linear fit is 0.949), it was expected that the output would not be entirely linear. Fitting a second-order polynomial to the data, a closer fit is achieved (Figure 3.13, R^2 value 0.995). An equation based on this trend line was then used to determine RMS repeatability and error. The RMS repeatability error of the measurements reaches a maximum of 0.099 N at 1 N of applied force. Calculating the RMS errors at each applied force, the largest RMS error is 0.11 N of force, occurring again at 1 N of applied force. These results are consistent with the normal force sensor and right transverse shear sensor.
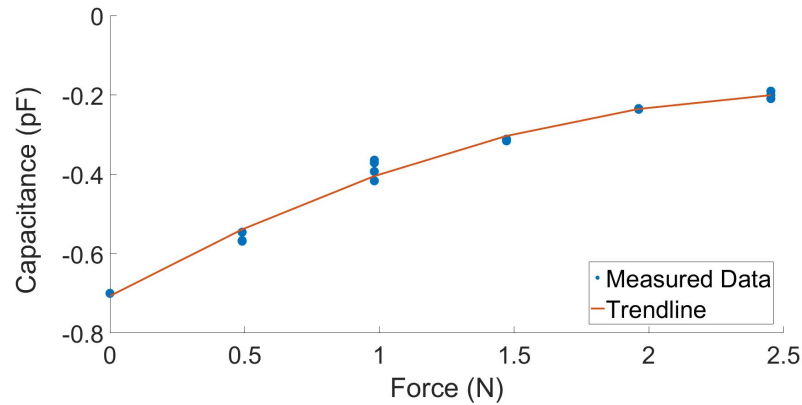
Figure 3.13: Sensor characterization of the left transverse shear sensor. A second-order trendline was fit to the collected data.

A dynamic response was observed by applying a 2.45 N load a minimum of four times in sequence. Looking at the application of 250 g (Figure 3.14), it can be seen that there is a small settling period after the weight is applied or removed. This period occurs when the dielectric is deforming under the load viscoelastically. The settling time when 2.45 N was applied was found to average 2.2 s on both the transverse shear sensors and the normal force sensor (time to reach 95% of the maximum measured force). As would be expected, the settling time is dependent on load.
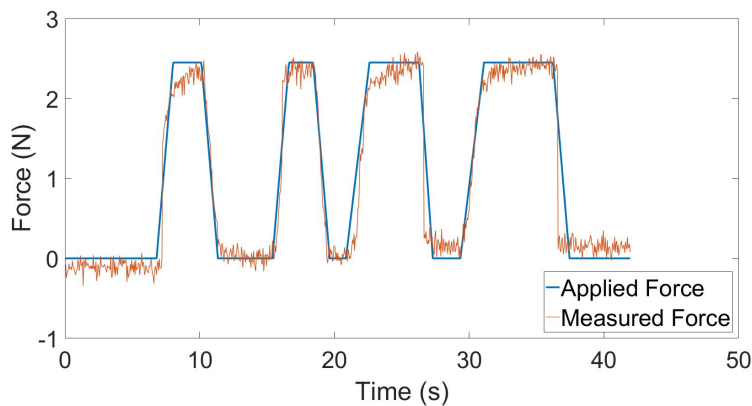
Figure 3.14: Dynamic loading of the right transverse shear sensor. The sensor was loaded and unloaded four times with 250 g of weight.

3.4.3 Experimental Discussion

Based on the experimental evaluation of the first prototype, several opportunities for improvement were identified. The axial shear sensor was identified as the first critical area of improvement. Upon analysis, the low sensitivity and large amount of noise associated with the axial shear sensor was caused by two factors: first, the use of cyanoacrylate adhesive (used to bind the dielectric sheet to the FPCB and to the aluminum electrode) caused the assembly to to be too stiff, limiting forward movement of the aluminum electrode; second, the angled front of the aluminum electrode was not perfectly in line with the angle of the front electrode. Therefore, the two electrodes were not perfectly parallel. These problems can be rectified by changing to a more flexible adhesive and changing the front face of the bottom jaw so that it is perpendicular to the bottom.

Further, the maximum force application (2.45 N) was limited due to adhesive and material choices. Using the sheets of flexible dielectric requires the use of an additional adhesive to bind the dielectric, FPCB, and aluminum electrode. The chosen adhesive (in this case cyanoacrylate) was too brittle and limited the forces that could be applied. Therefore, it was decided to explore the possibility of replacing the sheet of dielectric material with a curing elastomer that can act as both the dielectric and adhesive to bond the aluminum electrode and the FPCB.

Manufacturing the FPCB was very time consuming, and creating multiple copies of the FPCB at one time was not possible with the Atometric MMM. Therefore, a new method of manufacturing the FPCB (using available equipment at Western University) was a goal for the next iteration device.

This testing was far from comprehensive, in part due to the poor results of the axial sensor, and the smaller than expected sensing range. The aforementioned calibration matrix was not completed, as the restrictions prevented it from having any real meaning. The tests did however demonstrate the feasibility of the system, and highlighted areas of improvement.

Chapter 4

Design and Realization of the Second Prototype

4.1 Introduction

Moving forward from the first prototype, it was evident that several improvements were needed to create a truly functional MIS grasper. Following the same structure as Chapter 3, this chapter details the changes that were made to the design of the instrument, including testing and evaluation. The updated design is tested more rigorously, and recommendations are presented.

4.2 Mechanical Design

The most significant design modification was made to SL1, changing the design of the lower jaw to make the front perpendicular to the bottom, instead of joining at shallower angle (Figure 4.1). This change helps to decouple the axial shear sensor from the normal sensor, and increases the sensitivity of the axial sensor. Along with this, the height of the lower jaw was raised slightly to increase the surface area of the axial shear sensor. To keep the overall size of the grasper the same, the increase in the height of the lower jaw required an equal decrease in the height of the upper jaw. Apart from the reduced height, the shape of the upper jaw was unchanged .
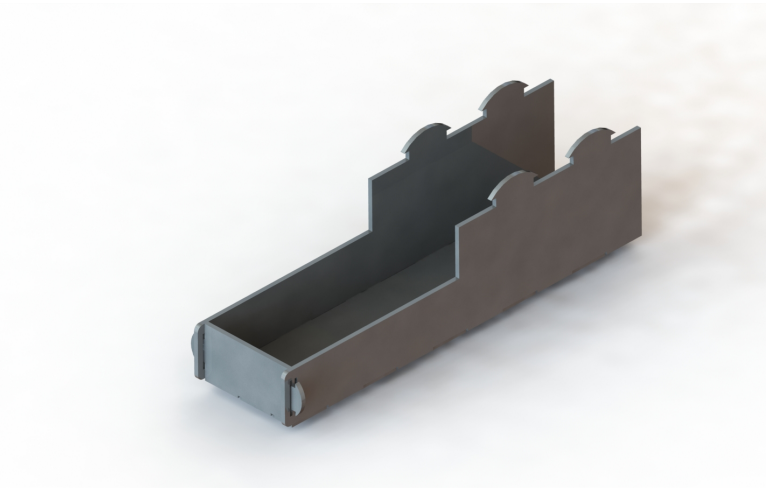
Figure 4.1: Sublaminate 1 modified for second version grasper.

The first generation grasper used castellated hinges for all joints. However, as shown in [14], plastic hinges can provide more strength for joints that only need to fold once. In a plastic hinge, the perforated layer deforms plastically during assembly of the device. Although plastic hinges are not meant to survive more than a few bending cycles, they provide more strength than castellated hinges. To take advantage of this, hinge designs for folds required strictly for assembly of the device were changed to use plastic hinges for one stainless steel layer (Figure 4.2). Thus, while the hinge upon which the upper jaw rotates continues to use a castellated hinge design because it endures many flexion cycles (due to opening and closing the jaw) other joints have stainless steel layers that are perforated instead of castellated.
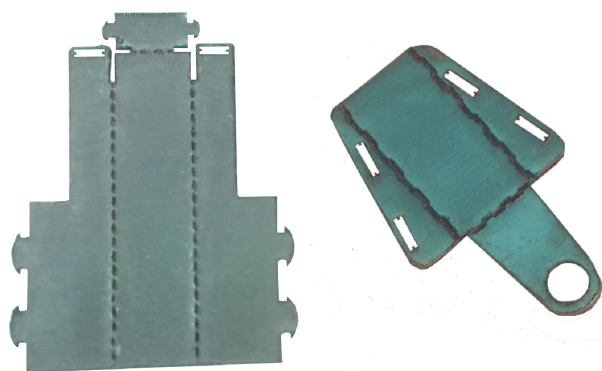
Figure 4.2: Sublaminates 1 (left) and 2 (right) displaying plastic and castellated hinges respectively.
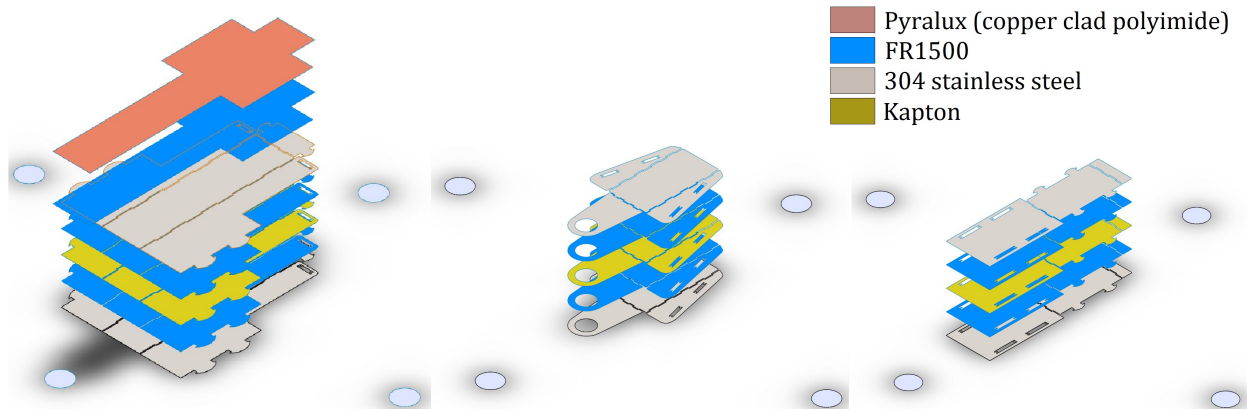
Figure 4.3: Completed sublaminate structures of second-generation grasper. From left to right: Sublaminates 1, 2 and 3. The four circles in each diagram represent the alignment pins.

The layer order and materials for each of the sublaminates remain the same. For the second-generation instrument the support frame was not modeled, due to the reasons outlined in Section 3.2. The updated layer designs are shown in Figure 4.3. The completed device looks very similar to the original design, as can be seen in Figure 4.4.

4.3 Sensing System Design

The dimensions of the FPCB were modified to match the new lower jaw design but the components and layout remained the same. The transverse shear and normal force sensor electrodes were lengthened, as the electrodes could now run the entire length of the jaw—in the first prototype it was necessary to stop the electrodes where the lower jaw became angled.

The flexible dielectric sheet used in the prototype was replaced with a curing silicone compound. The compound served to bond the aluminum electrode to the FPCB, acted as a dielectric, and provided the elastic element for the sensors. It was important that the chosen compound have a high bond strength to metals, to prevent the electrode from dislodging under higher forces, as happened with the cyanoacrylate in the first prototype. To maximize sensor sensitivity, the compound needs to be extremely flexible. It was also required that the compound is biocompatible.

Using these criteria, MS910Med from MasterSil was chosen as the adhesive compound. MS910Med is a one part acetoxy type silicone that meets USP Class VI requirements for biocompatibility. A

(a): PCMEMS grasper mounted in stainless steel shaft for testing.
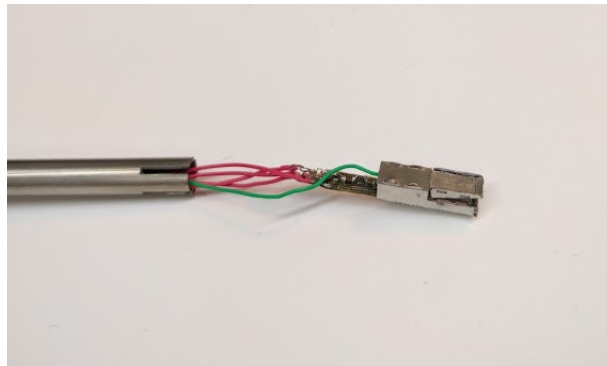
(b): PCMEMS grasper before mounting into instrument shaft.

Figure 4.4: Completed second-generation PCMEMS grasper.

10–20 minute tack-free time and moderate viscosity allowed for easy assembly of the sensor system. The full specifications of the compound can be found in Table 4.1.

A small guide was 3D printed to centre the electrode and contain the adhesive during assembly (Figure 4.5). The guide was placed at the back of the lower jaw and a pea sized mass of MS910Med was placed in the center of the lower jaw. The aluminum electrode was then aligned using the guide and pushed down into the centre of the adhesive, pushing MS910Med around all sides of the electrode evenly. Then, a flat metal plate was scraped across the top of the lower jaw to remove any excess adhesive and level the electrode with the top of the lower jaw. The guide was removed after 10 minutes.

Typical Properties of MS910 Med	
Specific gravity, 24 °C	1.1
Viscosity, 24 °C	paste
Colour	translucent
Tack-free time, 24 °C	10–20 minutes
Tensile lap shear strength, 24 °C, aluminum to alumnum	400–500 psi
Tensile strength, 24 °C	1300–1600 psi
Elongation, 24 °C	400–600%
Hardness, 24 °C	20–30 Shore A
Delectric constant, 24 °C, 60 Hz	2.75
Dissipation factor, 24 °C, 60 Hz	0.003
Volume resistivity, 24 °C	$>10^{15}$ Ω-cm
Shelf life at , 24 °C, in original unopened containers	6 months
Service temperature range	-59 °C to +204 °C

Table 4.1: Typical properties of MS910 Med silicone adhesive.
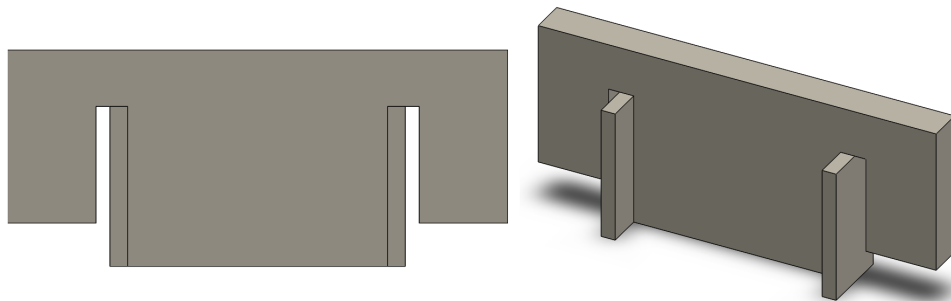
Figure 4.5: Adhesive guide for MS910Med silicone. Outer slots are used to secure the guide to the walls of the lower jaw.

4.3.1 Manufacture of the Circuit Boards

To reduce manufacturing time, a new method of fabricating the FPCBs was used. First, sheets of Pyralux were cut to standard A4 paper size (210 x 297 mm). Next, the sheets were cleaned using a 5% acetic acid solution to promote toner adhesion, and an Epson laser printer was used to print the circuit design in black toner onto the Pyralux sheets. The printer files were PDF images of the circuits, converted using EAGLE PCB layout software. The printed copper sheets were then exposed to a chemical etching solution to remove the copper in any areas that were not covered in toner. A summary of the procedure is presented in Table 4.2.

Process	Description
Cut	Sheets of Pyralux cut to standard A4 paper size
Clean	5% acetic acid solution used to polish and clean the surface of the Pyralux. Note that during the entire process care must be taken to avoid getting finger prints or other dirt/oils on the Pyralux, as this prevents the ink from properly adhering to the material. Sheers were handled using nitrile gloves.
Print	Pyralux sheet(s) placed in the bypass tray of a commercial laser printer.
Etch	Pryalux sheets cut into smaller pieces, each containing two circuits. Circuits etched using ferric chloride to remove copper.

Table 4.2: FPCB manufacturing procedure using laser printer.

The procedure was not always successful, with roughly half of the etched circuits not suitable for use. The most common cause of failure was uneven etching, resulting in traces with small gaps, or adjacent traces that were connected together (Figure 4.6). However, due to the speed of the laser printing process and the small size of the circuit, it was very easy to create many copies of the circuit at once on a single sheet of Pyralux. During etching, the Pyralux sheets floated in the tank of etchant and it was more difficult to etch a large sheet evenly. Therefore, the large sheets were cut to etch the circuits in groups of two.

On longer traces, over etching was a more common problem than under etching. It is believed that this was caused by the etchant eating into the traces from the sides once the top layer of copper was etched away, causing small breaks in the thin traces. Greater success was seen by modifying the traces from 8 mil (0.2032 mm) width with 8 mil spacing, to 10 mil width, with 6 mil spacing.
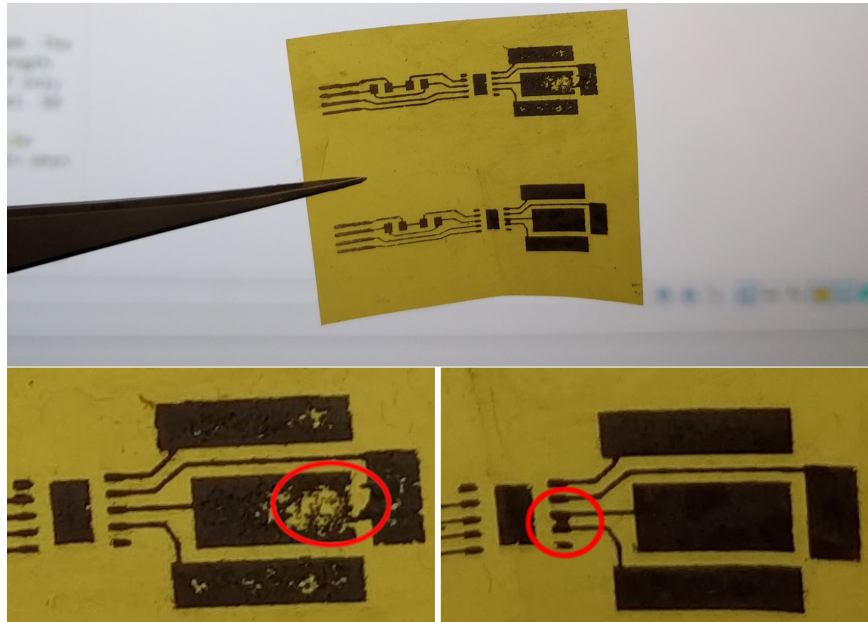
Figure 4.6: FPCB manufacturing defects caused by over and under etching of the copper layer. (bottom left) Over etching has removed copper on the sensor electrodes. (bottom right) Traces for two electrodes are connected due to under etching.

4.4 Evaluation and Discussion—Second Prototype

4.4.1 Experimental Setup

To characterize the sensor, a slightly different setup was used than was described in Section 3.4.1. A 3D printed mount was made that secured the lower jaw of the grasper on three sides. The lower jaw was fit into this mount and secured using cyanoacrylate adhesive. The mount was used to hold the grasper more securely and prevent any misalignment. To apply forces to the grasper, a small piece of acetate was adhered to the grasping surface (the aluminum electrode) of the lower jaw using cyanoacrylate adhesive. Weights were hung from a wire which was attached to the acetate and run over a pulley. The hanging weights pulled the acetate, and therefore the grasping surface, to produce a measured force response. The setup was rotated $90°$ three times—pulling on the acetate in a different direction each time—to measure the force response in each direction (Figure 4.7).
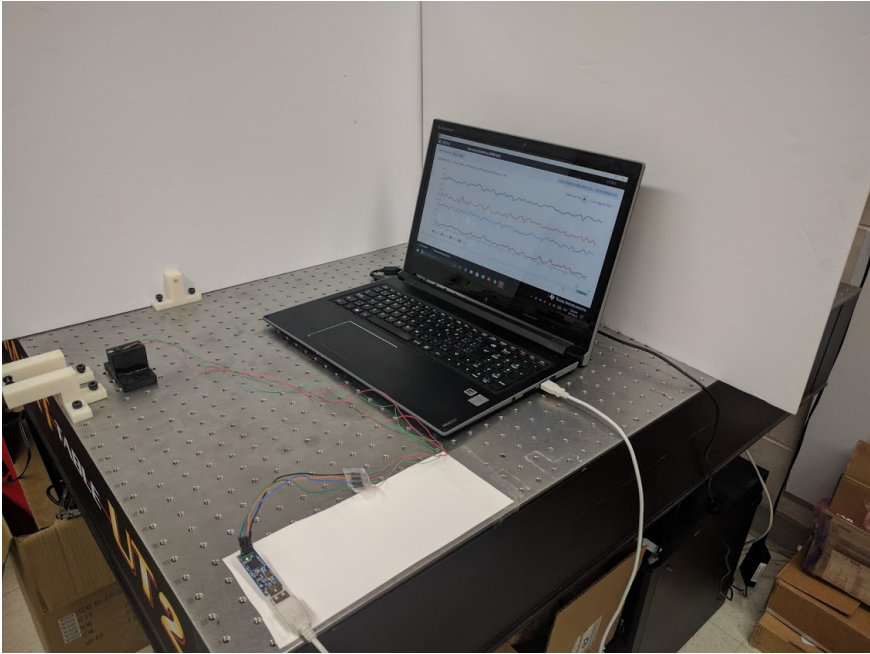
(a): Testing setup overview showing the FDC1004 evaluation board and PC used to collect data.
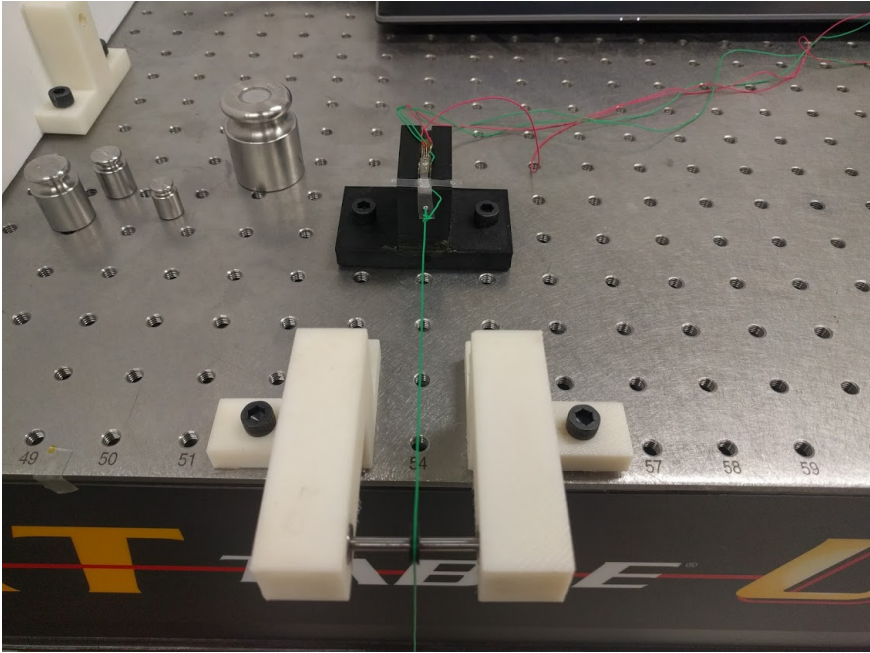
(b): View of bottom jaw in mounted setup.

Figure 4.7: Sensor characterization testing setup.

This was sufficient for measuring axial and transverse shear forces, however to measure normal forces the mount was moved such that the sensorized jaw now extended over the edge of the optical table. Weights were then hung down directly from the jaw, applying a downward force on the normal force sensor.

After characterizing the sensor in this setup, the sensor was tested again with the grasper mounted in the stainless steel instrument shaft, to ensure that there was no difference in measurements. It was confirmed that there was no difference between the two methods. Although it was easier to ensure forces were applied purely in one axis when using the 3D printed mount, the sensor performance in the 3D printed mount and in the instrument shaft were the same.

With the grasper mounted in the stainless steel shaft, four 32 AWG wires were connected to the FPCB and were passed through the instrument shaft, then connected to an evaluation board (FDC1004EVM, Texas Instruments) for data collection. The data was sent from the evaluation board to a PC running the FDC1004 evaluation board graphical user interface (GUI) program. The data was then exported from the GUI to MATLAB (Math Works MATLAB R2016a) for data processing. Note that when the data was first processed in MATLAB it was still raw capacitance values, and did not yet directly refer to force values.

4.4.2 Verification and Characterization of the Instrument

4.4.2.1 Characterizing The Sensors

Weights of 10, 20, 30, 50, 100, 150, 160, 200, 250, 260, 300, 350, and 400 grams were used to characterize the response of the sensor, corresponding to maximum forces of ±3.92 N. Each weight was loaded and unloaded 5 times, and an average response was used to generate a characteristic force curve. To reduce noise, the data was run through a moving average filter with a window length of 9 samples. The characteristic curves for the three sensors (axial shear force, transverse shear force, and normal force) are shown in Figure 4.8.

A second-order polynomial fit line has been added to each figure, showing that for each sensor the measured data approximately follows a quadratic trend. The quadratic equations displayed in Figure 4.8(d) are the equations needed to convert the measurements from a capacitance to a force
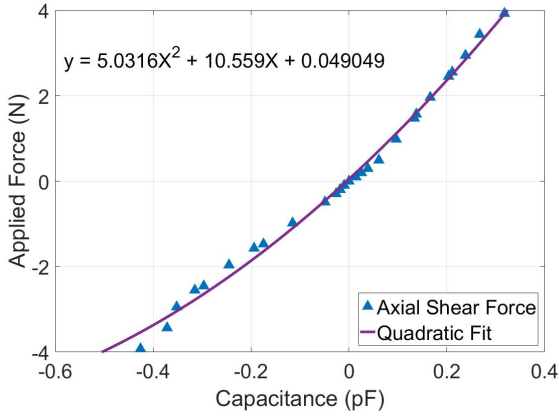
(a): Axial shear force calibration curve.
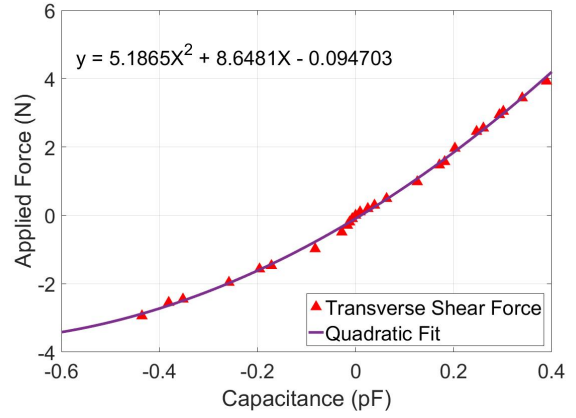
(b): Transverse shear force calibration curve.
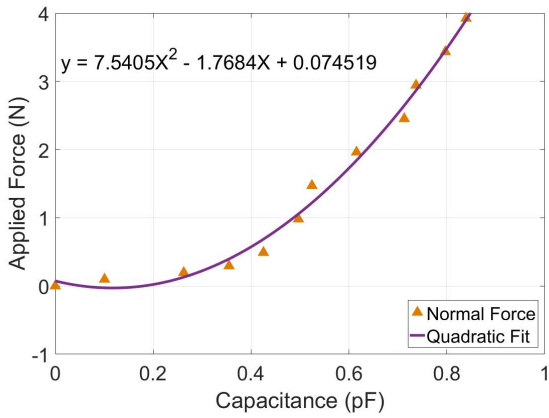
(c): Normal force calibration curve.

Sensor	Characteristic Equation
Axial Shear Force	$5.0316X^2 + 10.559X + 0.049049$
Transverse Shear Force	$5.1865X^2 + 8.6481X - 0.094703$
Normal Force	$7.5405X^2 - 1.7684X + 0.074519$

(d): Characteristic equations for each sensor

Figure 4.8: Calibration curves for sensorized instrument.

value. It must be noted though that the data does not follow the curve exactly, therefore a small amount of error for the characterization must be accepted. The root-mean-square (RMS) error of the sensors is 0.159 N, 0.085 N, and 0.133 N for the axial shear, transverse shear, and normal force sensors respectively.

Sensor	RMS Error (N)
Axial Shear	0.159
Transverse Shear	0.085
Normal Force	0.133

Table 4.3: RMS error of sensors.

4.4.2.2 Repeatability

Each point in Figure 4.8 is an average of five measurements. It was important to measure the repeatability of the system at each force level, and for each sensor. The maximum deviations from the mean value of the force measurements are displayed in Figure 4.9. Error bars are used to indicate the maximum deviation above and below the mean.

The repeatability for each sensor was calculated as RMS repeatability, expressed as an average percentage of the individual measurements, not the full scale range. The RMS repeatability for the axial shear, transverse shear, and normal force sensors is 3.7%, 2.3%, and 3.0% respectively. In the same order, the mean deviation was 0.064 N, 0.069 N, and 0.056 N. This information is summarized in Table 4.4.

Sensor	RMS Repeatability Error	Mean Deviation
Axial	3.7%	0.064
Transverse	2.1%	0.069
Normal	3.0%	0.056

Table 4.4: Repeatability of the sensing system.

The maximum deviation from the mean for each sensor was also calculated, which can be thought of as the maximum error due to repeatability (Table 4.5). Table 4.5 also includes the largest characterization error (difference between the mean and the characterization equation) and the largest total error for each sensor. The largest total error was calculated as the largest difference between any one measurement and the characteristic equation. Note that this is not simply the addition of the maximum deviation and maximum characterization error—it is the "worst case", displaying the largest differences between a single measurement point and the characterization equation. The large error values in Table 4.5 are often due to a single outlying data point.
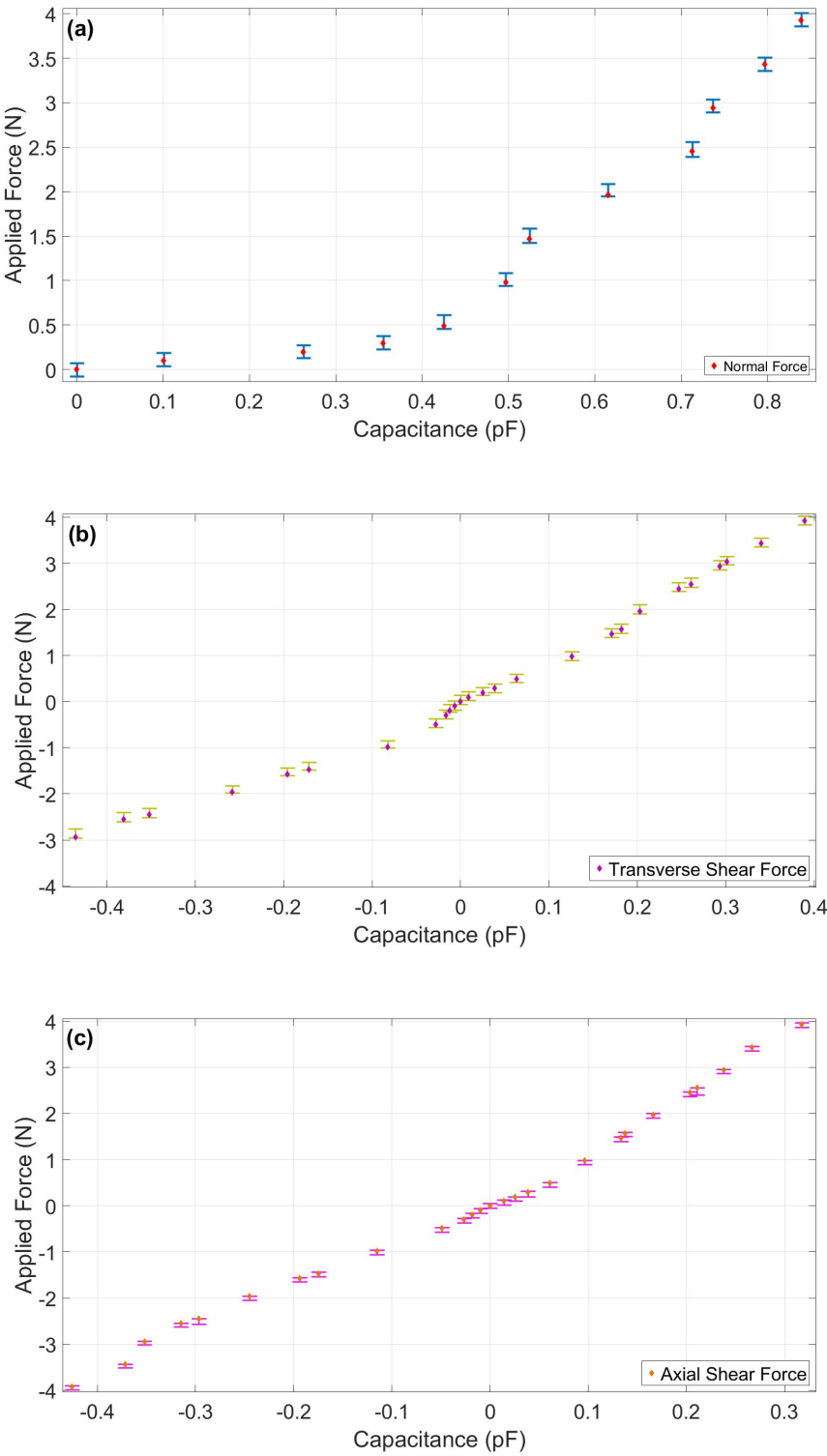
Figure 4.9: Measurement of forces shown with error bars to indicate variance in the measurements. (a) Normal force sensor. (b) Transverse shear sensor. (c) Axial shear sensor.

Sensor	Maximum Characterization Error (N)	Maximum Repeatability Error (N)	Maximum Error (N)
Axial	0.389	0.148	0.442
Transverse	0.209	0.095	0.244
Normal	0.194	0.127	0.365

Table 4.5: Largest measured errors in each of the three sensors.

4.4.2.3   Dynamic Response

The dynamic response of the sensor was measured by suddenly applying and removing multiple weights and measuring the response of each sensor. Overall, the dynamic response was excellent, with the exception of the axial sensor in the negative direction (an applied force towards the handle of the instrument). The response time of this sensor grew quickly as the applied force was increased, and after 3 N of force, did not return to the same baseline zero value when the force was removed (Figure 4.10). The results of this test are shown in Table 4.6, where the settling time was measured as the time to within 95% of the final value.
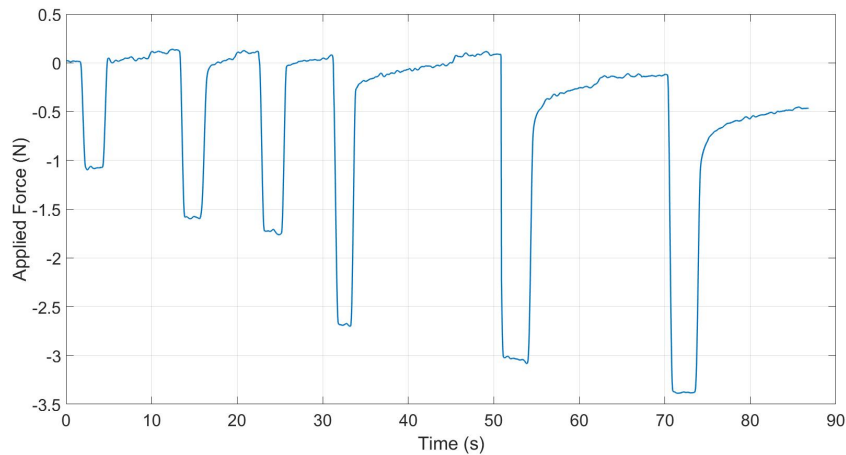
Figure 4.10: Dynamic response of axial sensor in negative direction.

The dynamic response of the transverse and normal sensors were similar to each other, with a settling time of 1.1 s and 0.8 s respectively under the maximum load of approximately 4 N. For both of these sensors the settling time correlated with the magnitude of the applied force.

Applied Force (N)	Settling Time (s)
1.0	0.25
1.5	0.4
1.6	0.1
2.6	1.2
3.0	2.45
3.5	Does not return

Table 4.6: Dynamic response of axial sensor in negative direction.

Interestingly, the response time of the axial sensor when force was applied in a positive direction (force applied away from the instrument handle) got smaller as larger forces were applied. A full summary of the dynamic response is presented in Table 4.7.

Sensor	Applied Force (N)	Settling Time (s)
Axial (+)	1.5	0.8
	2.5	0.65
	4	0.3
Axial (-)	1.5	0.25
	2.6	1.2
	3.5	Does not return
Transverse	1.5	0.4
	2.5	0.4
	4	1.1
Normal	1.5	0.45
	2.5	0.5
	4	0.8

Table 4.7: Dynamic response of sensors. Settling time is taken as 95% of time to reach final value.

4.4.3 Force Transformation of Coupled Forces

Due to the proximity of the sensors in this design, it was expected that there may be some coupling between sensors. Therefore, it was important to calibrate the device to determine the factors of influence between sensors. Given that the incoming data was received as capacitance values (in pF), the three raw sensor values are represented by: C_A, C_T, and C_N, corresponding to axial shear

capacitance, transverse shear capacitance, and normal capacitance respectively.

When a force is applied purely along one axis, there is an applied measurement, and two coupled measurements. For example, applying force purely along the axis of the shaft of the grasper creates an *applied* axial shear response (that can later be converted into a force measurement), and any readings on the transverse shear and normal force sensors are *coupled* responses. The relationship between the applied response and the coupled responses is then measured, and an equation can be used to quantify the transverse shear and normal responses that are created when an axial force is applied. This relationship was determined experimentally for each sensor, using the testing methods outlined in Section 4.4.2.1. For coupled responses, the following notation will be used,

Measured Response	Axial Load	Transverse Load	Normal Load
Axial Sensor	C_A	$C_{T,A}$	$C_{N,A}$
Transverse Sensor	$C_{A,T}$	C_T	$C_{N,T}$
Normal Force Sensor	$C_{A,N}$	$C_{T,N}$	C_N

Table 4.8: Variable notation for coupled and applied forces.

Using the example of a purely axial load, C_A is the capacitance measured from the axial shear sensor (the applied response). $C_{A,N}$ and $C_{A,T}$ are the capacitances measured from the normal and transverse sensors respectively (the coupled responses). A calibration matrix, Equation 4.1, can then be used to determine the actual capacitance value being read by any sensor. Essentially, the portion of the response on a sensor that is due to an applied force on the other sensors is subtracted from the measured value to get the true capacitance response. The true capacitance response is then used to find the measured force, using the calibration curves from Figure 4.8.

$$\begin{bmatrix} C_A & -C_{T,A} & -C_{N,A} \\ -C_{A,T} & C_T & EC_{N,T} \\ -C_{A,N} & -C_{T,N} & C_N \end{bmatrix} = \begin{bmatrix} C'_A \\ C'_T \\ C'_N \end{bmatrix} \tag{4.1}$$

$C'_{A/N/T}$ is the updated response value (still in pF) reflecting the changes made by removing the coupled responses due to the other sensors. The value is simply converted to a real force value

using the sensor characterization data,

$$
\begin{bmatrix} E_A(C'_A) \\ E_T(C'_T) \\ E_N(C'_N) \end{bmatrix} = \begin{bmatrix} F_A \\ F_T \\ F_N \end{bmatrix}.
\tag{4.2}
$$

Where $E_{A/T/N}$ is the equation relating capacitance to force values (shown in Figure 4.8(d)), and $F_{A/T/N}$ is the resulting force measurement for each sensor. Filling in the matrix with equations is simply the result of the sensor characterization. The full loading pattern of the sensors can be seen in Figure 4.11. This was used to determine the relationship between the sensors and the coupled responses when a force is applied purely in the axial, transverse, and normal directions.

The relationship between the applied and coupled forces is demonstrated in Figure 4.12 for the axial shear sensor, as an example. The equation in Figure 4.12, $C_{AT} = -0.1474C_A^2 + 0.013665C_A - 0.0064356$, represents the amount of capacitance that is induced on the transverse sensor when an axial load is applied to the grasper. Visually, it can be seen that an approximately quadratic relationship exists between the sensor for the applied force, and the coupled sensors—this was true for the coupled responses under transverse shear and normal force loads as well. Each of the equations for the coupled responses of the sensors is shown in Table 4.9.

Applied Force	Coupled Response	Quadratic Equation of Coupled Response
Axial	$C_{A,T}$	$-0.1474C_A^2 + 0.013665C_A - 0.00064356$
	$C_{A,N}$	$-0.22329C_A^2 - 0.0064418C_A - 0.0039241$
Transverse	$C_{T,N}$	$-0.53809C_T^2 + 0.068581C_T - 0.0046655$
	$C_{T,A}$	$-0.25022C_T^2 + 0.05002C_T - 0.0050331$
Normal	$C_{N,T}$	$-0.053675C_N^2 + 0.091621C_N + 0.001501$
	$C_{N,A}$	$-0.288228C_N^2 + 0.339168C_N + 0.013437$

Table 4.9: Sensor coupling in response to loads applied purely in one axis.
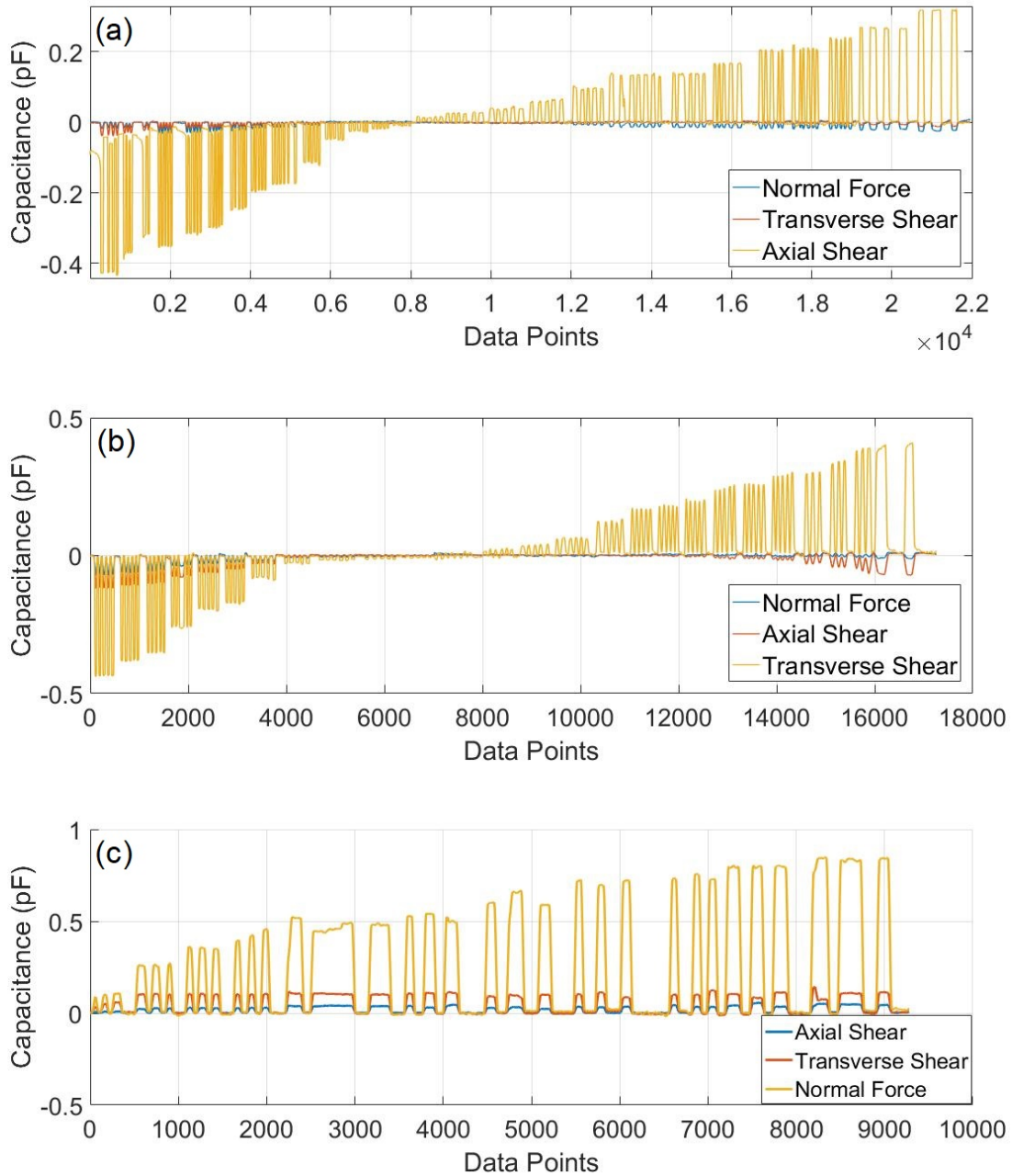
Figure 4.11: Response to principle applied forces. (a) Axial shear force is applied from -4 to 4 N. (b) Transverse shear force is applied from -4 to 4 N. (c) Normal force is applied from 0 to 4 N.

.
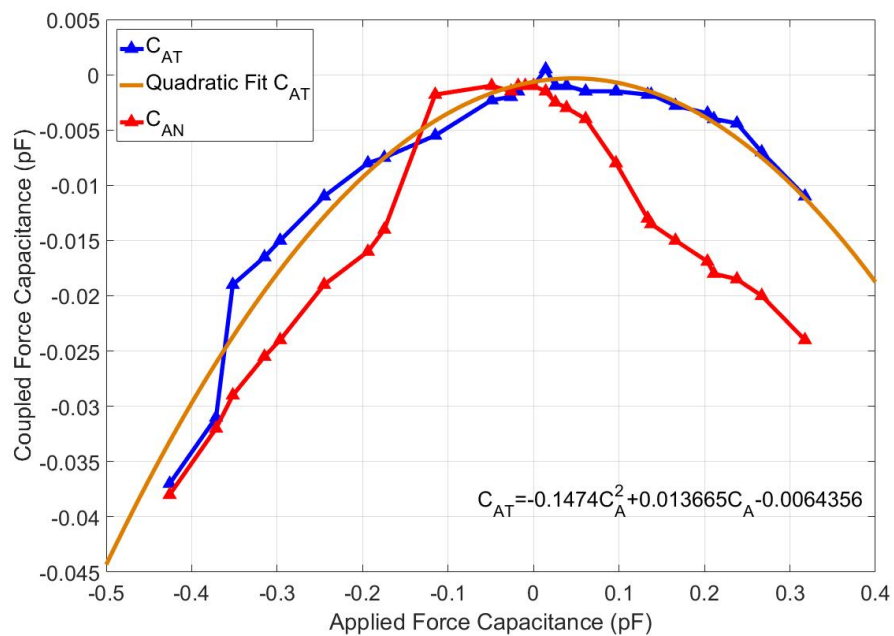
Figure 4.12: Relationship between sensors under an axial load. Equation describes the capacitance induced on the transverse sensor, related to the capacitance measured from the axial sensor when a purely axial force is applied.

A simple matrix that relates measured capacitance to actual capacitance (removing the effects of coupled forces) was presented in Equation 4.1. Recall from Table 4.8 the variables $C_{A,N}$ and $C_{A,T}$, which represent the coupled forces for an axial load. These variables are really the equations for the coupled force responses—the equations in Table 4.9. Because the resulting equations in Table 4.9 are quadratic, the coupled equations, such as $C_{A,N}$ and $C_{A,T}$ are a combination of three terms. Therefore, the calibration matrix is actually a bit more complicated. As an example, the quadratic equation for the coupled response of the normal force sensor under axial load can be given the form,

$$C_{A,N} = a_{AN} C_A^2 + b_{AN} C_A + c_{AN}, \tag{4.3}$$

where a_{AN}, b_{AN}, and c_{AN} are the coefficients from the quadratic equation of coupled response from Table 4.9. The full calibration matrix to generate the true capacitance response values is then in the form,

$$\begin{bmatrix} 0 & 1 & 0 & -a_{TA} & -b_{TA} & -c_{TA} & -a_{NA} & -b_{NA} & -c_{NA} \\ -a_{AT} & -b_{AT} & -c_{AT} & 0 & 1 & 0 & -a_{NT} & -b_{NT} & -c_{NT} \\ -a_{AN} & -b_{AN} & -c_{AN} & -a_{TN} & -b_{TN} & -c_{TN} & 0 & 1 & 0 \end{bmatrix} \begin{bmatrix} C_A^2 & 0 & 0 \\ C_A & 0 & 0 \\ 1 & 0 & 0 \\ 0 & C_T^2 & 0 \\ 0 & C_T & 0 \\ 0 & 1 & 0 \\ 0 & 0 & C_N^2 \\ 0 & 0 & C_N \\ 0 & 0 & 1 \end{bmatrix}$$

$$= \begin{bmatrix} C_A & -(a_{TA} C_T^2 + b_{TA} C_T + c_{TA}) & -(a_{NA} C_N^2 + b_{NA} C_N + c_{NA}) \\ -(a_{AT} C_A^2 + b_{AT} C_A + c_{AT}) & C_T & -(a_{NT} Nc^2 + b_{NT} tC_N + c_{NT}) \\ -(a_{AN} C_A^2 + b_{AN} C_A + c_{AN}) & -(a_{TN} C_T^2 + b_{TN} C_T +_{TN} n) & C_N \end{bmatrix}$$

$$= \begin{bmatrix} C_A & -C_{T,A} & -C_{N,A} \\ -C_{A,T} & C_T & -C_{N,T} \\ -C_{A,N} & -C_{T,N} & C_N \end{bmatrix} = \begin{bmatrix} C_A' \\ C_T' \\ C_N' \end{bmatrix}. \tag{4.4}$$

Substituting the values from Table 4.9, the resultant equations are:

$$C'_A = C_A + 0.2502C_T^2 - 0.0500C_T + 0.28823C_N^2 - 0.33917C_N - 0.008407,$$

$$C'_T = C_T + 0.1474C_A^2 - 0.01367C_A + 0.05368C_N^2 - 0.091621C_N - 0.0008574,$$

$$C'_N = C_N + 0.2233C_A^2 + 0.006442C_A + 0.53809C_T^2 - 0.06858C_T + 0.008579. \tag{4.5}$$

The capacitance values can then be converted into measured forces using the equations from Figure 4.8(d). Therefore, the final equation for the applied force, using the values obtained from Equation 4.5, is,

$$F_A = 5.0316C'^2_A + 10.559C'_A + 0.049049$$

$$F_T = 5.18535C'^2_T + 8.4681C'_T - 0.094703$$

$$F_N = 7.5405C'^2_N - 1.7864C'_N + 0.074519. \tag{4.6}$$

4.4.4 Noise and Resolution

The incoming sensor data was run through a moving average filter with a window length of 9 samples to reduce noise. This filtering creates a delay of 200 ms. All values listed for noise calculations are done using the filtered data. The noise of the sensor is summarized in Table 4.10.

Sensor	RMS noise, pF (N)	Peak to peak noise, pF (N)
Axial Shear Force	0.0047 (0.0875)	0.0228 (0.2134)
Transverse Shear Force	0.0081 (0.0378)	0.0216 (0.0944)
Normal Force	0.0102 (0.0587)	0.0585 (0.1878)

Table 4.10: Sensor noise for instrument.

It was possible to clearly distinguish visually between differences of 100 mN in testing when observing the resultant capacitance or force measurement plots. This was true from forces of 100 mN up through the range of the sensors. However, the level of noise suggests that more filtering may be needed, as the peak to peak noise was often seen much larger than 100 mN. Given the

visual representation of the data, it is reasonable to say that 100 mN is the limit of realistic sensor resolution.

4.4.5 Temperature Response

The response of the sensors to a change in temperature was tested. Using a 40 W incandescent light bulb, the sensor was heated from room temperature (21.6 °C at time of measurement) to 37 °C, the internal temperature of the human body. The response of the sensor to a 2.45 N load applied in the positive transverse direction was measured at room temperature, at the elevated temperature, and again at room temperature. (Figure 4.13).
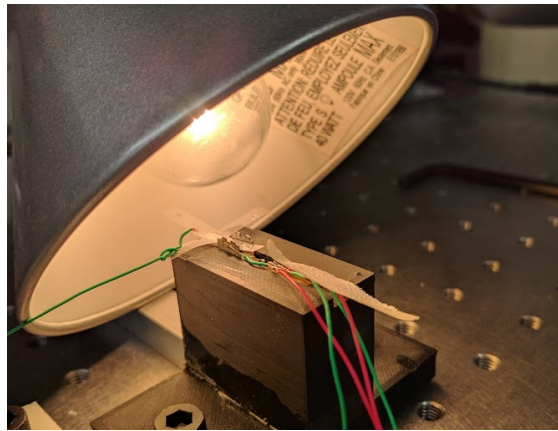
Figure 4.13: Setup for heating the sensor to 37 °C using a 40 W incandescent light bulb.

As the bulb began to heat up the sensor, the base level of capacitance dropped quickly, until it reached a steady value, then began to rise again once the heat was removed (Figure 4.14). The baseline capacitance dropped from 0 pF to -0.218 pF, and then returned to 0 pF once the sensor cooled back to room temperature.

The change in temperature had a small effect on the measured response between loaded and unloaded conditions. At room temperature, applying the 2.45 N load resulted in a 0.251 pF change in capacitance on the transverse shear sensor; at body temperature this was a 0.242 pF difference. This corresponds to a measurement difference of 101 mN (ignoring the change in baseline capacitance). These results suggest that some form of temperature compensation is needed for this device to function in a surgical setting.
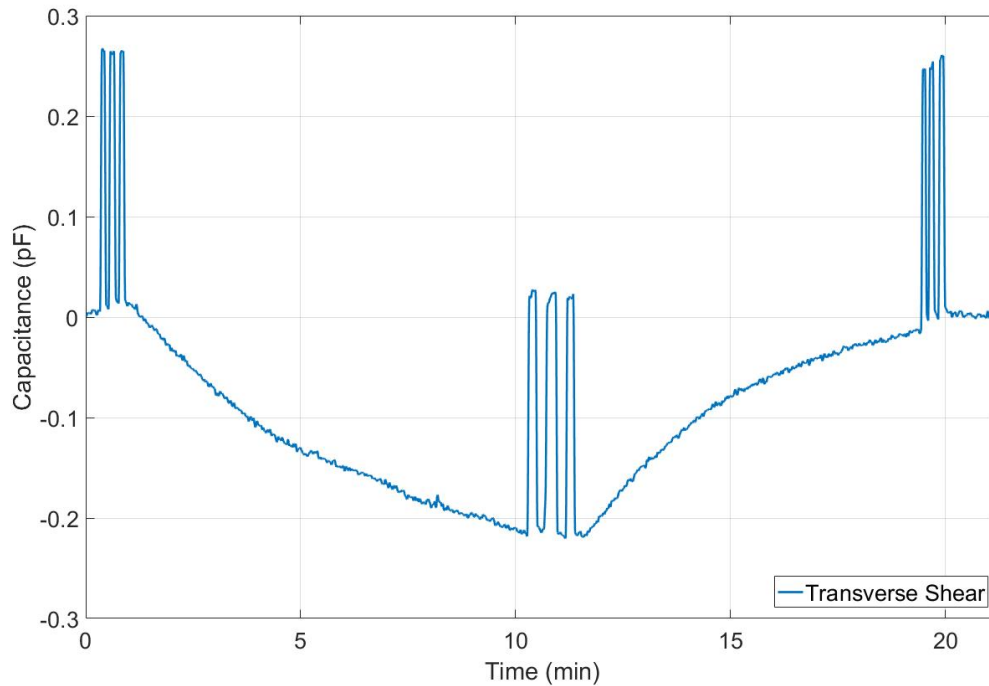
Figure 4.14: Transverse sensor response and drift when heated to 37 °C. 2.45 N of force applied starting at room temperature, heating the sensor, then removing the heat source.

4.4.6   Mechanical Testing and Simulated Grasping Task

Although the majority of the testing on the instrument focused on the sensing system, the body of the grasper also underwent testing to determine its strength and utility. A simulated grasping task was performed. To perform the task, the end effector was mounted into a stainless steel instrument shaft and the shaft was supported using 3D printed mounts. A piece of 0.5 mm thick silicone rubber with a shore hardness 20A of was placed in the grasper jaws. A weight was attached to the actuation cable and hung over a pulley to provide a constant grasping force. The silicone was then pulled by hand, measuring the sensor response.

The upper jaw of the grasper could open to a maximum of 44°, creating an opening of 5.4 mm at the distal tip of the jaw, which was more than wide enough to grab the rubber sheet. (Figure 4.15).

Pulling on the actuation cable successfully closed the grasper jaws, and the grasper was able to grab the rubber sheet. The friction between the jaws and the silicone rubber was low though, and a large amount of pressure was needed to grasp the material. Using an actuation force of 7 N
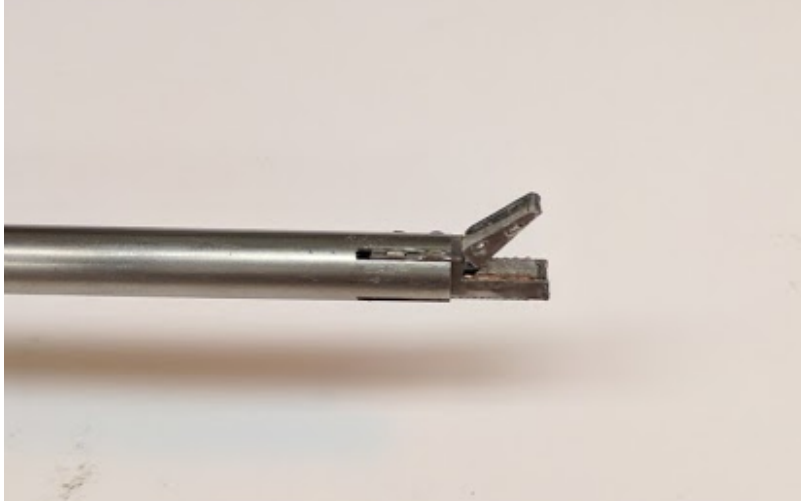
Figure 4.15: Range of motion of grasper jaw.

to pull the grasper jaw closed, forces greater than 2.5 N would cause the material to slip from the grasper. Increasing the actuation force to 8 N resulted in a tear in the polyimide hinge of the pull tab that attaches to the actuation cable on the upper jaw .

In Figure 4.16, the sensor response is shown for grasping the sheet of silicone rubber then pulling it away and to the right of the grasper.

The lower jaw supported forces up to 4 N in each direction during the sensor testing for many cycles without any signs of wear or failure. The upper jaw is strong when the grasper is closed. With the jaws closed around the simulated tissue sample, a force of 4 N was pushed into the side of the upper jaw without any material failure. However, with the jaw open when a force of 2 N was hung at the distal tip of the upper jaw, the jaw hinge began buckling. This would have damaged the grasper if allowed to hang.

4.5 Discussion

4.5.1 Performance of the Sensing System

Comparing the grasper performance, the closest available design would be the grasper design by Kim *et al.* from [47]. Overall, the performance of the Kim grasper was slightly better than the grasper presented in this thesis (Table 4.11). The differential sensing used by Kim for all
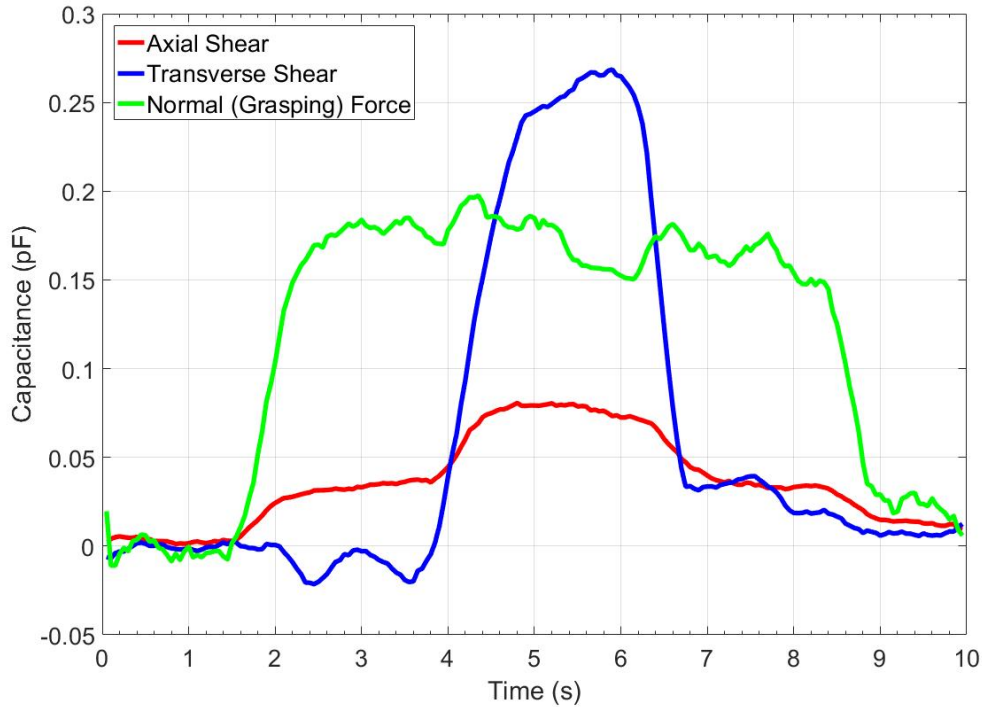
Figure 4.16: Simulated grasping task on sheet of silicone rubber. At approximately 1.5 s the jaw
is closed on the sheet, at 4 s the sheet is pulled diagonally forward and to the right,
the sheet is let go at 6.5 s, and the jaw is released at 8.5 s.

measurements may have helped reduce error, however, the grasper designed by Kim was also twice
as large, allowing relatively easier manufacturing and a larger sensor response. Further, the Kim
grasper was only tested in a range of ±2.5 N for two of the sensing directions. Kim also reported
repeatability as a percentage over the full scale range of the grasper, not as a percentage of each
measurement.

Category	Kim Grasper	PCMEMS Grasper
Force Range	±2.5 N axial; ±5 N transverse; 5 N normal	±4 N, axial and transverse; 4 N normal
Resolution	54.5 mN (average across all axes)	100 mN (average across all axes)
RMS Error	91.6 mN (average across all axes)	125.6 mN (average across all axes)
Repeatability	1.43% (average, measured over full scale range)	2.93% (average, measured over each force value)

Table 4.11: Comparison of Kim grasper [47] and PCMEMS grasper.

In many of the tests, the results showed the strongest performance for the transverse shear sensor, and the poorest performance for the axial shear sensor. This was true for RMS error, RMS repeatability, maximum error, and dynamic response. The most reasonable explanation for this is that the differential sensing used in the transverse shear sensor provided a more accurate and predictable response.

While the normal force sensor did not use differential sensing, the force range was limited strictly to the direction pushing into the sensor. Further, the sensor area on the normal force sensor was the largest, allowing for a larger sensor response to the same input.

One of the largest differences between sensors was the dynamic response. When large forces in the negative axial direction were applied, the axial shear sensor would not return to its base value. It is possible that because the axial sensor was single sided (attached only on the positive side of the sensor) when larger forces were applied, there was not enough of an elastic element under compression to restore the position of the electrode.

When assembling the sensor system, the jaw was held in place with a clamp while waiting for the MS910 Med to cure. If the adhesive cured in such a way that a force was constantly pulling the common electrode in the negative direction, then it is possible that at rest there would exist an imbalance in the internal tensions of the adhesive. This could reduce the force pulling the common electrode back to its neutral position after a negative force is applied. Further testing is required to determine the cause of this issue.

During the sensor characterization, the capacitance–applied force relationship was not linear, as predicted. A Hooke's Law approximation did not accurately describe the response, instead the system more closely followed a second-order polynomial trend. Some of the larger errors, especially for the axial shear sensor occurred at near the limit of the sensor, at 3.5 or 4 N of applied force.

Although some coupling between the sensors did exist, this was expected and accounted for by creating the calibration matrices. The coupling between sensors was significantly reduced and this arrangement of sensors was proven as a viable option for force sensing. The coupling equations were second-order polynomial approximations based on the gathered data. Therefore, there was another small amount of error introduced into the system.

The RMS noise may have been related to sensor electrode size, as there was a definite trend

with the largest sensor electrode (normal force) exhibiting the most noise, and the smallest sensor (axial) exhibiting the least. Additional testing would be needed to determine the outcome on noise from varying the sensor electrode size. Overall, the RMS noise was within an acceptable range, allowing for the measurement of forces as small as 100 mN. With the body of the grasper grounded, and the common electrode grounded, the shielding worked as intended. Touching an object to the instrument shaft or the grasper did not create noise in the measurements.

The significant shift in baseline capacitance due to a change in temperature suggests that some on board compensation may be needed to adjust for temperature. For an instrument that is designed to contact the human body, varying temperatures will certainly be encountered. Further testing is required to fully characterize the temperature response.

The sensing range of this grasper is one area where other designs have demonstrated a significant advantage. Ranges of ± 10 N for force measurements are seen with other MIS grasper designs. While a larger sensing range would be ideal, practical limitations must also be considered. Many MIS graspers presented in literature are designed for laparoscopic procedures, and they can therefore afford to be twice as large. The limitations of material strength in a PCMEMS design is another factor for review. A large sensing range is of no use if the device will break before the limit of this range.

4.5.2 Performance of Mechanical Components

The MS910 Med worked very well as an adhesive, and withstood all testing procedures without delamination or tearing. During the increased temperature testing the change in capacitance due to an applied force remained constant, therefore it appears that the adhesive maintained similar dielectric and elastic properties.

The failure of the pull tab hinge was at a reasonably high force, however it highlights what may be a significant challenge to the future development of PCMEMS instruments for MIS—material strength. Similarly, the strength of the upper jaw hinge should be increased to resist torsional loading at the distal tip of the jaw.

Increasing the friction of the jaws would have aided the grasper during the simulated grasping test. The task, though simple, illustrates that the grasper can perform basic functions, with all

three sensors successfully delivering data.

4.5.3 Concluding Remarks

There were many areas where the grasper showed promise, building on existing ideas and adding contributions to the area of PCMEMS for both the mechanical design and the sensing system. In some aspects, the performance of the device was not as strong as anticipated, such as the sensitivity to heat and the non-linear response to forces. There are also areas that will require further attention before a definite conclusion can be reached. Chapter 5 presents the conclusions and future work for this project.

Chapter 5

Conclusions and Future Work

5.1 Introduction

This thesis has presented a novel MIS grasper, manufactured using PCMEMS techniques, which uses capacitive sensors to measure forces in the axial, transverse, and normal directions. The current state of the art has suggested that PCMEMS may offer several advantages over traditional manufacturing techniques, especially when the goal is to economically produce complex items at larger volumes. In particular, several surgical devices have recently been realized using PCMEMS. One of the promising benefits of a PCMEMS surgical device is the possibility of reducing unit cost to a point where it is economically viable to dispose of the device after a single use.

The grasper presented herein was manufactured using unconventional techniques, even when compared to most PCMEMS devices. The finished grasper was evaluated to determine the efficacy of the sensing system. The mechanical strength of the design was also evaluated, to determine the limits of possible applied forces to the grasper.

Results from the evaluation show a promising sensing concept that could be adopted for other devices. While the performance of the PCMEMS grasper was slightly poorer than a similar conventionally-manufactured grasper, the device is the first PCMEMS surgical grasper to incorporate multi-axis force sensing, and does so over a force range larger than existing PCMEMS graspers.

5.2   Contributions

The device presented herein represents a step towards a commercially viable MIS instrument manufactured using PCMEMS, and single use MIS instruments. The ability to sense forces in multiple axes is of clinical importance when performing many MIS procedures, and instruments that can be disposed of after a single use will reduce contamination concerns and processing time. The contributions of this thesis may be summarized as follows:

1. A thorough exploration of alternative manufacturing techniques for a PCMEMS device. Using a micro-milling machine to manufacture the layers of the device is a first for a PCMEMS device, and proves that this is a realistic method for prototype or limited production manufacturing—where appropriate laser cutting machines are not available. Manufacturing on machines other than laser cutters may open opportunities for more researchers to begin experimenting with PCMEMS devices, accelerating the development process. Further, the described low-cost flexible printed circuit board (FPCB) manufacturing technique allows for rapid prototyping and inexpensive production. Although the FPCB manufacturing method is not unique to this thesis, there is limited academic discussion available on the subject. Commercial FPCB production is currently offered at a limited number of suppliers and is often prohibitively expensive when producing a small numbers of boards.

2. Multi-axis capacitive force sensing located at the tool tip. The sensing system presented is the first PCMEMS force sensing system that uses capacitive sensors. The grasper is also the first PCMEMS device to feature multi-axis force sensing, and the range of the system is larger than all other PCMEMS graspers. Sensor evaluation showed good dynamic response and relatively small errors across the force range. The FPCB is extremely simple, with only two capacitors and one CDC chip on a single layer FPCB. It has been shown that the board can be easily added as a material layer during the PCMEMS manufacturing process.

5.3   Additional Outcomes

The ease of manufacturing and the sensor performance have demonstrated that capacitive sensors are an area of research that is worthy of further investigation for PCMEMS devices. The foundation and proof of concepts developed in this thesis can be expanded upon for other uses; the system can be adapted for very small applications, and scaled up for larger force ranges as well. Tissue palpation tools that use an array of capacitive cells or a standalone sensor could be developed using these techniques.

It was shown that it was possible to assemble the body of the grasper both manually and using a support-frame-assisted assembly procedure. Using the support frame for the prototypes was limited due to manufacturing capabilities, but was successful on the 10:1 scale models. The design featured sarrus linkages to unfold sub assemblies and a system of slots and tabs to lock pieces together. As PCMEMS is a relatively new research field, developing a catalog of possible folding patterns and devices will aid in the creation of new designs in the future.

The simulated grasping task explored some challenges for PCMEMS—the robustness of designs, and the ability to vary texture (expressed as the low level of grip friction). The grasper presented in this thesis failed due to a material tear in the hinge connecting the jaw to the actuation cable. Additionally, it was necessary to pull the actuation cable with such high amounts force due to the low friction between the jaws of the grasper and the sample being grabbed. Adding texture such as grooves or ridges—something that has yet to be explored in depth for PCMEMS—to the grasping surface of the jaw would increase the friction.

5.4   Recommendations and Future Work

There exist several areas of improvement for both the design and the testing or validation of the proposed grasper. Due to the fact that the grasper was fabricated using a micro milling machine, additional questions exist regarding the assembly of the device. Additionally, this thesis has relied on existing literature to answer questions regarding economic viability and manufacturing times, as these could not be adequately answered when using the methods that were presented in this thesis. The following steps would be appropriate for building upon the conclusions of this thesis, and improving the performance of the grasper presented herein:

- The current design uses a differential pair of sensors for measuring transverse shear forces, and this was shown to perform better than the single axial shear sensor. Modifying the design in such a way that both the axial and transverse shear force sensors operate in differential pairs may improve the axial sensor performance. One limiting aspect of this approach is that the number of available measurement channels on the currently used CDC is 4. If two electrodes are angled at 45 degrees away from each other, such as [47], the information can be combined to measure forces in two axes, which could offer a solution to this problem. It would also be possible to use two CDC chips, with the option of including one in the upper jaw. The author is currently unaware of a commercially available CDC chip that is smaller than the FDC1004 with an equal or greater number of input channels, but smaller custom solutions do exist.

- The on board FPCB could be simplified even further by moving the decoupling capacitors to the data collection board (outside of the instrument). This would reduce unit cost by requiring fewer components and shrinking the length of the FPCB by over 30%. Moving the decoupling sensors to the other end of the instrument should not have a large impact on the amount of noise in the system, due to the fact that the signal has already been converted to a digital value at this point.

- The effects of heating the sensor were touched upon briefly, but a complete characterization of the sensor response to heat should be performed. Similarly, if the design can be modified

to include an on board temperature sensor, this would allow the temperature drift to be compensated for. Temperature sensing IC chips exist that are less than 1 mm × 1 mm in size (e.g., Texas Instruments LMT70), therefore, this is feasible. Additionally, several CDC chips feature on board temperature compensation. These are usually slightly larger than the FDC1004 (4 × 4 mm vs 3 × 3 mm) but may be able to fit into the grasper with a slight modification to the design of the instrument.

- The strength of the pull tab joint that failed during the simulated grasping task could be improved by using a thicker sheet of kapton for the flexible layer. Because the joint also moves through a relatively small angle of flexion, it may be possible for the joint to function and keep one or both of the structural layers solid, instead of using castellated hinges. The number of expected bending cycles over the lifetime of the instrument would need to be established, to determine if the stainless steel would fail due to fatigue.

- It is unclear whether a strength difference exists between PCMEMS hinges cut using a MMM or using a laser cutter. It is possible that the smoother edge finish of a laser cutter reduces the stress concentrations in the material. Comparing the tensile strength between a series of machined and laser cut hinge sub assemblies would answer this question.

- It would be beneficial to establish a relationship between sensor electrode size and sensor performance. This includes determining whether a larger sensor would produce a more linear response to applied forces than the sensor presented in this thesis. Characterizing sensor performance for a variety of electrode sizes would help extend the use of this technology into other tools. Additional MIS instruments and PCMEMS devices can be explored that use the sensing approach described in this thesis. Standalone sensors could be developed by creating a simple PCMEMS shell with an embedded FPCB in many configurations.

- In this thesis, only two elastomers were tested as the dielectric between sensor electrodes. Although the two elastomers were chosen for their specific properties, each was also tested in different scenarios—using a separate adhesive agent, or with the elastomer as the adhesive agent. Testing multiple dielectric and adhesive combinations may result in greater

performance, as well as improved consistency. Manufacturing consistency and repeatability between sensors was not discussed in this thesis, however this is an important consideration for a device that is intended for mass production. Design for manufacturing and design for assembly should be considered.

- The grasper was not tested to mechanical failure under all possible loading conditions. The strength of various PCMEMS structures—where sublaminates join or mate—should be both modeled and tested. The designed grasper featured a tube where one sublaminate, which folded to form three sides, mated with a second sublaminate through slots and tabs. It is unknown what the torsional, crush, and tensile strength of such a structure is. The optimal tab and slot size for strength is also unknown. If structure strength was modeled and validated for variables such as hinge design, slot and tab size/spacing, and material thickness, it would enhance the understanding of the PCMEMS community.

- The accuracy of the dynamic response and calibration of the sensors could be improved by testing the sensor in unison with a commercially available force sensor.

- During testing, the data processing was not happening in real time. The measurements were recorded, transfered, then processed in MATLAB. This is tedious, and also makes it impossible to determine total system delay or processing time. A custom user interface for testing and data collection should be developed to process and display the data in real time. This interface could also include preset tools for calibrating the sensors. If the interface is paired with a motorized system and a commercial force sensor, the calibration could be fully automated.

- Currently, when no grasping force is applied to the device, a restoring force exists that opens the jaws. The restoring force is only due to the bending of the material layers, and is relatively small. When the system is fit into a full instrument with a handle, the actuation cable should be replaced with a rigid link—a restoring force can then be applied with a spring at the proximal end of the instrument. There is enough space within the instrument shaft to do this, and additional space can be created by reducing the diameter of the wires that

run through the instrument shaft.

- Testing the response of the sensor when in contact with fluid (to simulate environmental conditions for surgery) is needed to determine if any protective coating is required over the circuitry to prevent short circuiting. Contact with fluid may also change the response of the capacitive sensor.

- All constituent materials have been certified as biocompatible, with the exception of the FR1500 sheet adhesive, for which further testing is required. Evidence suggests that after curing, FR1500 should be safe for surgical purposes. However, this has not been verified by the manufacturer (DuPont). A coating such as Parylene C could also be used to apply a thin flexible covering over any exposed FR1500.

- Sterilization testing is required for the grasper. All constituent materials and the MS910 Med adhesive can be subjected to ethylene oxide sterilization. The service temperature of MS910 Med is 204 $^\circ$C, and the maximum storage temperature of the FDC1004 chip is 150 $^\circ$C, therefore autoclave sterilization may also be possible. The additional processing time and cost of either of these sterilization methods has not been calculated.

- Several questions exist regarding the manufacturing of the device. Although some papers have provided general answers for other PCMEMS devices, the specifics for the device described in this thesis should be determined.

  - Manufacturing time from start to finish to create the device.
  - Unit and incremental cost of manufacturing.
  - Assembly time manually and using the scaffold support system.
  - Full procedure to ensure the finished device is sterile.

Ultimately, the end goal is to explore how PCMEMS can be best used in the medical industry, and create useful devices. This thesis has contributed to this goal, but the next steps and future work outlined above will ensure continued progress. PCMEMS has shown great promise in this area, but it is a technology that is still very much in development. It is important to continue this development and produce research that builds towards the end goals.

References

[1] J. P. Whitney, P. S. Sreetharan, K. Y. Ma, and R. J. Wood, "Pop-up book MEMS," *Journal of Micromechanics and Microengineering*, vol. 21, no. 11, p. 115021, 2011.

[2] P. Puangmali, K. Althoefer, L. D. Seneviratne, D. Murphy, and P. Dasgupta, "State-of-the-art in force and tactile sensing for minimally invasive surgery," *IEEE Sensors Journal*, vol. 8, no. 4, pp. 371–380, 2008.

[3] P. Modi, A. Hassan, and W. R. Chitwood, "Minimally invasive mitral valve surgery: a systematic review and meta-analysis," *European Journal of Cardio-thoracic Surgery*, vol. 34, no. 5, pp. 943–952, 2008.

[4] K. Fuchs, "Minimally invasive surgery," *Endoscopy*, vol. 34, no. 02, pp. 154–159, 2002.

[5] B. T. Bethea, A. M. Okamura, M. Kitagawa, T. P. Fitton, S. M. Cattaneo, V. L. Gott, W. A. Baumgartner, and D. D. Yuh, "Application of haptic feedback to robotic surgery," *Journal of Laparoendoscopic & Advanced Surgical Techniques*, vol. 14, no. 3, pp. 191–195, 2004.

[6] H. Mayer, F. Gomez, D. Wierstra, I. Nagy, A. Knoll, and J. Schmidhuber, "A system for robotic heart surgery that learns to tie knots using recurrent neural networks," in *IEEE International Conference on Intelligent Robots and Systems*, (Beijing, China), pp. 543–548, Oct 9–15 2006.

[7] A. Talasaz, A. L. Trejos, and R. V. Patel, "Effect of force feedback on performance of robotics-assisted suturing," in *IEEE RAS and EMBS International Conference on Biomedical Robotics and Biomechatronics*, (Roma, Italy), pp. 823–828, Jun 24–27 2012.

[8] M. MacFarlane, J. Rosen, B. Hannaford, C. Pellegrini, and M. Sinanan, "Force-feedback grasper helps restore sense of touch in minimally invasive surgery,," *Journal of Gastrointestinal Surgery*, vol. 3, no. 3, pp. 278–285, 1999.

[9] C. R. Wagner, N. Stylopoulos, and R. D. Howe, "The role of force feedback in surgery: Analysis of blunt dissection," in *10th Symposium on Haptic Interfaces for Virtual Environment and Teleoperator Systems, HAPTICS*, (Orlando, FL), pp. 68–74, Mar 24–25 2002.

[10] S. Russo, T. Ranzani, J. Gafford, C. J. Walsh, and R. J. Wood, "Soft pop-up mechanisms for micro surgical tools: Design and characterization of compliant millimeter-scale articulated structures," in *IEEE International Conference on Robotics and Automation*, (Stockholm, Sweden), pp. 750–757, May 16–21 2016.

[11] J. Gafford, T. Ranzani, S. Russo, A. Degirmenci, S. Kesner, R. Howe, R. Wood, and C. Walsh, "Toward medical devices with integrated mechanisms, sensors, and actuators via printed-circuit MEMS," *Journal of Medical Devices*, vol. 11, no. 1, p. 011007, 2017.

[12] J. B. Gafford, R. J. Wood, and C. J. Walsh, "Self-assembling, low-cost, and modular mm-scale force sensor," *IEEE Sensors Journal*, vol. 16, no. 1, pp. 69–76, 2016.

[13] J. Gafford, T. Ranzani, S. Russo, H. Aihara, C. Thompson, R. Wood, and C. Walsh, "Snap-on robotic wrist module for enhanced dexterity in endoscopic surgery," in *IEEE International Conference on Robotics and Automation*, (Stockholm, Sweden), pp. 4398–4405, May 16–21 2016.

[14] J. B. Gafford, S. B. Kesner, A. Degirmenci, R. J. Wood, R. D. Howe, and C. J. Walsh, "A monolithic approach to fabricating low-cost, millimeter-scale multi-axis force sensors for minimally-invasive surgery," in *IEEE International Conference on Robotics and Automation*, (Hong Kong, China), pp. 1419–1425, May 31–Jun 7 2014.

[15] J. B. Gafford, S. B. Kesner, R. J. Wood, and C. J. Walsh, "Microsurgical devices by pop-up book MEMS," *ASME/IDETC: Robotics and Mechanisms in Medicine*, pp. 1–7, Aug 4–7 2013.

[16] J. B. Gafford, S. B. Kesner, R. J. Wood, and C. J. Walsh, "Force-sensing surgical grasper enabled by pop-up book MEMS," in *IEEE International Conference on Intelligent Robots and Systems*, pp. 2552–2558, Nov 3–7 2013.

[17] A. L. Trejos, R. V. Patel, and M. D. Naish, "Force sensing and its application in minimally invasive surgery and therapy: a survey," *Institution of Mechanical Engineers, Part C: Journal of Mechanical Engineering Science*, vol. 224, no. 7, pp. 1435–1454, 2010.

[18] V. Gupta, N. Reddy, and P. Batur, "Forces in surgical tools: comparison between laparoscopic and surgical forceps," in *8th Annual International Conference of the IEEE Engineering in Medicine and Biology Society*, vol. 1, (Amsterdam, Netherlands), pp. 223–224, 1996.

[19] J. J. Van Den Dobbelsteen, A. Schooleman, and J. Dankelman, "Friction dynamics of trocars," *Surgical Endoscopy and Other Interventional Techniques*, vol. 21, no. 8, pp. 1338–1343, 2007.

[20] G. Picod, A. C. Jambon, D. Vinatier, and P. Dubois, "What can the operator actually feel when performing a laparoscopy?," *Surgical Endoscopy and Other Interventional Techniques*, vol. 19, no. 1, pp. 95–100, 2005.

[21] W. Sjoerdsma, J. L. Herder, M. J. Horward, A. Jansen, J. J. G. Bannenberg, and C. A. Grimbergen, "Force transmission of laparoscopic grasping instruments," *Minimally Invasive Therapy & Allied Technologies*, vol. 6, no. 4, pp. 274–278, 1997.

[22] J. C. Gwilliam, M. Mahvash, B. Vagvolgyi, A. Vacharat, D. D. Yuh, and A. M. Okamura, "Effects of haptic and graphical force feedback on teleoperated palpation," in *IEEE International Conference on Robotics and Automation*, (Kobe, Japan), pp. 677–682, May 12–17 2009.

[23] B. Demi, T. Ortmaier, and U. Seibold, "The touch and feel in minimally invasive surgery," in *HAVE 2005: IEEE International Workshop on Haptic Audio Visual Environments and their Applications*, (Ottawa, Canada), pp. 33–38, Oct 1–2 2005.

[24] M. Tavakoli, R. V. Patel, and M. Moallem, "Robotic suturing forces in the presence of haptic feedback and sensory substitution," in *IEEE Conference on Control Applications*, (Toronto, Canada), pp. 1–6, Aug 28–31 2005.

[25] P. S. Sreetharan, J. P. Whitney, M. D. Strauss, and R. J. Wood, "Monolithic fabrication of millimeter-scale machines," *Journal of Micromechanics and Microengineering*, vol. 22, no. 5, pp. 1–6, 2012.

[26] R. J. Wood, S. Avadhanula, R. Sahai, E. Steltz, and R. S. Fearing, "Microrobot design using fiber reinforced composites," *Journal of Mechanical Design*, vol. 130, no. 5, pp. 052304–052304–11, 2008.

[27] R. Malka, A. L. Desbiens, Y. Chen, and R. J. Wood, "Principles of microscale flexure hinge design for enhanced endurance," in *IEEE International Conference on Intelligent Robots and Systems*, (Chicago, IL), pp. 2879–2885, Sep 14–18 2014.

[28] B. Goldberg, M. Karpelson, O. Ozcan, and R. J. Wood, "Planar fabrication of a mesoscale voice coil actuator," in *IEEE International Conference on Robotics and Automation*, (Hong Kong, China), pp. 6319–6325, May 31–Jun 7 2014.

[29] R. Wood, S. Avadhanula, M. Menon, and R. Fearing, "Microrobotics using composite materials: the micromechanical flying insect thorax," in *IEEE International Conference on Robotics and Automation*, (Taipei, Taiwan), pp. 1842–1849, Sep 14–19 2003.

[30] M. I. Tiwana, S. J. Redmond, and N. H. Lovell, "A review of tactile sensing technologies with applications in biomedical engineering," *Sensors and Actuators, A: Physical*, vol. 179, pp. 17–31, 2012.

[31] G. Tholey, A. Pillarisetti, W. Green, and J. P. Desai, *Design, development, and testing of an automated laparoscopic grasper with 3-D force measurement capability*, pp. 38–48. Berlin, Heidelberg: Springer, 2004.

[32] J. Rosen, B. Hannaford, M. P. MacFarlane, and M. N. Sinanan, "Force controlled and teleoperated endoscopie grasper for minimally invasive surgery-experimental performance evaluation," *IEEE Transactions on Biomedical Engineering*, vol. 46, no. 10, pp. 1212–1221, 1999.

[33] D. S. Yurkewich, A. Escoto, A. L. Trejos, M.-E. LeBel, R. V. Patel, and M. D. Naish, "Low-cost force-sensing arthroscopic tool using threaded fiber Bragg grating sensors," in *5th IEEE RAS/EMBS International Conference on Biomedical Robotics and Biomechatronics*, (Sao Paulo, Brazil), pp. 28–33, Aug 12–15 2014.

[34] D. Tosi, M. Olivero, G. Perrone, and A. Vallan, "Improved fibre Bragg grating interrogation for dynamic strain measurement," *Deutsche Gesellschaft fur angewandte Optik, DGAO*, 2009.

[35] G. S. Fischer, T. Akinbiyi, S. Saha, J. Zand, M. Talamini, M. Marohn, and R. Taylor, "Ischemia and force sensing surgical instruments for augmenting available surgeon information," in *IEEE/RAS-EMBS International Conference on Biomedical Robotics and Biomechatronics, 2006*, (Pisa, Italy), pp. 1030–1035, Feb 20–22 2006.

[36] A. L. Trejos, A. Escoto, D. Hughes, M. D. Naish, and R. V. Patel, "A sterilizable force-sensing instrument for laparoscopic surgery," in *5th IEEE RAS/EMBS International Conference on Biomedical Robotics and Biomechatronics*, (Sao Paulo, Brazil), pp. 157–162, Aug 12–15 2014.

[37] J. Dargahi, M. Parameswaran, and S. Payandeh, "A micromachined piezoelectric tactile sensor for an endoscopic grasper-theory, fabrication and experiments," *Journal of microelectromechanical systems*, vol. 9, no. 3, pp. 329–335, 2000.

[38] S. Sokhanvar, M. Packirisamy, and J. Dargahi, "A multifunctional PVDF-based tactile sensor for minimally invasive surgery," *Smart Materials and Structures*, vol. 16, no. 4, pp. 989–998, 2007.

[39] G. S. L. Teo, M. S. Flander, T. R. Sepp, M. Corral, J. D. Diaz, A. Slocum, and K. Vakili, "Design and testing of a pressure sensing laparoscopic grasper," in *Design of Medical Devices Conference*, (Minneapolis, MN), pp. 1–8, April 12–14 2011.

[40] S. P. Chang and M. G. Allen, "Demonstration for integrating capacitive pressure sensors with read-out circuitry on stainless steel substrate," *Sensors and Actuators, A: Physical*, vol. 116, no. 2, pp. 195–204, 2004.

[41] B. Gray and R. Fearing, "A surface micromachined microtactile sensor array," in *IEEE International Conference on Robotics and Automation*, (Minneapolis, MN), pp. 1–6, Apr 22–28 1996.

[42] S. J. Chen, J. L. Huang, G. J. Wu, C. L. Wu, and S. S. Pan, "Design and characterization of a PCB based capacitive shear force sensor for robotic gripper application," *International Conference on Sensing Technology*, vol. 1, pp. 884–888, 2013.

[43] R. Brookhuis, H. Droogendijk, M. De Boer, R. Sanders, T. Lammerink, R. Wiegerink, and G. Krijnen, "Six-axis force–torque sensor with a large range for biomechanical applications," *Journal of Micromechanics and Microengineering*, vol. 24, no. 3, p. 035015, 2014.

[44] D. Kim, C. H. Lee, B. C. Kim, D. H. Lee, H. S. Lee, C. T. Nguyen, U. K. Kim, T. D. Nguyen, H. Moon, J. C. Koo, J.-D. Nam, and H. R. Choi, "Six-axis capacitive force/torque sensor based on dielectric elastomer," *SPIE Smart Structures and Materials + Nondestructive Evaluation and Health Monitoring*, vol. 8687, pp. 86872J–1–9, 2013.

[45] D. H. Lee, U. Kim, H. Jung, and H. R. Choi, "A capacitive-type novel six-axis force/torque sensor for robotic applications," *IEEE Sensors Journal*, vol. 16, no. 8, pp. 2290–2299, 2016.

[46] U. Kim, D. H. Lee, H. Moon, J. C. Koo, and H. R. Choi, "Design and realization of grasper-integrated force sensor for minimally invasive robotic surgery," in *IEEE International Conference on Intelligent Robots and Systems*, (Chicago, IL), pp. 4321–4326, Sep 14–18 2014.

[47] U. Kim, D. H. Lee, W. J. Yoon, B. Hannaford, and H. R. Choi, "Force sensor integrated surgical forceps for minimally invasive robotic surgery," *IEEE Transactions on Robotics*, vol. 31, no. 5, pp. 1214–1224, 2015.

[48] J. Peirs, J. Clijnen, D. Reynaerts, H. Van Brussel, P. Herijgers, B. Corteville, and S. Boone, "A micro optical force sensor for force feedback during minimally invasive robotic surgery," in *Sensors and Actuators, A: Physical*, vol. 115, pp. 447–455, Sep, 2004.

[49] B. Poulose, M. Kutka, M. Mendoza-Sagaon, A. Barnes, C. Yang, R. Taylor, and M. Talamini, "Human vs robotic organ retraction during laparoscopic nissen fundoplication," *Surgical endoscopy*, vol. 13, no. 5, pp. 461–465, 1999.

[50] G. Tholey, J. P. Desai, and A. E. Castellanos, "Force feedback plays a significant role in minimally invasive surgery: results and analysis.," *Annals of surgery*, vol. 241, no. 1, pp. 102–109, Jan, 2005.

[51] J. Rosen, J. D. Brown, S. De, M. Sinanan, and B. Hannaford, "Biomechanical properties of abdominal organs in vivo and postmortem under compression loads," *Journal of biomechanical engineering*, vol. 130, no. 2, p. 021020, 2008.

Appendix I: Permissions and Approvals

This appendix contains the following permission statements:

- Written permission from Sage Publications for Figure 2.1

- Written permission from Dr. Ana Luisa Trejos for Figure 2.1

- Online permission from IOP Publishing for Figures 2.2, 2.3

- Online permission from IOP for Figure 2.4

- Online permission from ASME for Figure 2.5

- Online permission from IEEE for Figures 2.6

  Figures 2.6–2.10, 2.12–2.16 are cited in text by IEEE standards

- Online permission from IOP for Figure 2.11

PermissionsUK < ████████ @sagepub.com>
to me ▾

Dear Dave Tripp,

Thank you for your email. I am pleased to report we can grant your request without a fee as part of your thesis.

Please accept this email as permission for your request as detailed below. Permission is granted for the life of the edition on a non-exclusive basis, in the English language, throughout the world in all formats provided full citation is made to the original SAGE publication.

As a courtesy, we ask that you contact the author to let them know the content will be republished. Please note this approval excludes any content which requires additional permission from a separate copyright holder. If the SAGE material includes anything not '© the Author' or '© SAGE', please contact the rights holder for permission to reuse those items.

Best Wishes,

Craig Myles
on behalf of **SAGE Ltd. Permissions Team**

SAGE Publications Ltd
██████████ Road
██████████
UK
██████████

SAGE Publications Ltd, Registered in England No.1017514
Los Angeles | London | New Delhi
Singapore | Washington DC
The natural home for authors, editors & societies

Thank you for considering the environment before printing this email.

Ana Luisa Trejos
to David ▾

Hi Dave,
Thanks for asking. As long as you have the journal's permission, I don't have a problem with you using the figure.
Good luck with the final stages of your thesis,
Ana Luisa

Copyright
Clearance
Center

Confirmation Number: 11651106
Order Date: 06/19/2017

Customer Information

Customer: Dave Tripp
Account Number: 3001164427
Organization: Dave Tripp
Email:
Phone:
Payment Method: Invoice

This is not an invoice

Order Details

Journal of micromechanics and microengineering : structures, devices, and systems

| Billing Status: |
| N/A |

Order detail ID:	70580509		**Permission Status:** ✅ Granted

ISSN:	0960-1317		**Permission type:** Republish or display content
Publication Type:	Journal		**Type of use:** Thesis/Dissertation
Volume:			**Order License Id:** 4132730020289
Issue:			
Start page:			
Publisher:	INSTITUTE OF PHYSICS PUBLISHING		

Requestor type	Author of requested content
Format	Print, Electronic
Portion	image/photo
Number of images/photos requested	3
Title or numeric reference of the portion(s)	Page 3 Figure 1, Figure 2, Figure 3
Title of the article or chapter the portion is from	Pop-up book MEMS
Editor of portion(s)	N/A
Author of portion(s)	J P Whitney, P S Sreetharan, K Y Ma and R JWood School
Volume of serial or monograph	21
Issue, if republishing an article from a serial	11
Page range of portion	1--7
Publication date of portion	14 October 2011
Rights for	Main product
Duration of use	Current edition and up to 5 years
Creation of copies for the disabled	no
	no

Copyright Clearance Center

Note: Copyright.com supplies permissions but not the copyrighted content itself.

1	2	3
PAYMENT	REVIEW	CONFIRMATION

Step 3: Order Confirmation

Thank you for your order! A confirmation for your order will be sent to your account email address. If you have questions about your order, you can call us 24 hrs/day, M-F at ▮▮▮▮▮▮▮▮▮ Toll Free, or write to us at ▮▮▮▮▮▮▮.com. This is not an invoice.

Confirmation Number: 11651112
Order Date: 06/19/2017

If you paid by credit card, your order will be finalized and your card will be charged within 24 hours. If you choose to be invoiced, you can change or cancel your order until the invoice is generated.

Payment Information

Dave Tripp
▮▮▮▮▮▮▮▮▮▮
▮▮▮▮▮▮▮▮▮▮
Payment Method: n/a

Order Details

Journal of micromechanics and microengineering : structures, devices, and systems

Order detail ID:	70580534	**Permission Status:** ✅ Granted	
Order License Id:	4132750355183	**Permission type:**	Republish or display content
ISSN:	0960-1317	**Type of use:**	Thesis/Dissertation
Publication Type:	Journal		
Volume:		**Requestor type**	Author of requested content
Issue:			
Start page:			
Publisher:	INSTITUTE OF PHYSICS PUBLISHING	**Format**	Print, Electronic
		Portion	image/photo
		Number of images/photos requested	1
		Title or numeric reference of the portion(s)	Page 3, Figure 3
		Title of the article or chapter the portion is from	Monolithic fabrication of millimeter-scale machines
		Editor of portion(s)	N/A
		Author of portion(s)	

Copyright Clearance Center

Confirmation Number: 11651111
Order Date: 06/19/2017

Customer Information

Customer: Dave Tripp
Account Number: 3001164427
Organization: Dave Tripp
Email:
Phone:
Payment Method: Invoice

This is not an invoice

Order Details

Journal of micromechanics and microengineering : structures, devices, and systems

| Billing Status: |
| N/A |

Order detail ID:	70580529	
ISSN:	0960-1317	
Publication Type:	Journal	
Volume:		
Issue:		
Start page:		
Publisher:	INSTITUTE OF PHYSICS PUBLISHING	

Permission Status: ✅ Granted

Permission type: Republish or display content
Type of use: Thesis/Dissertation

Order License Id: 4132741283009

Requestor type	Author of requested content
Format	Print, Electronic
Portion	image/photo
Number of images/photos requested	1
Title or numeric reference of the portion(s)	Figure 8
Title of the article or chapter the portion is from	Pop-up book MEMS
Editor of portion(s)	N/A
Author of portion(s)	J P Whitney, P S Sreetharan, K Y Ma and R JWood School
Volume of serial or monograph	21
Issue, if republishing an article from a serial	11
Page range of portion	6
Publication date of portion	14 October 2011
Rights for	Main product
Duration of use	Current edition and up to 5 years
Creation of copies for the disabled	no
	no

Copyright
Clearance
Center

Confirmation Number: 11657594
Order Date: 07/20/2017

Customer Information

Customer: Dave Tripp
Account Number: 3001164427
Organization: Dave Tripp
Email:
Phone:
Payment Method: Invoice

This is not an invoice

Order Details

Proceedings of the ASME International Design Engineering Technical Conferences and Computers and Information in Engineering Conference 2013

Billing Status:
N/A

Order detail ID:	70608536	**Permission Status:** ✅ Granted	
ISBN:	9780791855935	**Permission type:**	Republish or display content
Publication Type:	Book	**Type of use:**	Republish in a thesis/dissertation
Author/Editor:	ASME Design Engineering Technical Conferences (2013 : Portland, Or.) ; et al	**Job Ticket:**	501290372
		Order License Id:	4160380096334

Requestor type	Academic institution
Format	Print, Electronic
Portion	image/photo
Number of images/photos requested	2
Title or numeric reference of the portion(s)	Figure 4, Figure 13
Title of the article or chapter the portion is from	Microsurgical Devices by Pop-Up Book MEMS
Editor of portion(s)	N/A
Author of portion(s)	Gafford, J.B.
Volume of serial or monograph	6A
Issue, if republishing an article from a serial	37
Page range of portion	3,6
Publication date of portion	2013
Rights for	Main product
Duration of use	Current edition and up to 5 years
Creation of copies for the disabled	no
With minor editing privileges	no
For distribution to	Canada

7/20/2017 Rightslink® by Copyright Clearance Center

Copyright Clearance Center — RightsLink®

Home | Account Info | Help | ✉

IEEE
Requesting permission to reuse content from an IEEE publication

Title: Force-sensing surgical grasper enabled by pop-up book MEMS
Conference Proceedings: Intelligent Robots and Systems (IROS), 2013 IEEE/RSJ International Conference on
Author: Joshua B. Gafford
Publisher: IEEE
Date: Nov. 2013
Copyright © 2013, IEEE

Logged in as:
Dave Tripp
Account #:
3001164427

LOGOUT

Thesis / Dissertation Reuse

The IEEE does not require individuals working on a thesis to obtain a formal reuse license, however, you may print out this statement to be used as a permission grant:

Requirements to be followed when using any portion (e.g., figure, graph, table, or textual material) of an IEEE copyrighted paper in a thesis:

1) In the case of textual material (e.g., using short quotes or referring to the work within these papers) users must give full credit to the original source (author, paper, publication) followed by the IEEE copyright line ⬦ 2011 IEEE.
2) In the case of illustrations or tabular material, we require that the copyright line ⬦ [Year of original publication] IEEE appear prominently with each reprinted figure and/or table.
3) If a substantial portion of the original paper is to be used, and if you are not the senior author, also obtain the senior author⬦s approval.

Requirements to be followed when using an entire IEEE copyrighted paper in a thesis:

1) The following IEEE copyright/ credit notice should be placed prominently in the references: ⬦ [year of original publication] IEEE. Reprinted, with permission, from [author names, paper title, IEEE publication title, and month/year of publication]
2) Only the accepted version of an IEEE copyrighted paper can be used when posting the paper or your thesis on-line.
3) In placing the thesis on the author's university website, please display the following message in a prominent place on the website: In reference to IEEE copyrighted material which is used with permission in this thesis, the IEEE does not endorse any of [university/educational entity's name goes here]'s products or services. Internal or personal use of this material is permitted. If interested in reprinting/republishing IEEE copyrighted material for advertising or promotional purposes or for creating new collective works for resale or redistribution, please go to http://www.ieee.org/publications_standards/publications/rights/rights_link.html to learn how to obtain a License from RightsLink.

If applicable, University Microfilms and/or ProQuest Library, or the Archives of Canada may supply single copies of the dissertation.

BACK ⬦⬦⬦ CLOSE WINDOW

Copyright Clearance Center

Note: Copyright.com supplies permissions but not the copyrighted content itself.

1	2	3
PAYMENT	REVIEW	CONFIRMATION

Step 3: Order Confirmation

Thank you for your order! A confirmation for your order will be sent to your account email address. If you have questions about your order, you can call us 24 hrs/day, M-F at ▮▮▮▮▮▮▮▮ Toll Free, or write to us at ▮▮▮▮▮▮▮▮. This is not an invoice.

Confirmation Number: 11658117
Order Date: 07/24/2017

If you paid by credit card, your order will be finalized and your card will be charged within 24 hours. If you choose to be invoiced, you can change or cancel your order until the invoice is generated.

Payment Information

Dave Tripp
▮▮▮▮▮▮▮▮
Payment Method: n/a

Order Details

Smart Materials and Structures

Order detail ID:	70610610	
Order License Id:	4155491218509	
ISSN:	0964-1726	
Publication Type:	Journal	
Volume:		
Issue:		
Start page:		
Publisher:	IOP Publishing	

Permission Status: ✅ Granted

Permission type: Republish or display content
Type of use: Thesis/Dissertation

Requestor type	Academic institution
Format	Electronic
Portion	image/photo
Number of images/photos requested	2
Title or numeric reference of the portion(s)	Page 991, Figures 3, 4
Title of the article or chapter the portion is from	A multifunctional PVDF-based tactile sensor for minimally invasive surgery
Editor of portion(s)	N/A
Author of portion(s)	S. Sokhanvar, M. Packirisamy, J. Dargahi

CURRICULUM VITAE

Name:	Dave Tripp
Post-secondary Education and Degrees:	The University of Western Ontario London, Ontario, Canada 2010–2015 B.E.Sc. Mechatronic Systems Engineering with Professional Internship The University of Western Ontario London, Ontario, Canada 2015–2017 M.E.Sc. Electrical and Computer Engineering
Honours and Awards:	Graduate Student Teaching Assistant Award, Western, 2017 Alexander Charles Spencer Admission Scholarship, Western, 2010 Aiming for the Top Tuition Scholarship, Western, 2010
Related Work Experience:	Teaching Assistant The University of Western Ontario 2015–2017 Research Associate The University of Western Ontario 2015–2017 Quality Engineering Intern Transform Automotive 2013–2014